BACHELOR THESIS

DESIGN AND THERMAL ANALYSIS OF A DIRECT STEAM GENERATION CENTRAL-RECEIVER SOLAR THERMAL POWER PLANT

Author: Carlos Garrido Camino

Director: Antonio Acosta Iborra

Degree: Bachelor in Mechanical Engineering

School of Engineering
Thermal and Fluid Engineering Deparment

Leganés, 30 September 2013

DESIGN AND THERMAL ANALYSIS OF A DIRECT STEAM GENERATION CENTRAL-RECEIVER SOLAR THERMAL POWER PLANT

DISEÑO Y ANÁLISIS TÉRMICO DE UNA CENTRAL TERMOSOLAR DE TORRE DE CONCENTRACIÓN CON EVAPORACIÓN DIRECTA

Autor: Carlos Garrido Camino

Director: Antonio Acosta Iborra

TRIBUNAL

Presidente: Antonio García García

Vocal: Eduardo Corral Abad

Secretario: Jose Alfonso Artero Guerrero

Realizado el acto de defensa y lectura del Proyecto Fin de Carrera el día 30 de SEPTIEMBRE de 2013 en Leganés, en la Escuela Politécnica Superior de la Universidad Carlos III de Madrid, acuerda otorgarle la CALIFICACIÓN de

PRESIDENTE VOCAL SECRETARIO

Acknowledgements

A todos los profesores del CP Regimiento Inmemorial del Rey, del IES Mariana Pineda y de la UC3M por su dedicación y ser parte importante en la consecución de este trabajo.

A mi profesor y director del proyecto, Antonio Acosta, por su infinita paciencia y haber sabido transmitirme su pasión por esta profesión.

A todos mis amigos, pero sobre todo a los 5 de toda la vida, por haber sabido mantenerme en tierra, a Santi y a Víctor por haber sido dos grandes compañeros con los que me gustaría volver a trabajar y a mi gran amigo Manu por su confianza infinita e incondicional y sus clases de física y química.

A mi chica Elena, que aunque no ha estado desde el principio, me ha apoyado y ayudado como nadie en momentos críticos y ha tenido la paciencia suficiente para aguantar mis horas estresantes de trabajo.

A mis abuelos y mi tío, que los siento muy cerca siempre aunque alguno me falte y que son una de las razones por las que lucho día a día.

A mi hermano Álvaro, por llevar conmigo 20 años sufriéndome y enseñándome como nadie a ser mejor persona.

Y a los grandes culpables de todo esto, a mis padres, que con su apoyo y sacrificio me han educado como pocos saben hacer y a los cuales les estaré eternamente agradecido y en deuda por enseñarme que con muy poco se pueden hacer grandes cosas.

Abstract

Thermo-solar central receiver power plants use radiation coming from the Sun, a clean energy source, to produce electricity. The best locations for this type of installations are the ones between 30º and 40º of latitude, both in the northern and southern hemisphere, what makes Spain to be one of the most suitable and attractive places all over the world for this energy source. However, this technology is not well developed yet comparing to other renewable energy sources such as wind energy or hydropower energy. This is what makes engineers to work hard in order to obtain better results from this source and make solar thermal plants competitive against other kinds of power plants.

Thereby, the present project develops a direct steam generation design in order to improve the plant performance introducing new configurations both for the receiver, adding a second row of tubes, and for the power cycle, using a reheating process. For those objectives, this report starts describing the process from the very beginning, solar radiation. The design method ends calculating a back-up system based on a natural gas-fired boiler. In the meanwhile, the present project describes the power cycle, a heat transfer analysis at the receiver and the distribution of the heliostats over a given area.

Finally, after having obtained the results for a 50MW power plant, a financial analysis is provided to preliminary characterize the investment in this kind of energy source. Besides, the different models developed across the project, as well as between those designs are compared to solar energy power plants already operating in Spain.

Resumen

Las plantas de energía solar de concentración en receptor central usan una fuente de energía limpia, como es la radiación del sol, para producir electricidad. Los mejores lugares para la instalación de dichas plantas son aquellos que se localizan entre los 30º y 40º de latitud, tanto en un hemisferio como en el otro, convirtiendo a España en un atractivo y prolífico territorio. Sin embargo, esta tecnología no está suficientemente desarrollada como para competir con otras energías renovables como son la eólica o la hidroeléctrica. Por ello, los ingenieros trabajan duro para obtener mejores resultados con este tipo de centrales para hacerlas competitivas frente a otras plantas que utilizan fuentes de energía diferentes.

Por lo tanto, el presente proyecto desarrolla un diseño de evaporación directa para mejorar el rendimiento de dichas instalaciones introduciendo nuevas configuraciones en el receptor, añadiendo una segunda fila de tubos, y en el ciclo de potencia, haciendo uso del recalentamiento. Para ello, este trabajo empieza describiendo el proceso de la creación de la radiación solar. Termina con el cálculo del sistema de apoyo con caldera de gas natural. Entre ello describe los ciclos de potencia, un análisis de transferencia de calor en el receptor y la distribución de los heliostatos sobre un determinado campo.

Finalmente, después de haber obtenido los resultados para el diseño de una planta de producción de 50MW de energía eléctrica, se presenta un análisis financiero del proyecto para así justificar la inversión. Además, al final de muestran comparaciones entre los diferentes diseños descritos en este proyecto, así como entre éstos y otras plantas de energía solar que ya funcionan en el territorio español.

Index

Figure Index

Table Index

Chapter 1 Introduction

1.1. State of the art and Motivation

1.1.1. Current Energy Problems around the Globe

Energy is the basis of every single sign of human life in this planet. The global energy problem faced by mankind today is set to worsen since energy sources have not been used properly.

For several decades, society has been facing a long term and important issue in energy production for the survival, as the most used but the less solid sources of energy are fossil fuels. Nowadays, fuel has become one of the most expensive commodities due to several reasons. Firstly, there is a huge concentration in oil production, which is mainly in Middle East countries. Secondly, due to the growing number of world population, energy demand will be also higher than it is today, accelerating the spending of fossil fuel. Furthermore, it is widely studied and accepted that the reserves of crude will not last more than a century since it is not possible to generate more.

As oil becomes scarce and more demanded, the price will rise up to numbers that only a few will be able to afford. The concern about the previous issue came stronger than ever in the 1970s due to the so called “oil crisis”. The six biggest oil producers met together to create an Organization of Petroleum Exporting Countries (OPEC), with which they decided to increase crude price by 70%.

On the other side, the way of obtaining energy from this source is also an important concern from an environmental point of view. Burning fossil fuels, no matter whether they are in solid, liquid or gas state generates several pollutant products.

That energy is based on combustion reaction which produces, among others, water (H_2O) and carbon dioxide (CO_2). This last agent, CO_2, is the main pillar of the "greenhouse effect". Such effect, which is not hazardous on itself, consists on keeping the Earth warm enough to allow living forms. However, CO_2 has been directly related to the global warming effect, which is the principal cause of the heating-up of the Earth. Apart from CO_2, NOx and SO_2 are indirect products of combustions, depending on reaction conditions and the composition of burned fossil fuels. They contribute mainly to Ozone layer depletion, acid rain and greenhouse effect.

1.1.2. Energy Sources

There are two main energy sources according to the possibility of replenishment:

1. Non-renewable or conventional energy sources.

This kind of energy sources are exhaustible and cannot be replaced as they are used. They are the main cause of pollution but they have been used for many years which mean that their exploitation techniques are well developed. The main conventional energy sources are fossil fuels such as coal, natural gas and oil as well as uranium for nuclear energy production.

2. Renewable or unconventional energy sources.

They are inexhaustible and can be used as many times as society need. The main source of renewable energies is the Sun. Planet Earth obtains much energy from solar radiation every day. As this energy reaches the planet, it starts to be dissipated, creating other energy sources such as wind.

The main Renewable Energy Sources are given a brief look in the following subsections.

1.1.2.1. Solar Energy

As it will be continuously highlighted across the present document, the sun is the origin of every single energy source in the planet. However, solar energy refers to the energy directly obtained from the sun. As it is the main renewable energy source in this report, it will be deeply developed in Chapter 2. However, for a brief summary about this kind of energy, is worth to say that solar energy is the most abundant and continuous energy source. Solar radiation is subjected to absorption, reflection and transmission through the atmosphere and the topography of the studied location has also a great impact on the performance of solar energy plants.

There have been many scientific studies to state models which define the irradiation data on the earth surface, apart from the technological development carried over coolers, heaters and solar energy electricity generators such as photovoltaic cells.

However, for high and middle power, central receiver solar power plants are the more feasible option. It usually uses Hitec molten salts as heat transfer fluid, but other technologies like direct steam generation may rise the system efficiency.

1.1.2.2. Wind Energy

This source of energy has experienced a great and fast development across the world. Due to factors such as technological development, wind energy has seen its cost reduced to levels which make it competitive in the energy market.

Wind has been used from ancient times for different purposes such as to take water to higher zones, windmills to grind grains or to move big ships. In fact windmills have been the major basis for the development of wind farms to produce electricity. The evolution of windmills can be observed in Figure 1.

Although it does not pollute the air with any contaminant matter, there is a noise and visual pollution from modern wind farms.

Figure 1: Past and Present of Windmills. Source: (EsAcademic 2013)

1.1.2.3. Biomass

This technology is mainly based on industrial and agricultural wastes. However, from prehistoric times biomass power has been a major energy source. Again, this kind of energy has the sun as its origin. The sun is the primary ingredient for photosynthesis in plants, which forms the main ingredient for this source.

Wood, crop wastes and animal dungs are the main materials that have its reason to be in photosynthesis. All across the world, wood is used to heat up houses and cook, and especially in developing countries. In developed countries, there are many studies and investments on biofuels in order to mitigate the CO_2 emissions into the atmosphere.

However, its efficiency is relatively low since the materials have to be burned to obtain energy. In Figure 2 it can be observed some of the materials which are used for biomass energy production.

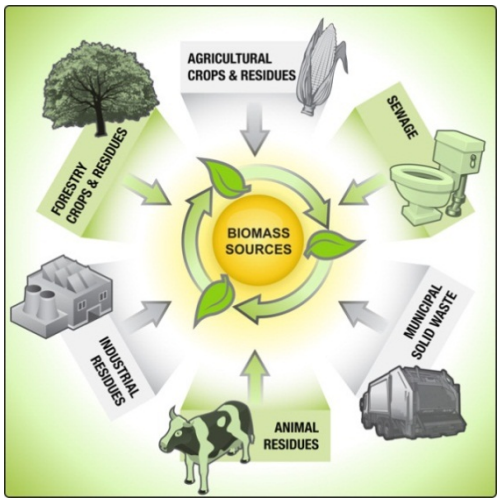

Figure 2: Biomass Sources. Source: (Greenewables 2013)

1.1.2.4. Geothermal Energy

This source of energy comes from heat escaping from the inside Earth layers. The potential of this energy is numbered as 35 thousand of millions times the world energy consumption (Johansson 1993). However, due to the limited depth to be exploited, 5km, only a tiny fraction of this energy can be obtained. In this depth, the temperature increases at an average of 30ºC per kilometer, but this value varies from zone to zone.

Natural spas and geysers are a result of geothermal energy. And these determined the best areas in the world to use technology in order to obtain energy from the heart of the earth. These zones are the Fire Belt, the Mid-Atlantic Ridge, the Alpine-Himalayan mountain chain, much of eastern Africa and western Arabian Peninsula, central Asia and a few archipelagos in the Pacific Ocean such as Hawaii and Samoa. Figure 3 shows in a map all those zones.

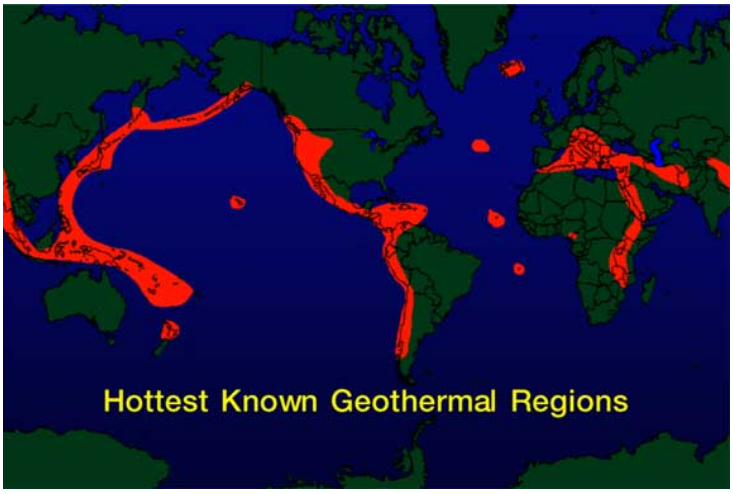

Figure 3: Suitable zones for geothermal energy. Source: (Geothermal Education Office 2000)

1.1.2.5. Hydraulic Energy

Electric power is generated in hydraulic energy systems when water stored by dams is released to make water turbines turn. Dams that store the water have two main purposes, to increase

water level, so that potential energy, and reserve water in order to compensate changes in river flow or power demand.

However, these reservoirs flood high areas affecting ecosystems that develop their live nearby the rivers. Furthermore, floodplains have rich soils for agricultural use and even when towns located close to these areas do not use them for agriculture, rivers provide of opportunities for fishing. These environmental issues go with the expropriation of areas zones needed to flood vast areas close to the rivers. This task plays an important role during the projects due to political reasons.

This source of energy is already widely spread and established all around the globe. In developed countries with large hydropower systems, large hydraulic power plants are already exploited to the limit. Therefore the focus now turns into small-scale hydro installations in order to obtain the marginal resources. An example of this technology is Hoover Dam which can be observed in Figure 4.

It needs to be highlighted that this mean of energy can be jeopardized by climate change. Stream flows may change in size in different areas, which would force to rebuild dams in other places. (Harrison and Whittington 2001)

Figure 4: Hoover Dam, Colorado River. Source: (Guia Sempio 2007)

1.1.2.6. Ocean Energy

Water covers almost two thirds of the earth, which means that the majority of the sun radiation is absorbed by oceans. This make the seas to become warmer, heating the air above up and giving air currents which move the water generating waves. Thereby, the oceans are a huge source of energy which mainly comes from four different sources: waves, tides, sea currents and salinity gradient. In Figure 5 some images show these four technologies.

Moreover, the gravity of the moon and the sun creates tides on the oceans. In continuous cycles, the oceans raise and lower their levels. The best point of this energy source is that is highly predictable in both timing and output. However, the tides are useful for energy

generation when are large enough, therefore, some places are more suitable than others to install this kind of power plants, such as United Kingdom and France.

Both in tropical and subtropical zones of the globe, natural temperature differences exist over the deep of the seas. Its production may be continuous since this difference in temperature lasts the whole day, 24 hours. The base of this technology is big pipes and pumps, and need to have at least a temperature gradient of 20ºC. The plants can be constructed in land, which gives direct electricity output, or in floating platforms, which need to convert this energy into other mean of energy by storage such as hydrogen production.

The salinity gradient that exists at oceans is also useful for energy generation. It is based on the osmotic pressure. Theoretically, a semipermeable membrane separates freshwater and a reservoir of saltwater. This reservoir would rise until a level which allows releasing it into a water turbine to obtain electricity.

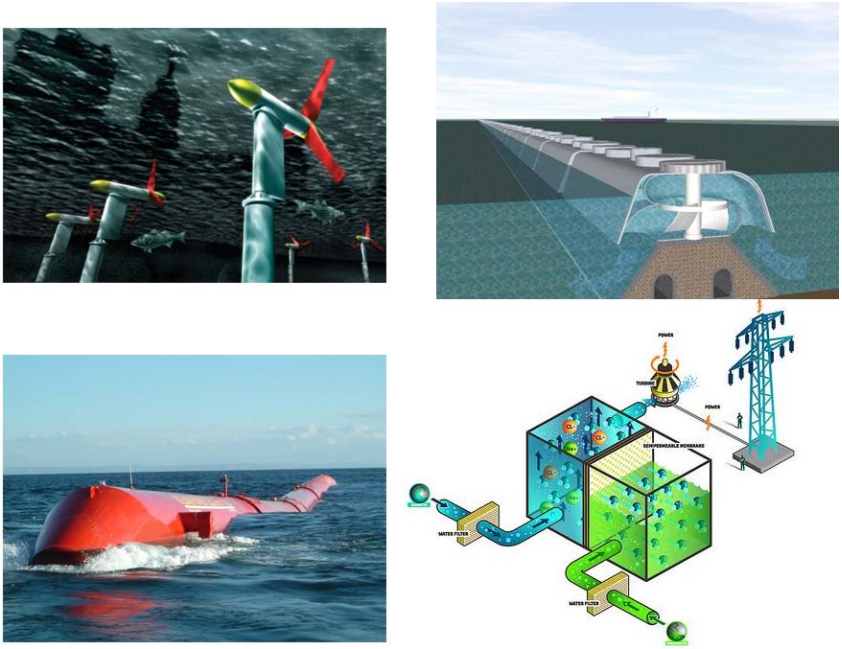

Figure 5: From left to right, from top to bottom; Current energy, Tide energy, Wave energy, Salinity gradient energy. Source: (Darvill 2012)

1.1.3. Renewable Energies as Solution

Renewable energies are being strongly enhanced as main alternatives to fossil fuel since they solve many of the inconvenient they have both economically and environmentally.

From an environmental perspective, there would be a new chance to mix both conventional and renewable technologies in order to improve efficiency and environmental care, meeting energy demand always at the best equilibrium. Since the average years to meet demand by oil and natural gas are 41 and 67 years respectively, natural gas would be the main resource to use as back-up in renewable energy power plants. In addition, the electrical energy coming

from renewable sources could be fed directly into the grid, substituting conventional sources, meaning a decrease to zero of energy storage.

Front an economic point of view, the introduction of new energy sources brings a wide range of ways to make the world run, diversifying energy producers, giving each region the opportunity to live with the more suitable source of energy. Besides, the diversity of renewable energies, taking into account their differences, would enhance competition in an important market which has been mostly controlled by oil producers. Therefore, they are an opportunity of offshoring energy production, making other countries participate in this market in many different ways since there are better locations than others to place renewable energy plants.

Apart from that, it would mean job creation in many different fields, levels and places. However, it has to be taken into account that this job creation would also mean a destruction of other positions in different sectors.

The penetration of renewable energies into energetic market depends on some changes on the market conditions. Firstly, private firms need to see clearly the benefits from this kind of energy in economic terms. There are many different ways to financially study a project, and renewable energy is a long term investment, which takes time to provide profits. Secondly, taxes and regulations should enhance investment decisions, taking also into account environmental costs which are not easy to dimension. Thirdly, governments should support research in renewable energy technologies, increasing funds and human capital in this area of investigation. And, finally, the creation of a large and strong organization similar to the OPEC in fossil fuel market.

In the EU the growth of RES-E[1] has much to do with the liberalization of energy markets, which happens in 1997 in Spain. In the same year, the so-called *Kyoto Agreement* took place during the third conference of parties made by the Climate Convention. The agreement aimed to reduce the greenhouse effect decreasing CO_2 emissions. That is why, during the 90s, the Member States of the EU decided to open energy markets to different competitors and end with the monopoly that was established until that date. The first step these states took was to divide clearly which of the parts of the market were able to be open for competition, like the direct service for customers, and the non-competitive parts such as the operation of the energy networks. Secondly, the operators that monopolized the market until that date were obliged to allow third parties to enter into the infrastructure and technology. As third step, these countries removed restrictions to customers to allow them to change from supplier enhancing the competition in this sector. And finally independent regulators were in charge of monitoring the sector to get a more objective view of the market.

However, even with such a great effort to enhance the competition, and therefore, the use of renewable energies in the market, it was not enough to definitely give new technologies a part of the sector. Thereby, the government started to introduce measures into the market in order to put the renewable technologies at the same level of competition as the traditional sources of energy. For this purpose, three main models have been developed across the EU. The first

[1] RES-E is related to the electricity production based on renewable energy resources.

one is the so called “Feed-in Model”, which consists on guaranteeing a minimum price for a long period of time for renewable electric energy production. It has been successfully implemented in countries like Spain, Germany and Denmark, proving its great efficiency when comparing specific renewable technology development such us wind power. It is a problem when introducing it in markets since it violates market rules. Another way to promote RES-E is the “Tender System”, developed in the UK. This system offers contracts in different intervals, with which a renewable energy plant is given a quota when presenting the lowest price of the tender. The winner of the tender sells its electric production at a fixed price for the whole life of the contract. Although it seems to be a better and more competitive system than the Feed-in Model, disagreements with the location of wind farms along the UK, due to landscape and bureaucratic reasons, have given worse results. In the Netherlands the used model is the “Certificates Trading Model”. In this model, the renewable energy producer sells the energy at the market price plus the market price of the green certificate. Green certificates are tradable commodities which guarantee that the energy was produced with renewable energies. (Meyer 2003)

1.1.4. Future of Energy

As it is described in the *IEA WEO2012* (International Energy Agency 2012), a scenario must be established to take a look into the future. As it follows, a new scenario is the base to describe the future development of energy. This means taking into account already implemented policies and the ones that have been planned but have not been implemented yet.

As one of the variables has already been fixed, government intervention, there are still two important factors, economic conditions and climate change. In a world, mainly developed countries, submerged in a deep economic and social crisis, the growth of the stake of renewable energies on the total world production can totter and be not easy to foresee as it was when economic growth was stable before 2008. However, the pressure of climate change is over entire world, what pushes the industry to move forward and invest in renewable energy.

In the other hand there are several trends which are explained next:

From an economic perspective, there are several trends affecting production and consumption of energy.

Firstly, the growth of energy demand in the short and medium term is a major issue since it is expected that world population will grow 1.700 million people from 2010 to 2035. This means the world will have over 30 times the current Spanish population, and more than once the Chinese population. That datum, transformed to energy demand, is equal to a 35% more of primary energy demands in the entire world for the same period, 1.2% per year. Depending on the assumed scenario, the new scenario already mentioned, gives a demand number between the current scenario, which would give a higher growth, 1.5% per year, and the 450 scenario, that would give a lower but consistent growth of 0.6%.

Secondly, the increasing trend in energy demand from developing countries in modern economy is a relevant fact that must be bear in mind. Since 1973 the share of non-OECD countries in world primary energy demand has raised up from 36% to 55%. This figure reflects the hard industrialization of countries like China and India, becoming the most active areas on world economy, getting a share of 64% on world primary energy demand. This would mean a saturation of energy market, giving high prices for conventional energy sources.

Thirdly, the present and future of fossil fuels must be considered at the time of taking a look into the future of energy. Nowadays they are the main source of energy of the whole world and it tends to increase during the mentioned period. The faster growth of fossil fuels belongs to coal, rising 59% until 2035. However, a faster growth is given in renewable energy sources, achieving a share of about 27%.

Following the main topic of this work, the fast growth of renewable energy production in the close future has to be highlighted. The expected electricity generation from renewables is 43% of the total electricity generation at 2035 in the EU. Among all the different renewable energy technologies, wind and hydro power are the most important. The factor that determines that solar thermal energy is not in that group is the immaturity of this technology. Much more investment, development and research have to be achieved in the next years. This is one of the reasons of the development of the presented project.

1.1.5. World Electric Production

According to the WEO 2012 (International Energy Agency 2012) the total world electricity generation was 21.408 TWh, where Coal covers the 40% compared to a 0.009% covered by Solar Thermal. In the European Union the total electricity generation was 3310 TWh, where Nuclear covered a 27% while only a 0.030% was covered by Solar Thermal. In Spain, according to *La energía en España* (Ministerio de Industria, Energía y Turismo de España 2012), the total demand in the Spanish Peninsula was 286TWh, where a 34% was covered by Natural Gas, and a 0.246% was covered by Solar Thermal technology.

This shows the great impact of Solar Energy in Spain, apart from the fact that its percentage of electric demand covered by Photovoltaic Technology is higher than both in the EU and in the World.

The distribution of energy demand in the whole world, Europe and Spain can be observed in Figure 6, Figure 7 and Figure 8.

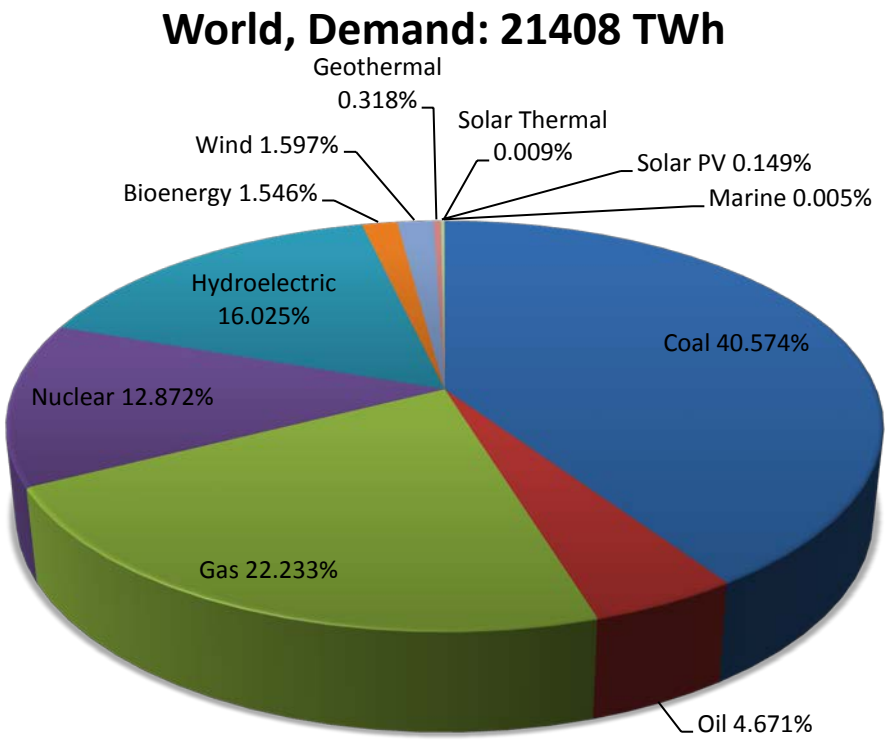

Figure 6: World energy demand. Source: (International Energy Agency 2012)

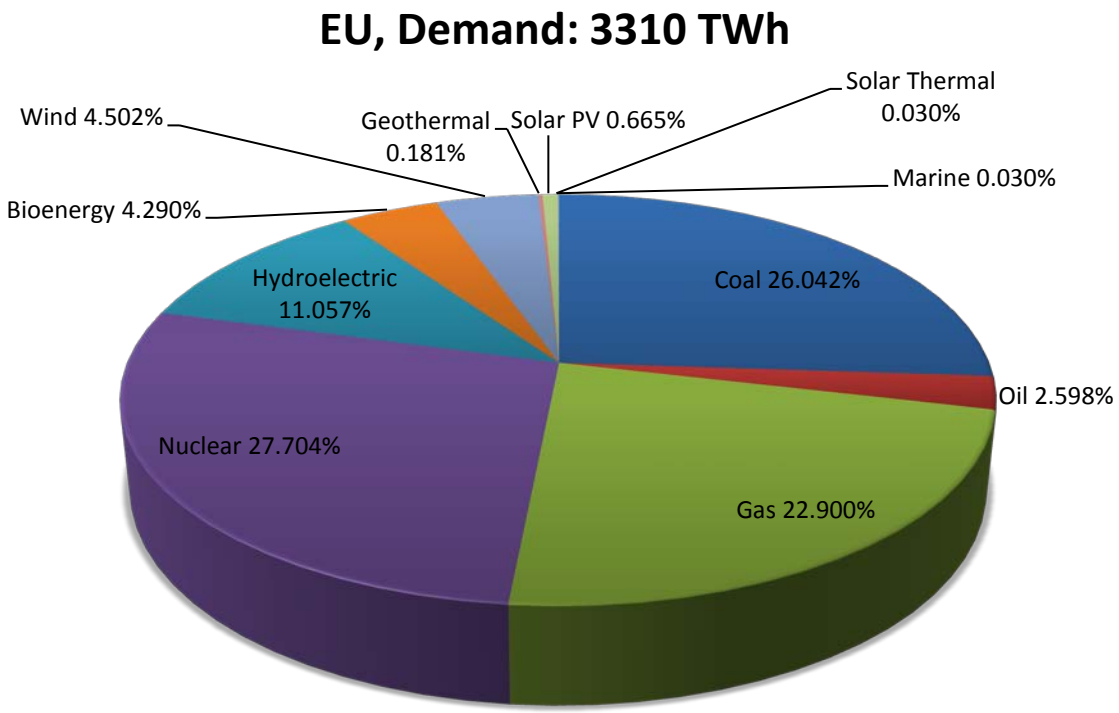

Figure 7: Energy demand in the European Union. Source: (International Energy Agency 2012)

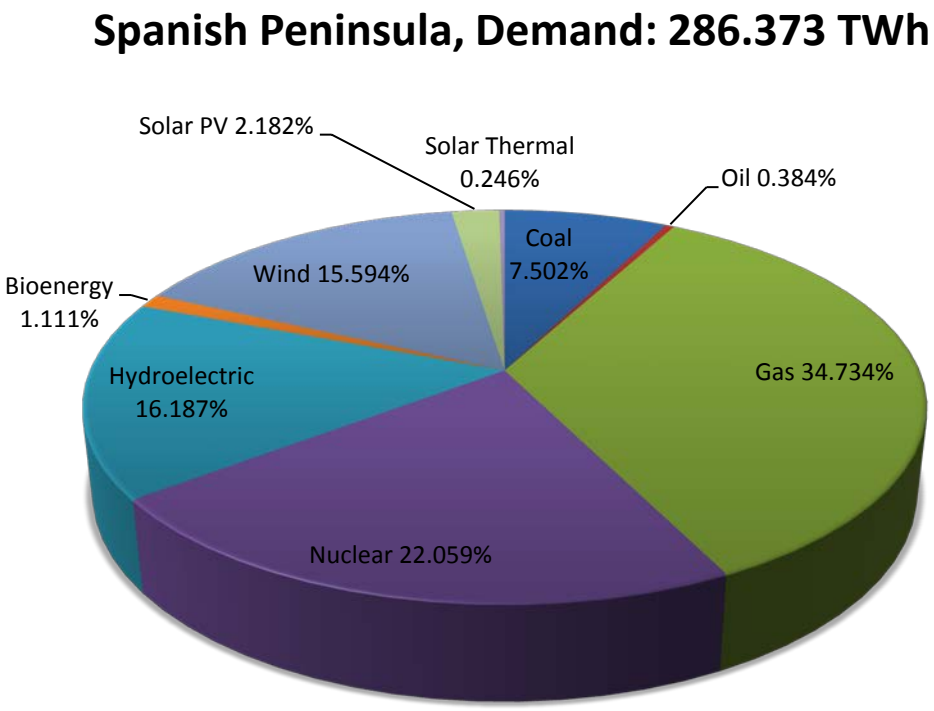

Figure 8: Energy demand in Spain. Source: (Ministerio de Industria, Energía y Turismo de España 2012)

In the New Policies Scenario defined by the *World Energy Outlook 2012* (International Energy Agency 2012), where both current energy commitments and the ones which have already been planned but not introduced are taken into account, the enormous growth from 2010 to 2035 in Solar Thermal Energy is mentioned, rising its electric installed production from 1.6TWh to 280TWh. In fact, it is highlighted that the majority of the new projects are planned to be fulfilled in the USA and Spain.

Apart from these many facts, there is a significant which makes solar energy an attractive field of study. By 2050 three fifths of electricity production will come from renewable energies, which will involve a 75% of CO_2 emissions in 1980. In 2050, with a normal growth rate, the total energy consumption would reach up to 835 EJ (United Nations Development Programme 2000). This is a small amount of energy compared to the 3.8million EJ of solar energy that visits the Earth each year (Johansson 1993).

1.1.6. Motivation

As already seen, solar energy is still a very immature technology which has the highest potential among the other alternatives to produce energy. This comes from the nature of its source, the Sun.

Apart from that, it is one of the cleanest energy source, very consistent and continuous in the time.

As far as the author knows, there has been no project such as this one at the University. The main new features in this project are the two-row receiver configuration, which improves the performance of the whole power plant, and the introduction of a reheating process, which also improves its performance.

Summing up these three facts, this project makes sense and it is very attractive and motivating to the author, who has put the best of him in its development in order to obtain a good research and to help as much as possible to progress of this energy, which seems to be the future in energy production.

1.2. Objectives

The main objectives of the present project explained as follows:

1. Creation of a simple a flexible model that helps to establish preliminary calculations for further research about the operation of a Direct Steam Generation, DSG, solar power plant. The DSG configuration generates steam directly in the receiver. This makes the plant to avoid the use of other kind of heat transfer fluid, HTF, such as oil or molten salts. Environmental and security risks appear when using HTF instead of steam. Apart from that, HTF need an intermediate exchanger because the power block is driven by a Rankine cycle which works with water. Two results come when not having this exchanger; lower investment and higher efficiency since this kind of exchanger have also its own heat losses.

2. Development of the necessary calculations to size and analyze a solar power plant with central receiver using a simple, fast and flexible method.

3. Analysis of the results of the calculations described in the previous point in order to help to understand and develop this type of technology.

4. Assessment of new designs of the receiver based on the addition of a second row of tubes, in order to improve the efficiency and profitability of solar energy as well as a more detailed field of heliostats distribution. These new designs aims to improve the net efficiency of the power plant and to decrease the number of heliostat needed.

5. Introduction of a reheating process in the power cycle of the power plant with the same aim of the previous point, the improvement of the efficiency of the whole plant decreasing the number of heliostats.

6. Setting of a starting point for further research that will be carried out by other students.

1.3. Methodology and stages of the project

During this section, an explanation of the steps taken in order to develop this project is given.

As in every type of project and research, the first step to take is to look for other projects and research done on the same field of study. In this case, one book, *Solar energy engineering: processes and systems* (Kalogirou 2009), and one paper among many others, *Simulation of an*

integrated steam generator for solar tower (Ben-Zvi, Epstein and Segal 2011), have been the base of the project. The work by Ben-zvi is a simulation of the behavior of the HTF in the receiver. Since it is a computer simulation, the range of study is limited due to cost calculations. Apart from those documents, the calculations have been based on two different bachelor thesis, *Diseño de una planta termosolar de receptor central con almacenamiento de sales fundidas,* (Joga López 2012) and *Diseño y análisis de una planta termosolar de torre central con configuraciones de único o doble receptor operando con sales fundidas,* (Heras Martín 2012).

The work by Ben-Zvi describes a two-row receiver. The receiver is compound of two rows of tubes where HTF passes through. The outer row serves as economizer and boiler while the inner row allows the superheating stage of the thermal cycle. This particular design has an opening sector at the outer row in order to collect more energy in the inner row in this section. For this project a similar design has been develop, which will be described in section 4.3.2.1. The main difference between this project and the work by Ben-Zvi is that calculation cost and its complexity is avoid along this report in order to give an easier, faster and more flexible calculations and designs.

Once the information is collected and selected and the state of the art is clear, the report of the present project is structured and developed as follows:

1. In Chapter 1, information is given about the real motivation that leads the author to work on this field, explaining both technological and economical present situations.

2. In Chapter 2 solar energy is presented in detail, giving descriptions of the parameters of planet Earth and the Sun that affect the performance and the application of this kind of energy.

3. During Chapter 3, the different solar energy technologies are explained as well as a rough notion of the advantages and drawbacks of these systems.

4. In Chapter 4 a model for the design of the power plant is presented. Firstly the thermal cycle is described, both for a regular Rankine cycle and for a reheating cycle. After that, the receiver is sized, following Ben-Zvi's paper, and divided into stages corresponding to the vapor, liquid water and mix of water phases. In order to characterize the solar radiation needed at the receiver, there is a description of the thermal losses which come from two different types of heat transfer modes, convection and radiation. Later, the load losses are presented in order to obtain the pumping power needed to run the cycle. With this, a procedure for calculating of the solar radiation value taken is given, which is needed for the design of the field of heliostats and the distribution of mirrors. Having the net power absorbed by the receiver and the efficiency of the Rankine cycle, the system is designed with a back-up of natural gas that allows continuous operation at the plant for months that have low solar radiation.

5. Consequently, Chapter 5 shows the results of the model described in Chapter 4 for a 50MW power plant. The location of the power plant is chosen to be Gibraleón, a little

town of the Spanish province of Huelva, in the south-east coast of the Iberian Peninsula.

6. Furthermore, an idea of the profitability of this project is given in Chapter 6 where an investment analysis is presented.

7. Before ending, Chapter 7 gives a clue of the environmental impact and, more important, how much CO_2 is saved to the atmosphere when producing electric energy with this power plant designed in this project.

8. Finally, Chapter 8 resumes the conclusions according to the results obtained through the whole project, analyzing them and giving future research paths stemming from this project.

Chapter 2 Solar Energy

2.1. Basics of Solar Energy

As is has been previously mentioned, the Sun, the star of the solar system where the Earth is found, is the main reason to explain the different sources of energy, both fossil and renewable energy ones. Its expected life is calculated as 5,000 million years. The 90% of the energy the Sun produces is estimated to be formed at a circumference of 0.23R, where R is the total Sun radius. The temperature at the core goes from 80 to 400 million Kelvin, while the atmosphere temperature at Earth goes from 270K to 350K. However, the outer layer of the Sun is at a temperature of 5,000K.

This high energy rate production has its origin in an exothermic nuclear fusion reaction. This reaction is given due to the plasma state of the Sun matter. It essentially contains H, Hydrogen, and He, Helium, apart from small portions of other elements. The reaction is the conversion of H into He through solar fusion. Being two different H protons, they combine to give a H double nuclei, which receives another H proton, giving a high exothermal reaction and He as products.

The annual total solar energy incident to Earth's surface is around 1.73×10^{14} kW, equal to 1.5×10^{18} kWh. This is equivalent to 1.9×10^{14} coal equivalent tons, cet, which exceeds the total annual energy consumption estimated at 10^{10} cet.

On top of all these facts, Earth must get an energy balance to preserve life on the planet. The Earth has to radiate to the sky the same amount of energy as the one received and absorbed from the Sun. If this balanced is not fulfilled, the average temperature of the planet tends to change. That is, If the radiation of the planet is higher than the energy absorbed from the Sun,

the temperature decreases and vice versa. This issue may remind the reader global warming, greenhouse effect and climate change.

2.2. Earth motion

There are several Earth movements in its orbital path around the Sun that definitely have influence on the amount of solar energy received on the planet and the temporal variations this has. The following ones, described in *Canon of Insolation and the Ice-Age Problem* (Milankovitch 1941), are the most important:

- The orbit is the rotational motion the Earth follows around the Sun with a cycle of one year. This path, having the Sun at its center, is not a circumference. It is an ellipse but with a low eccentricity. This means that the distance of the planet to the Sun is not the same along the entire cycle, which derives into variations along a year on the solar radiation received along a year both in the entire and in a specific area of the globe. That is why different seasons exist. The Earth receives more solar radiation when closer to the star, what happens around January 1.
- The tilt is the angle formed by the Earth's axis of rotation and the ecliptic plane. This plane contains the path of the Earth around the Sun. This movement accomplishes a cycle of 0.30º every 42,000 years, going back and forth from 21º15' to 21º45'. The larger the tilt is, the warmer the poles are due to the fact that they are longer exposed to solar radiation, and a larger difference can be found between summer and winter temperatures.
- The wobble or precession refers to the same movement that a spinning top makes when its axis of rotation is not vertical anymore. This movement not only affects the amount of solar radiation received by the earth, but also the distribution of this radiation on the different areas of the planet. A cycle of 23,000 years is got with this movement, giving climate changes every 100,000 years. The origin of wobbling on Earth is the tidal forces both from the Sun and the Moon.

These different movements are shown in Figure 9 for a better understanding.

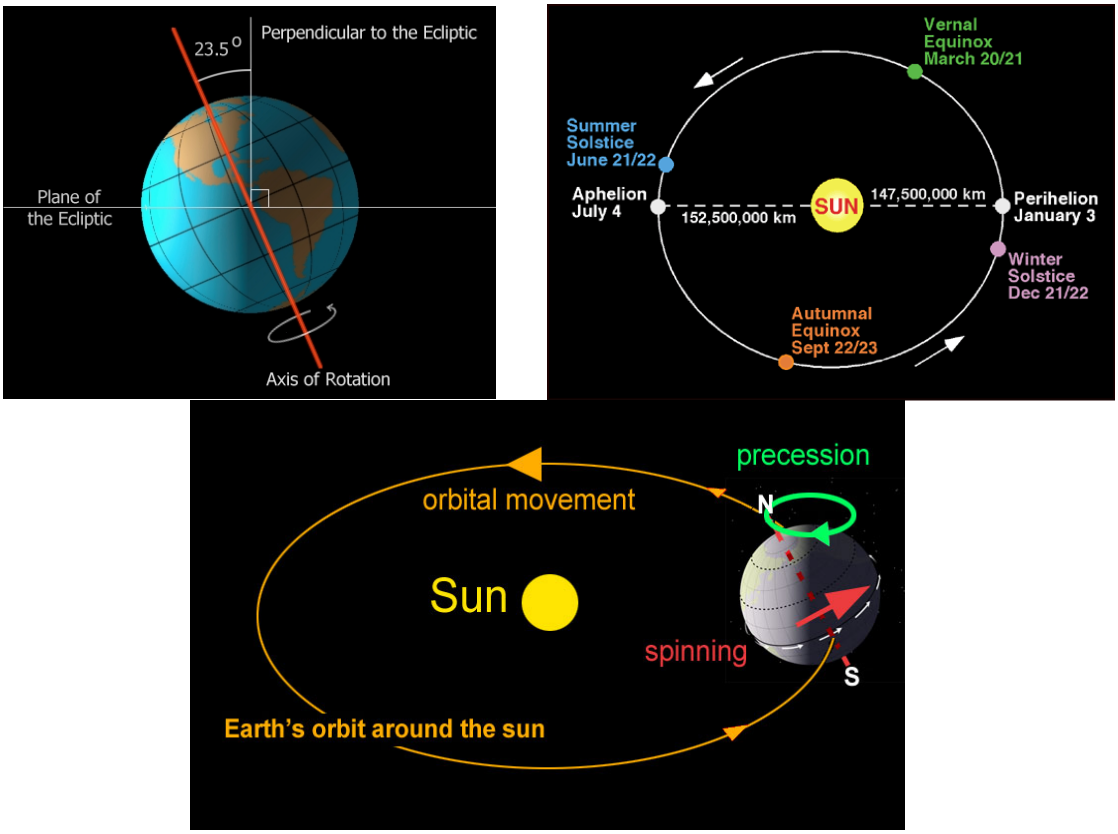

Figure 9: From left to right, from top to bottom; tilt angle, orbital movement and precession movement. Source: (World Mysteries 2011)

2.3. Factors

Taking into account the previous moevements, it has to be considered that solar energy systems are intermittent renewable energy sources. This intermittence comes from five main factors: day-light, clouds, topographical, latitude and astronomical effects (Şen 2004).

Day-light effects

It is basically the variation coming from the fact that a specific part of the globe does not receive solar radiation during the whole day due to day and night succession.

Cloud effects

As can be expected, clouds give shadow, which avoids solar radiation to get to the Earth. Direction, velocity, frequency and type, including size, transmissivity, and edge shape, of the clouds are the key-factors for designing solar energy systems (Favrat and Augsburger 2012).

Topographic effects

Among many others, the most important effects come from the type of surface. It is not the same to be in a forest, since its reflectivity is low, than in a desert or in an area covered by

snow. Furthermore, solar elevation and the geometry of the surface relative to the Sun affect the way solar energy approaches the ground.

Latitude effects

The albedo is the ratio between reflected solar energy and incident solar energy measured above the atmosphere. At latitudes less than 30º the albedo is relatively constant and at latitudes between 40ºN and 40ºS there is an excess in solar absorption. This fact gives a heat transfer from low latitudes to high latitudes giving atmospheric circulations. It can be observed in the Figure 10 that, integrating the difference between absorbed and emitted solar radiation, the maximum heat transfer happens in latitude between 30º and 40º.

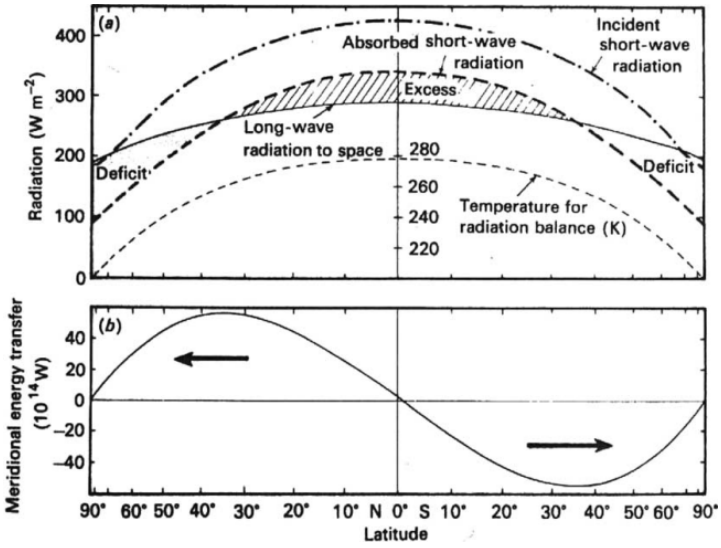

Figure 10: Latitude effect to Solar radiation. Source: (Şen 2004)

Astronomical effects

As already explained in section 2.2, since the Earth follows an elliptical path around the Sun, it is not at the same distance from the star during its trajectory, which mixed with fact that the Earth turns around a non-vertical axis on itself, gives different seasons during a year.

2.4. Position of the Sun from an Earth's perspective

Being on the Earth's surface, the Sun describes a movement along the day which varies depending on the point of the year the observer is at. The position of the star along its movement can be described at any time of the day from any position of the planet. To fulfill this purpose, 5 different angles may be used, as it can be observed in Figure 11:

1. Declination, δ, formed by the Earth-Sun line and the Equatorial plane. This angle changes with date and does not depend on the location of the observer. Its range varies from 23º45' on the north hemisphere summer solstice to -23º45' on the north hemisphere

winter solstice, passing through 0º at the equinoxes. It is defined by the following equation where D is the day of the year, being January 1st N=1 and December 31st N=365.

$$\delta = 23.45 \sin\left[\frac{360(284 + D)}{365}\right] \quad (2.1)$$

2. Hour angle, ω, which is the angle that the Earth rotates in a day, is defined as positive when having passed the meridian plane, or better said, west of the meridian plane. It is negative when east of the meridian plane, and means the angular distance to the solar noon. Being h the current solar hour, it is expressed as:

$$\omega = 15(12 - h) \quad (2.2)$$

3. Altitude or solar elevation, α, is the angle described by the observer-Sun line and the horizon. Due to declination angle, altitude varies along the year. It follows the equation below:

$$\sin(\alpha) = \sin(L) \cdot \sin(\delta) + \cos(L) \cdot \cos(\delta) \cdot \cos(w) \quad (2.3)$$

4. Zenith angle, θ_z, is the complementary angle of the altitude, with respect to the vertical axis.

$$\theta_z = 90º - \alpha \quad (2.4)$$

5. Azimuth angle, ψ, is formed by north direction and the projection of the line observer-Sun on the earth surface. Its sign follows the same rule as the hour angle.

$$\sin(\psi) = \frac{\sin(\omega) \cdot \cos(\delta)}{\cos(\alpha)} \quad (2.5)$$

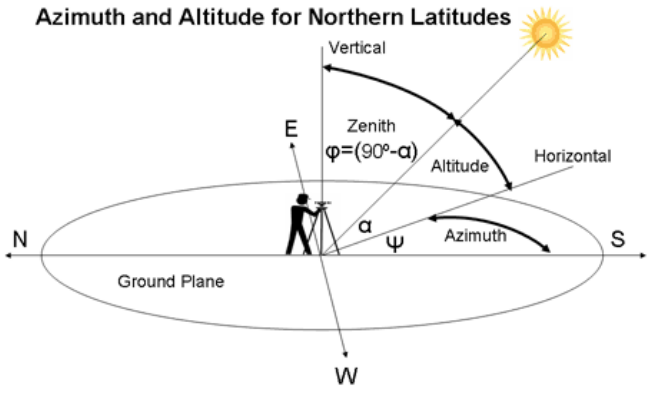

Figure 11: Zenith, Solar altitude and Azimuth angles. Source: (Woodbank Communications Ltd 2005)

Chapter 3 Solar Energy Systems

With the figures presented in Chapter 1, it is reasonable to think that solar energy is a good strategy to take up in order to meet the energy requirements in our society. Already in ancient times, solar energy was one of the main sources of energy available. In prehistoric times, it is known that food was dried by Sun in order to be preserved. But the biggest application, although it has been fought to be a myth by many modern scientists, was the one from Archimedes (287-212 BC). This great physicist designed a series of mirrors which concentrated solar energy in order to protect the city of Syracuse by burning ships approaching the coast. Centuries later, the French chemist Lavoisier built a furnace with mirrors reaching over 1000ºC of temperature. These two big developments show that the main way to use solar energy is by concentrating it at a point or series of them in order to reach high temperatures.

This is the key factor of the four main technologies that exist nowadays in the production of electricity from solar energy: parabolic-trough, parabolic-dish, Fresnel and central-receiver.

These four systems use the same general idea. This idea is based on four basic devices, collector, receiver, transport-storage, and power conversion. This process is shown in Figure 12.

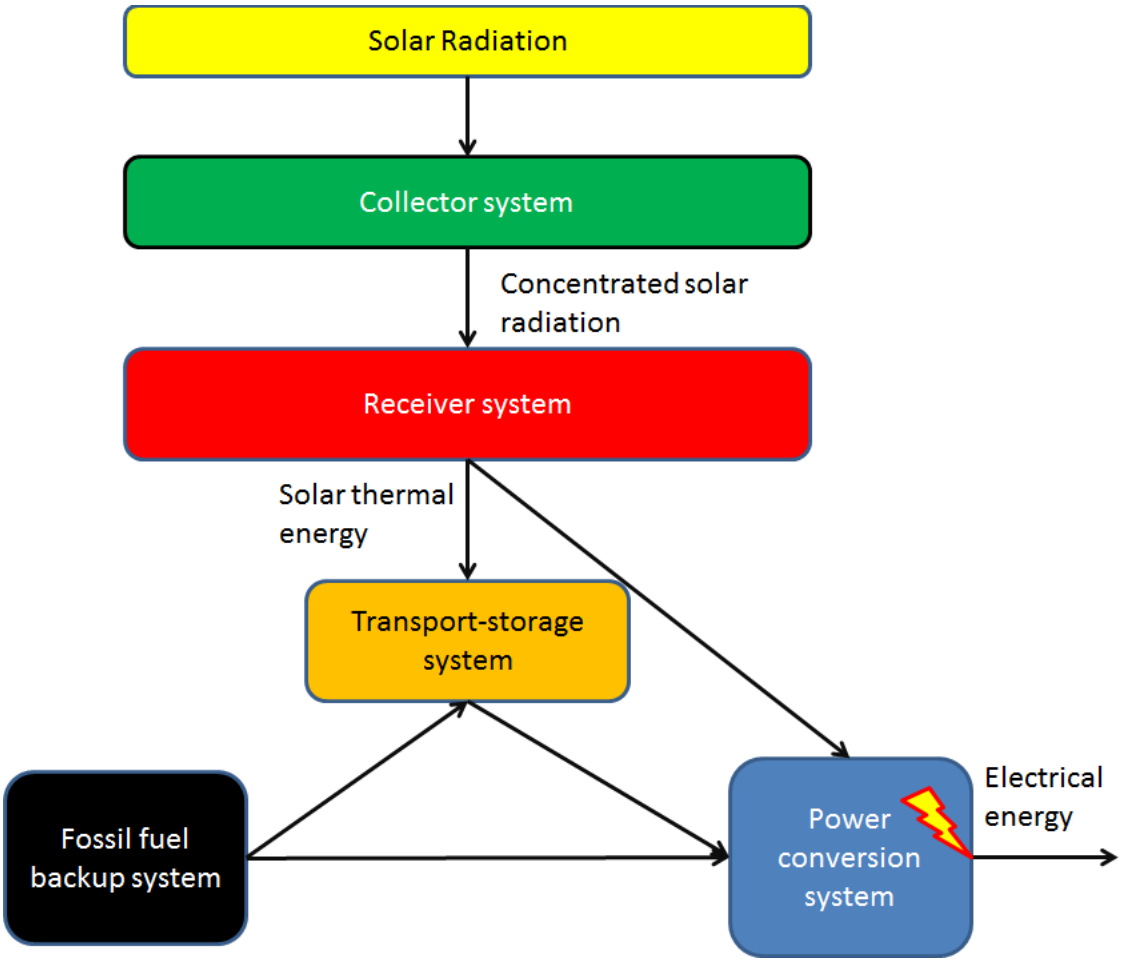

Figure 12: General Solar system Diagram. Source: Compiled by author

This flow of energy consists on concentrating the solar radiation with sun-tracking mirrors, or lens in Fresnel systems, on a receiver. At the receiver, a heat transfer fluid, from now on HTF, passes through tubes. These tubes receive the solar radiation, which rises the temperature. At the same time the tubes rise the HTF temperature. After this, whether the plants works with direct or indirect steam, the energy is delivered through a storage-transport system into a turbine that is driven by vapor. In case of indirect steam generation, the HTF may be oil or nitrate salts, which heats up and evaporates water at a thermal exchanger. Finally, the turbine is linked to a power generator which transforms thermal energy into electrical energy, providing electricity to the grid. In some plants there is a secondary system which works with fossil fuels, in order to deliver energy during low sunlight periods such as cloudy days.

3.1. Parabolic-trough systems

A parabolic-trough system consists in a linear solar collector with parabolic-form mirrors. These mirrors concentrate Sunrays in a pipe that passes by the focal line of the parabola formed by the mirrors, as it is observed in Figure 13. The HTF flows along black metal tubes heating up and being transported to a central point.

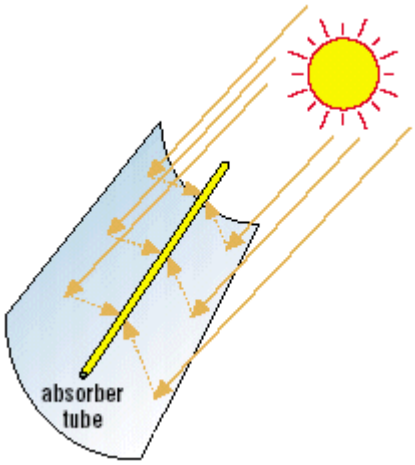

Figure 13: Parabolic-trough collector. Source: (Volker Quaschning 2003)

Due to the geometry of the parabola, these kind of collectors need almost no collector adjustment along the day due to Sun's trajectory. However, it has big losses during both sunrise and sunset due to large incident angles. Furthermore, the metal pipes are covered with glass tubes which avoid heat losses. Nonetheless, the glass adds transmittance losses, which get worse when tey are dirty.

The size of the tubes depends on the concentration ratio. This concentraton ratio, at the same time depends on the tolerances allowed in the mirrors. The concentration ratio comes in a range from 10 to 100, which is significantly lower to the central-receiver ratio. It operates at a temperature range from 100 to 400ºC. In contrast, it is the best developed technology.

Figure 14 shows a real parabolic-trough system and it can be observed how big they are.

Figure 14: Real parabolic-trough power plant. Source: (BVA Media Group 2012)

Parabolic-trough systems used to be coupled to a thermal storage device. One of the designs of these storage systems is a tank with a high specific heat coefficient fluid like molten salts, or change-phase fluids like paraffin or metals. It usually consists of two tanks, one at high temperature and another one at medium temperature. They are used at low solar radiation periods in order to help the HTF to get the appropriate energy.

Small Solar Power Systems Project/Distributed Collector System (SPSS/DCS) was constructed in Tabernas, Spain, in 1981 by the International Energy Agency. It was a pilot plant but it provided good information for the development of design and performance of parabolic trough, thermal-storage systems and power blocks. Moreover, the first two commercial projects were built in Dagget, California, and were called SEGS I and II with 14MW and 30MW in 1984 and 1985 respectively. The main difference of the second plant is that introduced a natural gas-fired boiler.

In Spain, this system is the most used one. In this country, 40 plants over 45 use this type of technology. All of them count with 50MW of power although their annual production depends much on the radiation obtained and whether they count with a storage system or not. All of them are installed in the southern half of the Iberian Peninsula, with only one in the north that is hybridized with a biomass system.

3.2. Fresnel systems

There are two main Fresnel systems. The first one is the Fresnel lens collector. It consists on lenses which are made of plastic and track solar rays into a point receiver, as it is shown in Figure 15.

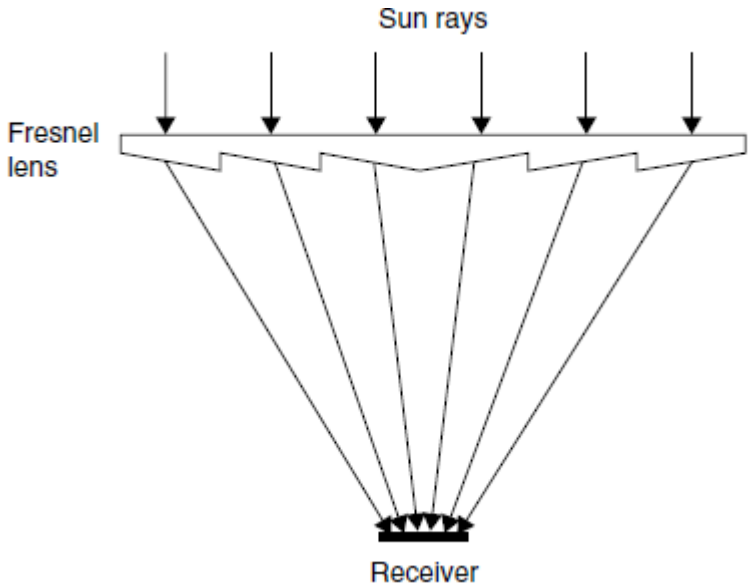

Figure 15: Fresnel lens collector. Source: (Kalogirou 2009)

The second one is the linear Fresnel reflector, Figure 16. This kind of system works as the parabolic-trough systems but with flat mirrors. This makes the construction of the collectors cheaper. The flat reflectors are positioned as arrays of linear mirrors strips, which form a curved form due to the different inclination of each mirror. The solar radiation is concentrated in a linear receiver.

Figure 16: Real linear Fresnel reflectors. Source: (Novatec Solar 2012)

The problem of this system is the shadow that each mirror project to adjacent mirrors. This can be solved separating the reflectors and/or constructing higher receiver. However, this increases the price of the structures of the receivers. Furthermore, another solution has been developed recently as shown in Figure 17. It is called Compact linear Fresnel Reflector and it consists on interleaved adjacent reflectors. Since several receivers can be installed in a field of mirrors, they can be placed closely. This fact makes that the mirrors are close enough to at least two different receivers. Thereby, it gives each mirror the possibility to track solar radiation to the receiver in which its reflection can be better absorbed.

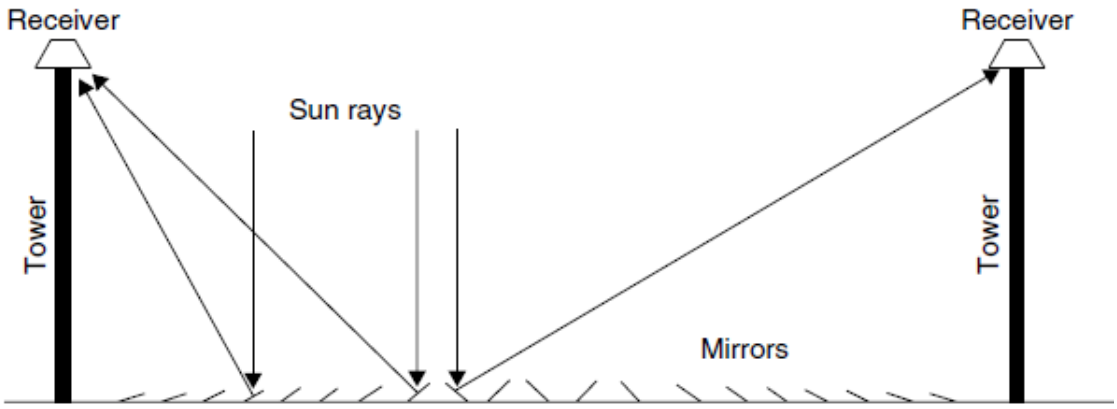

Figure 17: Interleaved linear Fresnel lens distribution. Source: (Kalogirou 2009)

It is important to highlight that even when this system is quite exotic for solar thermal energy, Spain counts with two Fresnel based solar power plants. These plants are located at the Spanish province of Murcia, called Puerto Errado I and II, with 1.4 and 30 MW of power respectively.

3.3. Parabolic-dish systems

This system concentrates rays in a solar receiver which is located at the focal point of the dish, Figure 18. This operation heats up a fluid that can be introduced directly to an engine-generator to give electrical energy or may be transported to a central power-conversion system. The concentration ratio varies from 600 to 3000, being the highest of the three compared systems. Moreover, this system may achieve 1500ºC. The problem comes when designing the piping systems in order to reduce losses. It also has the disadvantage of no possibility of storage.

Figure 18: Real Parabolic-dish system. Source: (Xah Lee 2011)

Another great advantage of this system is that they are the most efficient since they are always pointing to the sun. This fact implies that the structure must have a device which allows the collector to move in two directions, north-south and east-west.
However, they are separate units which does not depend one on another. This makes them to be independent and work almost continuously even in maintenance periods. A diagram of this system is observed in Figure 19.

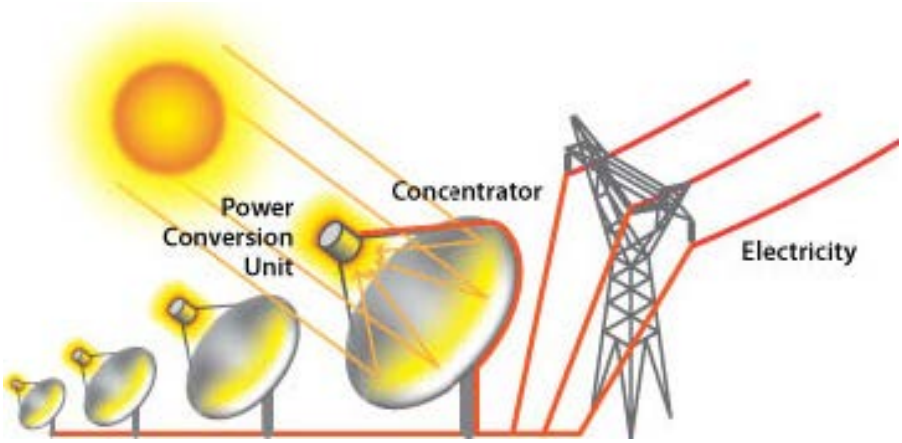

Figure 19: Parabolic-dish diagram. Source: (Solar Energy Topics 2012)

In Spain, although there are no power plants of this type already installed across the country, there are 3 projects to be developed in Ciudad Real with around 10MW of power.

3.4. Central-receiver systems.

This last system consists of a field of Sun-tracking mirrors, or so-called heliostats, which reflect solar energy. The solar energy is concentrated at a receiver mounted at the top of a tower in

the center of the field, Figure 21. The heliostats can be flat mirrors or slightly concave mirrors, giving both high temperatures and pressures. The absorbed energy is transferred to a circulating fluid which can be stored for later use, or directly piped to a turbine in order to generate electricity.

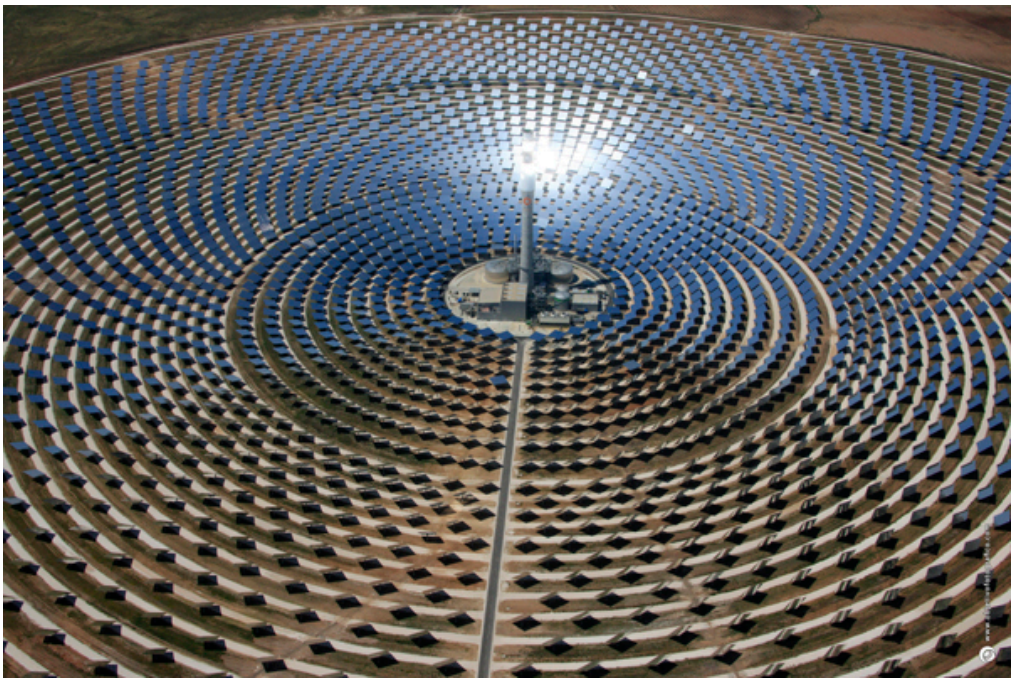

Figure 20: Gemasolar Central-receiver system in Seville. Source: (Torresol Energy 2010)

Some key factors are:

- They can collect solar energy and transfer it to a single receiver which minimizes thermal losses.
- They achieve concentration ratios in a range of 300 to 1500.
- They can efficiently store thermal energy.
- They are usually large, more than 10MW, which benefits from economies of scale.

Each heliostat has from 50 to 150 m^2 of reflective surface. There are three main configurations for the field of heliostats. The first one places the heliostats surrounding completely the tower. In the second one the heliostats are place at the north side (in the northern hemisphere) of the receiver tower with an enclosed heat-transfer surface. The third one is similar to the second one but with a receiver which has a north-facing heat-transfer surface.

The receiver is placed at a tower of at least 100m high. It is formed by several tubes which contains the HTF. This HTF can be water, which is delivered directly to the turbine, or molten salts, which will need a heat exchanger.

Molten salts counts with some disadvantages. These are the need of continuous heat delivered since the its solidification is quite dangerous due to oxidation processed and the own damage of the salt. Apart from that, the molten salts are more expensive than the water.

These systems usually have a natural gas boiler coupled for low sunlight periods.

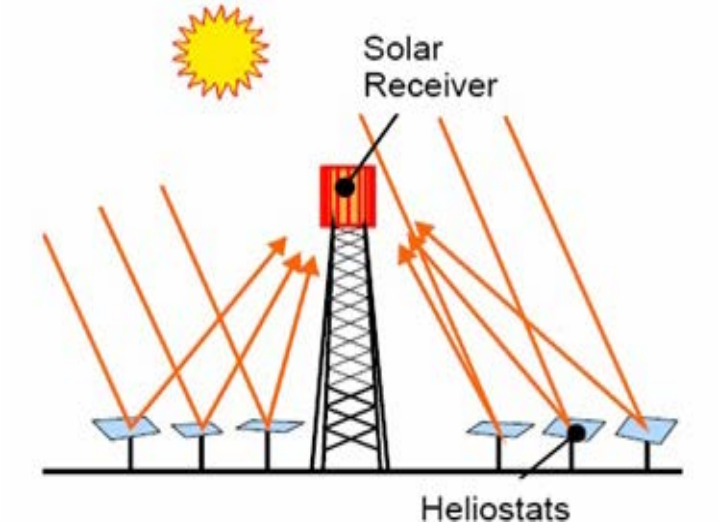

Figure 21: Central-receiver system diagram. Source: (Alexopoulos and Hoffschmidt 2010)

The first central-receiver plant was connected to the grid in 1981 in Adrano, Sicily, Italy, with 1MW of electric power. It was named Eurelios and sponsored by the Commission of the European Communities. Its aimed was to prove that solar power plants could be connected directly to the grid. One year later, Solar One, located in Southern California was constructed. The Department of Energy of the USA, Southern California Edison, Los Angeles Department of Water and Power and the California Energy Commission jointed in a venture in order to build a power plant where they could develop the technology. With 10MW of electric power it was shut down after 6 years. In 1984, in Tabernas, Spain, was constructed another 1MW power plant sponsored by the Spanish Ministry of Industry and Energy, with the prime aim of testing the plant feasibility.

According to *Localización de centrales solares termoeléctricas en España* (Protermosolar 2013), there are 3 power plants across the Iberian Peninsula in Spain, two with DSG technology and another one with nitrate salt as HTF. The three of them are located in Seville and are called PS10, PS20 and Gemasolar, Figure 20, with 10, 20 and 20 MW of power generation respectively. The PS10 commercial power plant has the honor to be the first power plant of this type installed in Europe.

3.5. Spain

In 1997, the European Union, EU, reported the White Paper, in which consumption control and energy efficiency together with renewable resources, RES, defined and promoted a new frame for energy in the old continent. In the Directive 2001/77/EC, Member States were required to regulate and reduce barriers for electricity production with RES as well as to set national targets. The Directive 2009/28/EC aimed targets for the EU Countries and established the requirements to adopt national renewable energy action plans, NREAP, in order to meet the objectives. A total average of 20% share of RES was required by the end of 2020, for the EU as

a whole. The final target for each country varied according to their initial levels and their potential.

In this frame, Spain plays a major role in the EU. This importance can be highlighted by the comparison of the targets applied to Spain and Germany. By the end of 2005, their initial levels of RES share were 8.5% and 5.8%, respectively, and their goals for 2020 are 20% and 18%. These data were set for the overall use of RES. However, national plans were broken apart by sector: electricity, RES-E, heating and cooling and transportation. Finally, the Spanish NREAP targeted an overall RES share of 22.7% and a RES-E share of 37.5%.

All these values lead to the point in which RES are about to be the main pillar of the economy regarding energy production and consumption. Altogether, state of the art, solar energy sytems and solar energy description will guide the present study.

Chapter 4 Designing Method

4.1. Thermal Cycle

The very first step of this project is the election of the variables in the vapor cycle. To begin with, it has to be chosen an electric power to be given by the whole plant. In this case a Rankine cycle is going to be the base of the development.

Due to the objectives of the present project, two different designs are going to be taken into account. The first one consists on a regular Rankine cycle, while the second one consists on a Rankine cycle with reheat, dividing the turbine into two smaller ones, one at higher pressure and another one at a lower pressure.

4.1.1. First design, regular Rankine cycle

A regular Rankine cycle consists on a boiler, which in a solar power plant is the receiver, a condenser, a turbine and a pump. The temperature at points 1 and 4 in Figure 22, which are the entrance and the exit of the condenser, are determined by the ambient temperature of the chosen location. Both in the boiler and the condenser, the pressure does not change in the processes that happen in them. According to bibliography (Kalogirou 2009), ordinary values for the pressure, both in the boiler and in the condenser, are 60bar and 0.1bar, respectively.

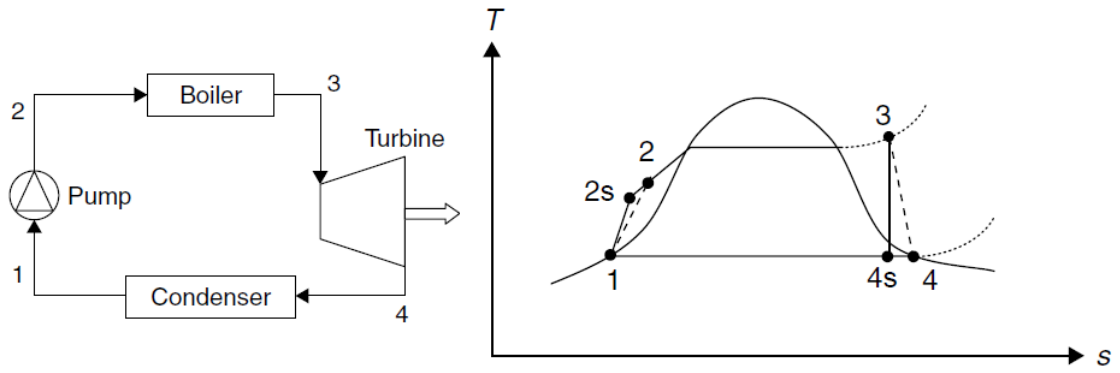

Figure 22: Regular Rankine cycle diagram. Source: (Kalogirou 2009)

In order to ensure the integrity of the turbine blades, the fraction of water drops in the vapor must be lower than 10%.

Next step is to fix a value for the maximum temperature which is achieved at point 3. The main restriction for this temperature is the maximum temperature that the tubes of the boiler can achieve without damaging its properties.

The cycle starts at point 1. This point is the entry to the pump and the exit of the condenser. The fluid is saturated water at this stage. When it enters the pump, it suffers an isentropic compression to the pressure at which the fluid has to boil. However, due to inefficiencies in the operation of mechanical components, the pump usually gives a 85% of overall yield. With this value the next step is to get point 2. The properties of this point can be achieved with equation (4.1), where h_1 and h_2 are the HTF enthalpies at points 1 and 2 of the cycle, v is the specific volume of the HTF at the condenser, P_{boiler} and $P_{condenser}$ are the pressure values for each device and η_{pump} is the pump efficiency.

$$h_2 = h_1 + \frac{v \cdot (P_{boiler} - P_{condenser})}{\eta_{pump}} \qquad (4.1)$$

All the values of equation (4.1) are known but the specific volume. This will be chosen as the specific volume at temperature and pressure of the condenser.

After the compression at the pump, the following element is the boiler where the water evaporates and gets the maximum temperature already fixed. Since maximum temperature and boiler pressure have been already prompt, it is needed to find the properties of the saturated steam at point 3. The needed properties are the entropy and enthalpy of the steam. Apart from this, the entropy and enthalpy of the vapor and liquid are needed at the conditions of the condenser.

Then, having these properties it is time to calculate point 4, the exit of the turbine and entrance of the condenser. This point comes from an isentropic expansion at the turbine. Unfortunately, this does not happen in real life since turbine efficiency is lower than 1. Consequently, the first thing to do is to get the vapor fraction of point 4s, X_{4s}, the exit of the turbine for the ideal Rankine cycle with isentropic expansion. This is achieved with equation

(4.2). In this equation, it can be found entropies of saturated water and steam at condenser pressure, s_l and s_v, and the entropy of point 3, s_3.

$$\chi_{4s} = \frac{s_3 - s_l}{s_v - s_v} \tag{4.2}$$

Consequently, enthalpy value for point 4s, h_{4s}, in the ideal Rankine cycle, can be achieved. The overall yield of the turbine is estimated at 0.85, datum needed to calculate the real enthalpy at point 4, h_4, in equation (4.4). In equation (4.3) the enthalpies of saturated water and saturated steam, h_l and h_v, are given data, as well as the enthalpy at the entrance of the turbine, h_3.

$$h_{4s} = (1 - \chi_{4s})h_l + \chi_{4s}h_v \tag{4.3}$$

$$h_4 = h_3 - \eta_{turbine}(h_3 - h_{4s}) \tag{4.4}$$

As has been explained before, the fluid at the exit of the turbine must have a vapor quality higher than 90%. Therefore, next step to take is to calculate the vapor quality at point 4, X_4. If this is not accomplished, iteration would be needed rising boiling pressure until this condition is fulfilled.

$$\chi_4 = \frac{h_4 - h_l}{h_v - h_l} \tag{4.5}$$

Once the Rankine cycle of the present design is completely defined the yield of the entire cycle can be obtained, η_t. In a Rankine cycle like the one already described, there are two energy inputs and one energy output. The energy extracted from the turbine is the output of the energy plant, while the energy to pressurize the fluid at the pump and the heat needed at the boiler to evaporate and rise the temperature of the fluid up are the energy inputs of the thermal cycle. This is shown in equation (4.6) where W_{cycle} is the net power and Q_{cycle} is the heat introduced to the system.

$$\eta_t = \frac{W_{cycle}}{Q_{cycle}} = \frac{(h_3 - h_4) - (h_2 - h_1)}{h_3 - h_2} \tag{4.6}$$

$$P_{thermal\ cyle} = \frac{P_{central}}{\eta_{total}} \tag{4.7}$$

For the design of the present project, an output power of **50MW** has been fixed. Using this value and the performance of the thermal cycle, the thermal power needed, $P_{thermal\ cycle}$, can be obtained with equation (4.7). However, if electrical and mechanical inefficiencies are taken into account, the thermal efficiency decreases around 1%. Thereby, the overall performance of the cycle comes from the product of the thermal, electrical and mechanical efficiencies, described in equation (4.8).

$$\eta_{total} = \eta_t \cdot \eta_{mec} \cdot \eta_{elec} \qquad (4.8)$$

Once the thermal power of the cycle is obtained, the mass flow of water can be calculated for this plant as it can be seen at equation (4.9), where ΔT_{eco} and ΔT_{sh} are the temperature differences between the inlet and the outlet of each stage. Specific heat capacities of the HTF have been used for this purposed instead of enthalpy differences in order to be able to use temperature differences. These specific heat capacities, $C_{p,eco}$ and $C_{p,sh}$, are taken as the average of the whole stage the belong to. Of course, enthalpy differences for each stage could have been used as well.

$$\dot{m} = \frac{P_{thermal\ cycle}}{(Cp,eco \cdot \Delta T_{eco} + L_{boil} + Cp,sh \cdot \Delta T_{sh})} \qquad (4.9)$$

4.1.2. Second design, Rankine cycle with reheat

In this second design, a second turbine at lower pressure is installed. The cycle works as the first design but with an important difference. The steam that enters the first turbine is depressurized until a medium pressure. And this medium pressure the steam follows a reflow, going back to the boiler, which is a receiver in this case. In the receiver is reheated until a high temperature which is depressurized again until the pressure at which the condensation takes place.

It is important to highlight that this design needs an iteration process since the temperature of point 5 is obtained during the following sections for the two-row design without opening sector. Firstly, a value will be given to this variable, which will be compared and modify in order to get to a close value at the beginning and at the end of the iteration. Meanwhile, in the design with a two-row receiver with an opening sector the temperature at point five is fixed to be the same as temperature at point 3.

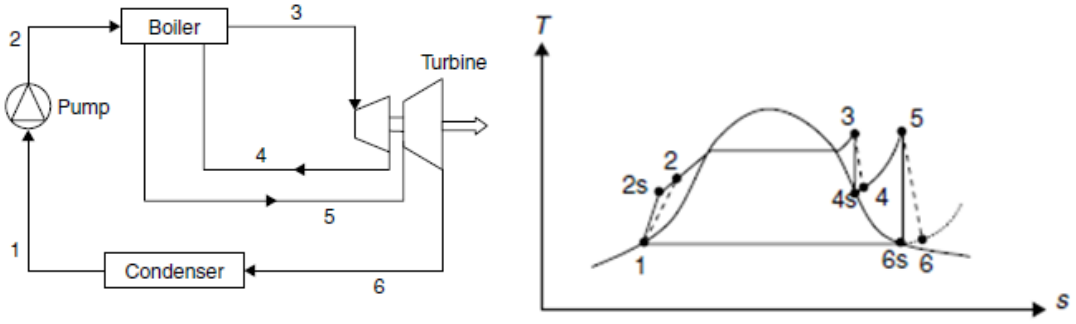

Figure 23: Reheating Rankine cycle. Source: (Kalogirou 2009)

Both the cycle and the diagram of the described design are shown in Figure 23: Reheating Rankine cycle. In order to describe point 4, this time is a little bit different. This difference is based on the fact that the isentropic enthalpy is chosen at the point where the expansion coincides with the line of saturated steam. As in the first design, the efficiency of the turbines is 85%. With these conditions, equation (4.10) gives the real enthalpy value for point 4.

$$h_4 = h_3 - \eta_{turbine}(h_3 - h_{4s}) \quad (4.10)$$

Furthermore, once the pressure at the outlet of the first turbine is reached, point 5 can be obtained as the intersection of the given pressure and the temperature described in the previous paragraph. Finally point 6 is similarly obtained as point 4 in the first design. It is shown at equation (4.13). In equation (4.11), entropies of saturated water and saturated steam are used, s_l and s_v.

$$\chi_{6s} = \frac{s_6 - s_l}{s_v - s_v} \quad (4.11)$$

Consequently, enthalpy value for point 6s, in the ideal Rankine cycle, can be achieved. The overall yield of the turbine is estimated at 0.85, datum needed for the previous purpose. In equation (4.12) the enthalpies of saturated water and saturated steam, h_l and h_v, are given data.

$$h_{6s} = (1 - \chi_{6s})h_l + \chi_{6s}h_v \quad (4.12)$$

$$h_6 = h_5 - \eta_{turbine}(h_5 - h_{6s}) \quad (4.13)$$

As has been explained before, the fluid at the exit of the turbine must have a vapor quality higher than 90%. Therefore, next step to take is to calculate the vapor quality at point 6. If this is not accomplished, iteration would be needed rising boiling pressure until this condition is fulfilled.

$$\chi_6 = \frac{h_6 - h_l}{h_v - h_l} \quad (4.14)$$

This kind of design does not imply the performance of the cycle. However, it makes the installation to need less quantity of HTF. The calculation of the mass flow rate of HTF follows equation (4.15). Furthermore, it avoids the increase of water droplets at the outlet of the first turbine, which can damage this device.

$$\dot{m} = \frac{P_{thermal\ cycle}}{(Cp_{eco} \cdot \Delta T_{eco} + L_{boil} + Cp_{sh1} \cdot \Delta T_{sh1} + Cp_{sh2} \cdot \Delta T_{sh2})} \quad (4.15)$$

For this design, the equation for the cycle efficiency is slightly different, since there are two heater stages as well as two expansion stages.

$$\eta_t = \frac{W_{cycle}}{Q_{cycle}} = \frac{(h_3 - h_4) + (h_5 - h_6) - (h_2 - h_1)}{(h_3 - h_2) + (h_5 - h_4)} \quad (4.16)$$

Nevertheless, this option needs a different design at the receiver, which will be described at section 4.3.2.2.

4.2. Design of the Receiver Geometry

As already developed in section 3.1.4, the receiver is the part of the plant where sun rays are concentrated in order to get the necessary energy to evaporate and heat up the transfer fluid, which in this case is water.

Based on *Simulation of an integrated steam generator for solar tower* (Ben-Zvi, Epstein and Segal 2011), the number of tubes is fixed with the same value as that project. The number of panels in this kind of receiver oscillates from 8 to 15 panels. In this project 12 panels are going to be chosen. The number of tubes is going to be fixed at 1512 tubes. Ben-Zvi fixes this number at 1506 tubes, but the number of tubes needs to be multiple of the number of panels. These tubes are ¾" diameter, schedule 80 pipes, which have an internal diameter of 0.754 inches, 1.88 cm, and an external diameter of 1.05 inches, 2.67cm. The receiver is rectangular form, 12m high and 16m of diameter. To pass from one panel to another, the HTF must pass through a collector. These collectors have been designed to have a diameter of 38 cm.

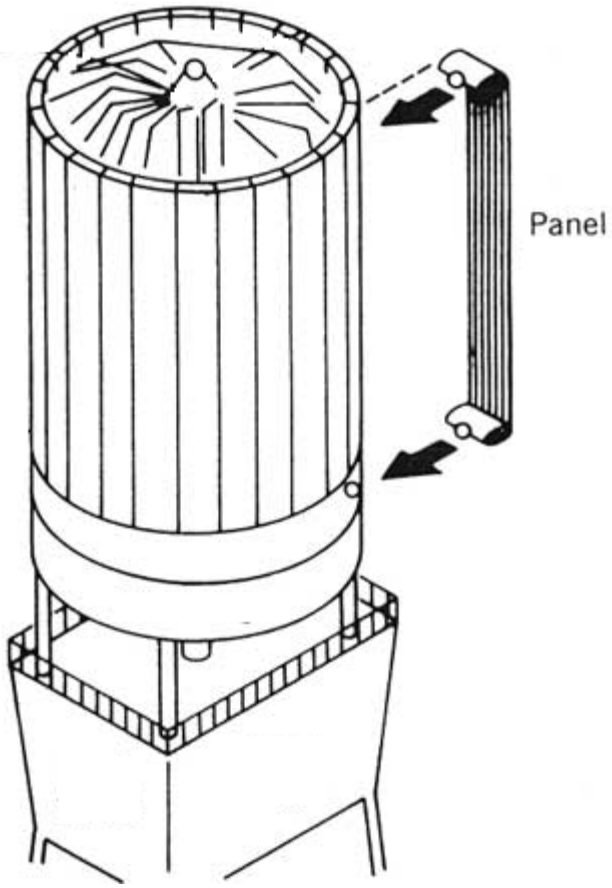

Figure 24: Receiver for one-row design. Source: (Johansson 1993)

In this project a comparison is going to be done from the very beginning. This means, from the design of one-row, passing through the addition of a second row with reheat, converting it to Ben-Zvi's design where a regular Rankine cycle has a two-row receiver with an opening sector, and finally the last described receiver with a reheating cycle.

Comparing to a solar power plant with salt as HTF, a plant like this one, with water must follow a different model due to phase change. As it can be observed in 4.1.1, the water goes into three different situations when passing through the receiver or boiler.

Firstly the fluid is a saturated liquid which heats up until the temperature at which starts to boil. During this stage the receiver behaves like an economizer. However, from the first bubble to the last drop of water, the receiver works as a boiler. Finally, when having only vapor as HTF, the receiver is expected to make transform the fluid into superheated vapor. These stages can be seen clearly illustrated at Figure 25.

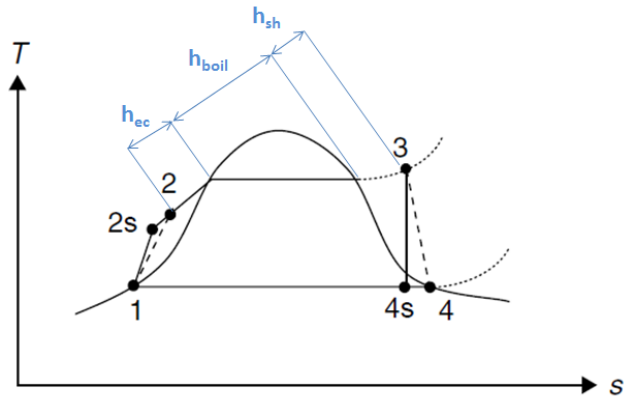

Figure 25: Distribution of boiler stages over the cycle

In order to divide the receiver into the previously described stages, the enthalpies at the main points of the stages are going to be used. Better to say, what is going to be assigned to each situations are the panels. Having the total enthalpy in the whole process, each stage gives to this total a portion. That is the fact that will be used to distribute the stages along the tube length. It has to be observed that the HTF is divided into two flows ate the entrance of the receiver. That means the tower behaves as a symmetric device. This is shown at Figure 26.

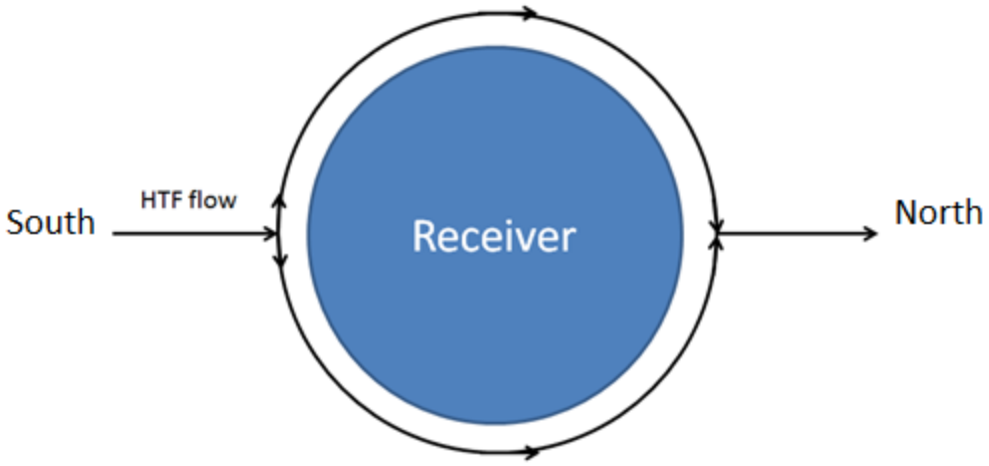

Figure 26: HTF path through the receiver

$$N_{panels,ec} = \frac{h_{ec}}{h_{ec} + h_{boil} + h_{sh}} N_{panels}$$

$$N_{panels,boil} = \frac{h_{boil}}{h_{ec} + h_{boil} + h_{sh}} N_{panels} \quad (4.17)$$

$$N_{panels,sh} = \frac{h_{sh}}{h_{ec} + h_{boil} + h_{sh}} N_{panels}$$

Having this distribution it can be calculated the length in which each stage dominates the process. First, the total length that a particle of fluid experience during its way along the receiver must be calculated. This can be obtained using both the number of panels and the length of tubes. Afterwards, having the number of panels of each stage of the boiler and this total length, the prime aim can be achieved.

$$L_{total} = N_{panels} \cdot L_{tubes} \quad (4.18)$$

$$L_{ec} = L_{total} \cdot \frac{N_{panels,ec}}{N_{panels}}$$

$$L_{boil} = L_{total} \cdot \frac{N_{panels,boil}}{N_{panels}} \quad (4.19)$$

$$L_{sh} = L_{total} \cdot \frac{N_{panels,sh}}{N_{panels}}$$

Therefore, it may happen that two of the tubes share stages. This means that one of the tubes will have a stage of economizer and a stage of boiler, and another tube will have a stage of boiler and a stage of superheater. Once the stages are perfectly located along the tubes, it is easier to establish properties for the HTF in the panels and the heat transfer correlations that should be used, due to the this helps to establish the difference of temperature between the inlet and outlet of each panel in the economizer and the superheater.

Consequently the problem faces a new aim, the calculation of the heat transfer at the receiver to feed the turbine at the previously established conditions. The general expression for heat transfer is shown in (4.20). ΔT is the difference in temperature between the inlet and the outlet of the tube or stage. It is taken as constant for each tube-stage following other bachelor thesis (Heras Martín 2012). Besides, this supposition gives an uniform heat flux for the heliostat field design which simplifies calculations.

$$q = \frac{\Delta T}{R} \quad (4.20)$$

In order to get the thermal resistance, R, the heat transfer coefficient, h, has to be obtained. This thermal resistance consists of a conduction part, convection part and phase change part at the suitable stage. The general expression for this thermal resistance is shown in (4.21).

$$R_t = \left[\frac{1}{\pi \cdot d_{tube,int} \cdot L_{tube} \cdot h} + \frac{ln\left(\frac{d_{tube,ext}}{d_{tube,int}}\right)}{2 \cdot \pi \cdot L_{tube} \cdot k_{tube}} \right] \quad (4.21)$$

The heat transfer coefficient, HTC, is defined as *h* and the *k* is the conduction coefficient of the tube material. The conduction part will be the same during the whole process. Thereby, all the effort in the following section will be put in the heat transfer coefficient.

All the HTC are obtained using the Nusselt number, where *d* is the internal radius of the tube and *k* the conduction coefficient of the fluid.

$$Nu = \frac{h \cdot d}{k} \quad (4.22)$$

4.2.1. Heat transfer in the economizer

During this stage there is a temperature rise but there is only one phase in the HTF. While this process happens, the thermal resistance to have into account is the one from conduction of the tube and the convection in internal turbulent flow for circular tubes (Re>2300).

In this case, the Dittus-Boelter correlation is used in (4.23) for a heating process.

$$Nu_D = 0.023 Re_D^{0.8} Pr^{0.4} \quad (4.23)$$

This correlation is confirmed experimentally, and will have to be considered, under the following conditions. (Incropera 2006)

$$0.7 \leq Pr \leq 160$$
$$Re_D \geq 10000 \quad (4.24)$$
$$\frac{L}{D} \geq 10$$

The previous correlation shows its dependency in Reynolds and Prandtl numbers, where ρ is the density, *v* the fluid velocity, *d* the internal radius of the tube, μ the dynamic viscosity of the fluid and *Cp* the specific heat of the fluid.

$$Re_D = \frac{\rho_l \cdot v \cdot d_{tube,int}}{\mu_l} \quad (4.25)$$

$$Pr = \frac{Cp \cdot \mu}{k} \quad (4.26)$$

4.2.2. Heat transfer in the boiler

In this case, there is a phase change to deal with. From (Thome 2004), the Chen's correlation is going to be used. This correlation divides the two phase HTC into two different contributions, nucleate boiling and convection.

$$h_{tp} = h_{nb} + h_{conv} \tag{4.27}$$

However, this contribution is not directly used due to two factors. First, Chen observed that the increase in temperature close to the wall under forced convection reduced the nucleation of boiling sites, therefore, reducing the contribution of the nucleate boiling. Secondly, the vapor formed in the phase change increased the fluid velocity also increasing the convective heat transfer contribution.

That is why the final relation between the two contribution and the total HTC is expressed in (4.28) where four variables need to be established.

$$h_{tp} = S \cdot h_{FZ} + F \cdot h_{DB} \tag{4.28}$$

The nucleate pool boiling correlation found on *Dynamic of vapor bubbles and boiling heat transfer* (Forster and Zuber 1955) is expressed by h_{FZ}.

$$h_{FZ} = \left[\frac{k_l^{0.79} c_{pl}^{0.45} \rho_l^{0.49}}{\sigma^{0.5} \mu_l^{0.29} h_{vap}^{0.24} \rho_g^{0.24}}\right] \Delta T_{sat}^{0.24} \Delta p_{sat}^{0.75} \tag{4.29}$$

The wall superheat, ΔT_{sat} , is the local temperature difference between the inner tube wall and the local saturation temperature. The pressure difference, Δp_{sat}, is the obtained from the vapor pressures of the fluid at the wall temperature and at the saturation temperature.

$$\Delta T_{sat} = T_{wall} - T_{sat} \tag{4.30}$$

$$\Delta p_{sat} = p_{wall} - p_{sat} \tag{4.31}$$

As well as in the previous stage, the convection HTC, $h_{DB,}$ is obtained by the Dittus-Boelter correlation, which in (4.32) comes integrated the definition of the Nusselt number with the correlation, using the properties of the liquid.

$$h_{DB} = 0.023 Re_l^{0.8} Pr^{0.4} \frac{k_l}{d_{int,tube}} \tag{4.32}$$

In this case the Reynolds number is calculated using the vapor quality, *x*. Also the Prandtl number uses the properties of the liquid.

$$Re_l = \frac{\dot{m}(1-x) d_{int,tube}}{\mu_l} \tag{4.33}$$

$$Pr = \frac{Cp_l \cdot \mu_l}{k_l} \tag{4.34}$$

The increase in the liquid-phase convection due to the two-phase flow is given by the two-phase multiplier shown in *F*.

$$F = \left(\frac{1}{X_{tt}} + 0.213\right)^{0.736} \tag{4.35}$$

In (4.36) the Martinelli parameter, X_{tt}, is used for the two-phase effect of the convection. It has to be noticed than when $1/X_{tt} \leq 0.1$, F is set equal to 1.

$$X_{tt} = \left(\frac{1-x}{x}\right)^{0.9} \left(\frac{\rho_g}{\rho_l}\right)^{0.5} \left(\frac{\mu_l}{\mu_g}\right)^{0.1} \tag{4.36}$$

The nucleate boiling suppression factor identified by *S*.

$$S = \frac{1}{1 + 0.00000253 Re_{tp}^{1.17}} \tag{4.37}$$

In this case, the Reynolds number depends on the Reynolds number calculated for the Dittus-Boelter correlation and the two-phase multiplier.

$$Re_{tp} = Re_l F^{1.25} \tag{4.38}$$

4.2.3. Heat transfer in the superheater

In the superheater the Dittus-Boelter correlation is also used but in this case using the properties of the vapor.

$$Nu_D = 0.023 Re_D^{0.8} Pr^{0.4} \tag{4.39}$$

$$Re_D = \frac{\rho_g \cdot v \cdot d}{\mu_g} \tag{4.40}$$

$$Pr = \frac{Cp_g \cdot \mu_g}{k_g} \tag{4.41}$$

4.3. Thermal losses in the receiver

For the thermal losses in the receiver, two main reasons bring important inefficiency. The first one is the thermal losses due to convection and the second one is due to radiation losses, shown in Figure 27.

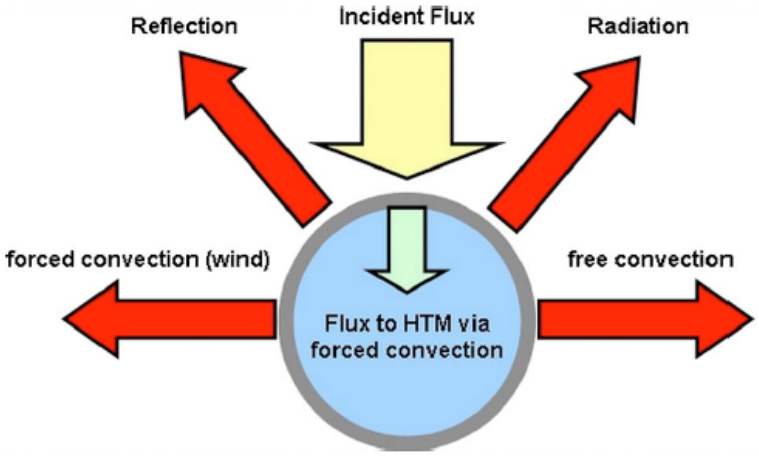

Figure 27: Heat Transfer System at the receive. Source: (Schmitz, et al. 2006)

The thermal losses due to reflection are estimated to be around 7.5% of the incident flux. This comes from the fact of considering both the sky and the tubes as grey surfaces, what is the same, their emissivity and absorptivity are equal. From (4.42) which establishes that for a semitransparent body the sum of the absorptivity, transmissivity and reflectivity is equal to the unit. If an opaque body is considered, the term of transmissivity disappears. From *Compound Parabolic Concentrators for Solar Water Heat Pasteurization: Numerical Simulation* (Denkenberger and Pearce 2006) it is obtained that the emissivity of the tubes is equal to 0.925. This gives a reflectivity of 0.075 from equation (4.42) considering τ=0.

$$\alpha + \tau + \rho = 1 \qquad (4.42)$$

As first step, the thermal losses by convection will be calculated. Secondly, the thermal losses due to radiation will be obtained for the different geometries of the receiver that the present project aims to study. All this procedure makes easier to design the field of heliostats the plant needs to give the expected power.

4.3.1. Thermal losses due to convection

The thermal losses due to convection come from two sources. The first one is the forced convection due to the wind that blows around the tubes. The second one is the free convection in the exterior of the tubes. For this purpose the (4.43) is used, where the tube temperature, T_{tube}, and the ambient temperature, T_{amb}, are introduced as well as the external area of the tube, A.

$$q_{conv} = \mathrm{A} \cdot h(T_{tube} - T_{amb}) \tag{4.43}$$

Ambient temperature is the average temperature of the chosen day for the dimensioning of the installation. For the tube temperature the (4.45) will be used, where *q* is the heat transfer calculated in section 4.2 and the temperature T_{htf} will be calculated through a geometric mean of the temperature at the entrance and at the exit of each stage, equation (4.44).

$$T_{htf} = \sqrt[4]{\frac{T_{in}^4 + T_{out}^4}{2}} \tag{4.44}$$

$$T_{tube} = T_{htf} + q \cdot R_t \tag{4.45}$$

For the HTC the equation (4.46) will be used, which have into account both forced and free or natural convection.

$$h = \sqrt[4]{h_{fc}^4 + h_{nc}^4} \tag{4.46}$$

For both designs, the forced convection is calculated with the Churchill and Bernstein (Incropera 2006) correlation as shown in (4.47).

$$Nu_d = 0.3 + \frac{0.62 Re_D^{0.5} Pr^{1/3}}{\left[1 + (0.4/Pr)^{2/3}\right]^{0.25}} \left[1 + \left(\frac{Re_D}{282{,}000}\right)^{0.625}\right]^{0.8} \tag{4.47}$$

To obtain the Reynolds number the properties of the wind are taken at the ambient temperature already established, as well as the Prandtl number.

$$Re_D = \frac{\rho_{air} \cdot v_{wind} \cdot d_{ext,tube}}{\mu_{air}} \tag{4.48}$$

$$Pr = \frac{Cp_{air} \cdot \mu_{air}}{k_{air}} \tag{4.49}$$

This finally allows the final calculation of the HTC due to forced convection.

$$Nu = \frac{h_{fc} \cdot d_{ext,tube}}{k_{air}} \tag{4.50}$$

In order to get the HTC due to natural convection, Churchill and Chu (Incropera 2006) correlation is used in (4.54). There is a condition that has to be fulfilled if this correlation for vertical cylinders is used as shown in (4.51). The Grashof number is established in (4.53).

$$\frac{D}{L} \geq \frac{35}{Gr_l^{0.25}} \tag{4.51}$$

$$Gr_L = \frac{g \cdot \beta (T_s - T_\infty) L_{tube}^3}{\nu^2} \tag{4.52}$$

$$Ra = Gr_L \cdot Pr \tag{4.53}$$

$$Nu_L = \left[0.825 + \frac{0.387 \cdot Ra^{1/6}}{\left(1 + \left(\frac{0.492}{Pr}\right)^{9/16}\right)^{8/27}} \right]^2 \tag{4.54}$$

The Rayleigh number is the product of Grashof and Prandtl number. Having obtained the Nusselt number, it is easy to obtain the HTC due to natural convection as shown in (4.55).

$$Nu_L = \frac{h_{nc} L_{tube}}{k_{air}} \tag{4.55}$$

4.3.2. Thermal losses due to Radiation

4.3.2.1. First Design. One row of tubes at the receiver

In the Figure 29, it is shown the shape to be studied in order to obtain the thermal losses due to radiation. This is the first geometry taken into account for this design, in which the receiver consists on one row of tubes, having a reradiating refractory surface in the core, right behind the tubes. This surface is taken as adiabatic, this is, there is no thermal flux that goes through it, it reflects all the received radiation. Although the receiver has a cylindrical shape, for this section a planar approximation is given in order to simplify calculations.

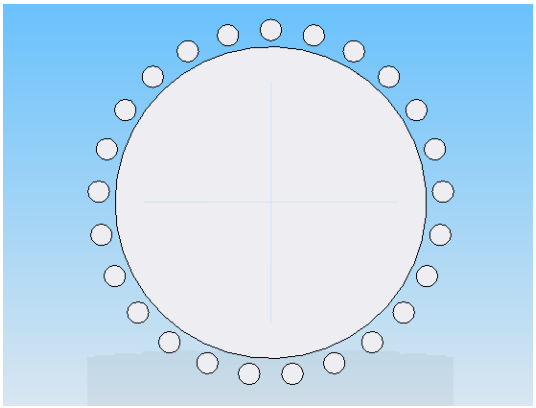

Figure 28: Simulation of the Design1, one-row receiver.

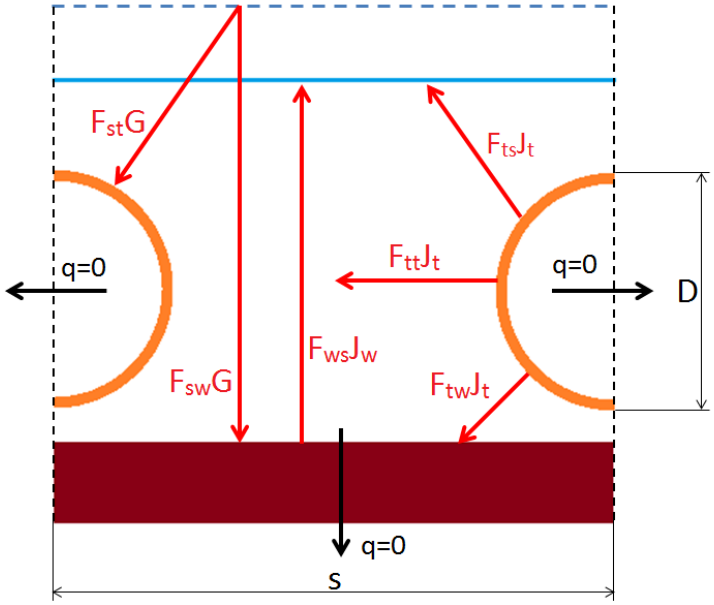

Figure 29: View factors diagram for a one-row of tubes configuration

Following the scheme, next step is to calculate the view factors of the shape between surroundings (s), tube (t) and wall (w). Equation (4.56) is obtained from the bibliography (Incropera 2006), while equation (4.57) follows the summation rule of view factors and the equation (4.58) is based on the reciprocity relation. The summation rule of view factors consists on the fact that all the radiation leaving a surface must be intercepted by other surfaces if the geometry of design is an enclosure. The reciprocity relation gives a relation between surfaces and says that the product of the view factor from one surface to another and the area of the first one is equal to the product of the inversed view factor and the area of the second surface.

$$F_{wt} = 1 - \left[1 - \left(\frac{D}{s}\right)^2\right]^{1/2} + \left(\frac{D}{s}\right) \cdot \tan^{-1}\left[\left(\frac{s^2 - D^2}{D^2}\right)^{1/2}\right] \qquad (4.56)$$

$$F_{ws} = 1 - F_{wt} - \cancel{F_{ww}} \qquad (4.57)$$

$$F_{st} = F_{wt} \qquad (4.58)$$

It has to be taken into account that the planar approximation gives that the view factor from a plane surface to itself is 0, which is used in (4.57) with the wall to wall element. Moreover, the two plane surfaces taken, both surroundings and the refractory wall, have the same view area, which ends to a view the same reciprocating view factor between them.

With all the view factor the problem is ready to consider the thermal circuit to solve, . Due to the geometry that has been previously described, the problem counts with 3 radiosities, J_s for the surroundings, J_w for the reradiating wall and J_t for the tubes. To make it clear, the radiosity is the rate at which radiation leaves a surface because of both emission and reflection per unit

area. There are another two variables to be defined, E_s and E_t, which are the emissive power of the surroundings surface and the tubes surface, respectively. The emissive power is defined as the rate at which radiation leaves a surface due to emission per unit area.

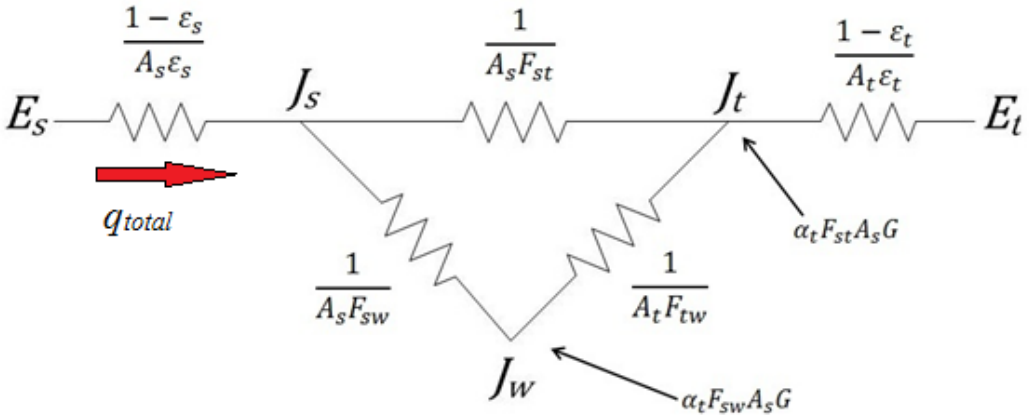

Figure 30: One-row radiation circuit where t=tube surface, s=surroundings surface, w=radiant wall surface

There are another three parameters in the circuit which have not been described. The first one is the emissivity, ε, both for the surroundings and the tubes. The emissivity is the ratio of the radiation emitted by a surface to the one emitted by a blackbody at the same temperature. The values of the emissivities come from *Compound Parabolic Concentrators for Solar Water Heat Pasteurization: Numerical Simulation* (Denkenberger and Pearce 2006).

$$\varepsilon_{earth} = 0.5$$

$$\varepsilon_{sky} = 1$$

$$\varepsilon_t = 0.925 \qquad (4.59)$$

$$\varepsilon_s = \frac{\varepsilon_{earth} + \varepsilon_{sky}}{2}$$

The second one is the attenuation coefficient, α, which is defined as the ratio between the total radiation leaving the heliostats and the direct radiation approaching the receiver. This ratio comes from the inefficiencies forced by the lack of precision of the beam of light coming from the heliostats. The value of the attenuation coefficient comes from (Thermal Engineering and Fluid Mechanics Department s.f.).

$$\alpha = 0.85 \qquad (4.60)$$

And last but not least is the concentrated radiation coming from the heliostats, G. This radiation reaches both the tubes and the reradiating wall depending on the view factors between the surroundings and those two components. This parameter will be one of the unknowns of the problem.

In addition, the areas A_s, A_t and A_w must be defined in order to complete the description of all the parameters of the circuit.

$$A_s = A_w = s \cdot L_{tube}$$
$$A_t = \pi \cdot d_{tube,ext} \cdot L_{tube} \quad (4.61)$$

In order to resolve the circuit, a nodal analysis is going to be carried out. This analysis consists on making equal the heat transfer rates getting to each node by all the branches that end/start at it. The starting energy to be introduced into the problem is the total heat involved in the receiver. This covers the heat needed in the tubes plus the heat lost by convection outside the tubes, which depends on wind velocity. q_{total}

$$q_{total} = q_{tube} + q_{conv} \quad (4.62)$$

$$q_{conv} = q''_{conv} \cdot \pi \cdot d_{tube,ext} \cdot L_{tube} \quad (4.63)$$

Finally, the problem to solve has 4 different unknowns. These are the three radiosities, J_s, J_w and J_t, and the concentrated radiation from the heliostats, G. The first variable to be solved is the radiosity of the tube, J_t, using equations (4.64) and (4.65)

$$q_{total} = \frac{J_t - E_t}{\frac{1 - \varepsilon_t}{A_t \varepsilon_t}} \quad (4.64)$$

$$E_t = \sigma \cdot T_t^4 \quad (4.65)$$

$$E_s = \sigma \cdot T_s^4 \quad (4.66)$$

For the temperature of the surroundings of the receiver, an estimation must be established. The surroundings receive radiation both from the sky and the ground. Therefore this estimation is based on this fact, having into account view factors from the surroundings of the receiver to the ground and the sky, which will be 0.5 for each one, and the temperature of both ground and sky.

$$T_{ground} = T_{amb} + 10K \quad (4.67)$$

$$T_{sky} = 273K \quad (4.68)$$

$$T_s = \sqrt[4]{\frac{F_{sky} \cdot \varepsilon_{sky} \cdot T_{sky}^4 + F_{ground} \cdot \varepsilon_{ground} \cdot T_{ground}^4}{\varepsilon_s}} \quad (4.69)$$

After this, the problem is reduced to a system of equations with 3 unknowns and three equations derived from the thermal circuit in Figure 30 and described as follows. It has been introduced the Stefan-Boltzmann constant, σ, whose value is 5.67×10^{-8} (W/m^2K^4).

$$q_{total} = \frac{J_w - J_t}{\frac{1}{A_t F_{tw}}} + \frac{J_s - J_t}{\frac{1}{A_s F_{st}}} + \alpha F_{st} A_s G \tag{4.70}$$

$$\frac{E_s - J_s}{\frac{1-\varepsilon_s}{A_s \varepsilon_s}} + \frac{J_w - J_s}{\frac{1}{A_s F_{sw}}} + \frac{J_t - J_s}{\frac{1}{A_s F_{st}}} = 0 \tag{4.71}$$

$$\frac{J_t - J_w}{\frac{1}{A_t F_{tw}}} + \frac{J_s - J_w}{\frac{1}{A_s F_{sw}}} + \alpha F_{ws} A_w G = 0 \tag{4.72}$$

Following several operations, the aim is to get a matrix calculation, which is easier to program in mathematical software such as MATLAB. This system is briefly defined as A·x=B, where x contains the three unknowns.

$$A = \begin{pmatrix} A_t F_{tw} & A_s F_{st} & \alpha A_s F_{st} \\ A_s F_{sw} & -(\frac{A_s \varepsilon_s}{1-\varepsilon_s} + A_s F_{sw} + A_s F_{st}) & 0 \\ -(A_s F_{st} + A_t F_{tw}) & A_s F_{sw} & \alpha A_s F_{sw} \end{pmatrix} \tag{4.73}$$

$$\vec{B} = \begin{pmatrix} q_{total} + J_t (A_w F_{wt} + A_s F_{st}) \\ -\frac{A_s \varepsilon_s}{1-\varepsilon_s} \sigma T_s^4 - J_t A_s F_{st} \\ -J_t A_w F_{wt} \end{pmatrix} \tag{4.74}$$

$$\vec{x} = \begin{pmatrix} J_w \\ J_s \\ G \end{pmatrix} \tag{4.75}$$

Having solved the previous system, the problem is close to its end calculating the final heat loss due to radiation.

$$q_{turbo.rad} = \frac{J_s - \sigma T_s^4}{\frac{1-\varepsilon_s}{A_s - \varepsilon_s}} \tag{4.76}$$

$$q_{rad} = q_{turbo.rad} \cdot n_{tube} \cdot n_{panel} \tag{4.77}$$

4.3.2.2. Second Design. Two rows of tubes at the receiver.

For the second design, a two row receiver is considered. This receiver is based on the one described in *Simulation of an integrated steam generator for solar tower* (Ben-Zvi, Epstein and Segal 2011). It consists of two rows of tubes, one closer to the reradiating wall than the other. However, in comparison to the design by Ben-Zvi, the outer row is closed, covering 360º, a whole circumference around the refractory wall.

The aim of this idea is to prove that having a divided receiver, in which one of the rows is a boiler and the other play the role of a superheater, the control of the fluid is better and there are less radiation losses. This receiver is more compact than other designs in which the division is vertical and not horizontal as at the present project. In Figure 31 the scheme of the new design is shown.

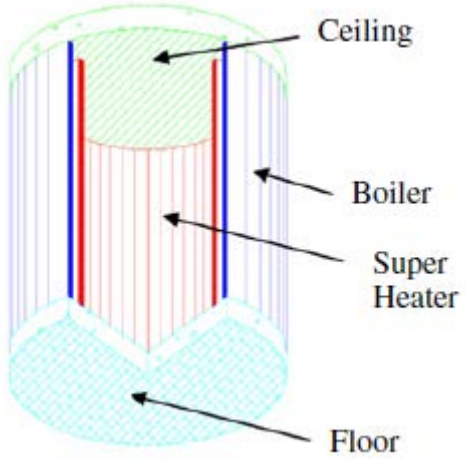

Figure 31: Two-row receiver. Source: (Ben-Zvi, Epstein and Segal 2011)

In this case the problem becomes more complicated due to the presence of more elements, which interact among them. In Figure 33 is easy to compare the increase in the number of relations between components with the previous design, Figure 30.

The design includes two types of tubes, inner and outer rows, the reradiating refractory wall and the surroundings, Figure 32.

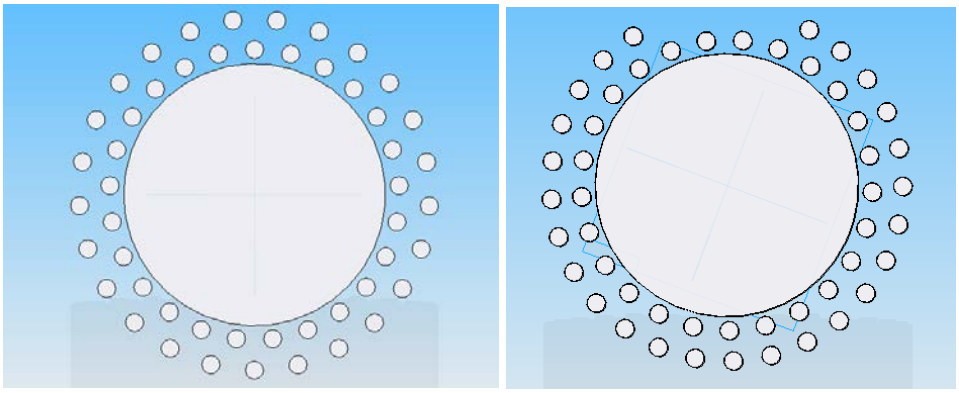

Figure 32: Simulation of the Design2, two-row receiver, right with opening sectors based on the work by Ben-Zvi.

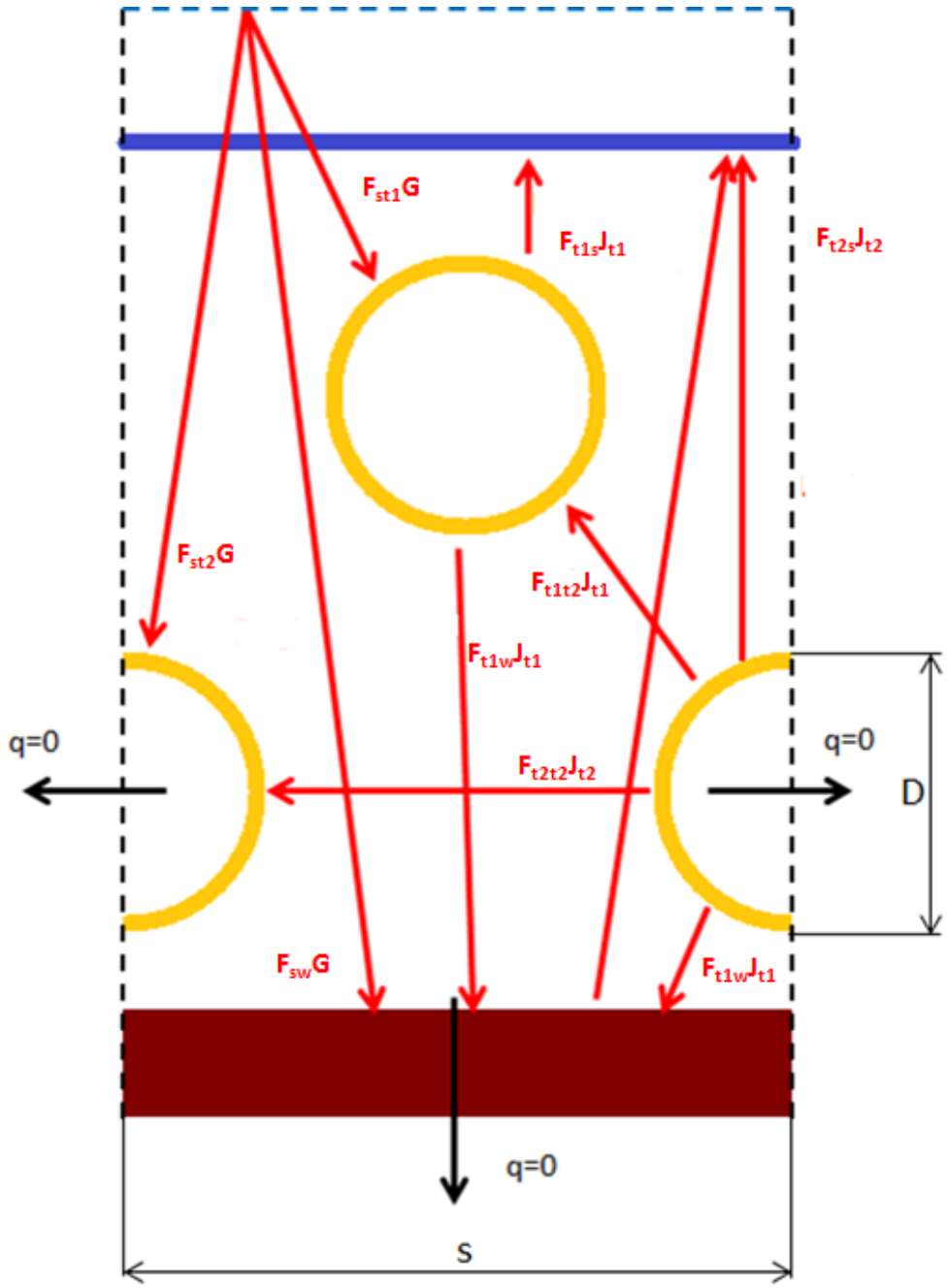

Figure 33: View factors diagram for a two-row of tubes configuration

An important factor that enables the view factor calculation is that the tubes of both rows must form an equilateral triangle among them. It can be considered a distribution where the tubes of the inner row are right behind the tubes of the outer tubes. This distribution is considered to be not as efficient as the equilateral triangle one. All this discussion can be found in *Radiant heat transmission between surfaces separated by non-absorbing media* (Hottel 1931). Also from this bibliography can be described the view factor formula from a plane to two rows of tubes above and parallel to the defined plane depending on the ratio center-to-center distance and the tube diameter, Figure 34.

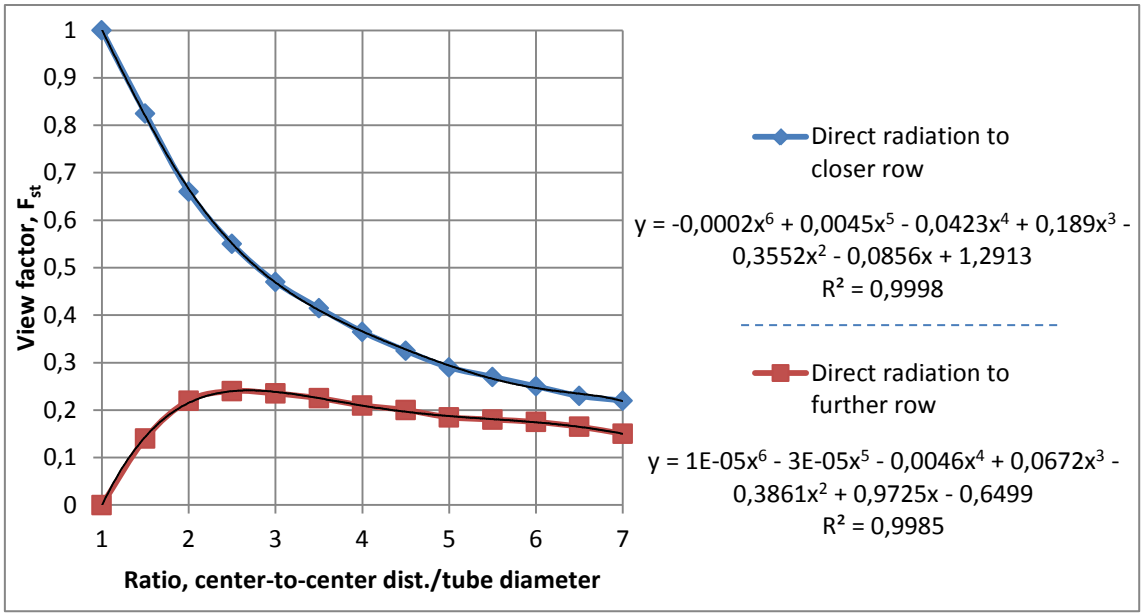

Figure 34: Direct view factors for a two-row configuration from a planar surface parallel to the rows of tubes. Source: (Hottel 1931)

A polynomial fitting curve was obtained from the previous figure for the view factors from the wall to the tubes, calling t1 to the inner row and t2 to the outer row.

$$R = \frac{s}{D} \tag{4.78}$$

$$F_{wt1} = -0.0002R^6 + 0.0045R^5 - 0.0423R^4 + 0.189R^3 - 0.3552R^2 - 0.0856R + 1.2913 \tag{4.79}$$

$$F_{wt2} = 0.00001R^6 - 0.00003R^5 - 0.0046R^4 + 0.0672R^3 - 0.3861R^2 + 0.9725R - 0.6499 \tag{4.80}$$

$$F_{st2} = F_{wt1}$$
$$F_{st1} = F_{wt2} \tag{4.81}$$

From (4.82) it can be obtained the view factor from the wall to the surroundings.

$$F_{ws} = 1 - F_{wt1} - F_{wt2} - \cancel{F_{ww}} \tag{4.82}$$

In order to get the view factors between the tubes a system of equations has to be solved. As well as the previous step, the equations are established following the summation rule which forms the system of equations for view factors, (4.82), and the reciprocity relation, (4.83).

$$F_{t1t1} + F_{t1t2} + F_{t1w} + F_{t1s} = 1$$
$$F_{t2t2} + F_{t2t1} + F_{t2w} + F_{t2s} = 1 \tag{4.83}$$

Since the diameter of the tubes is the same for both inner and outer rows and the distance between them is the same due to the equilateral triangular distribution, using the reciprocity relation, it can be established that the view factors between the tubes, both between different rows and the same row, are equal.

$$F_{tt} = F_{t2t2} = F_{t2t1} = F_{t1t1} = F_{t1t2} \tag{4.84}$$

$$F_{t1w} = \frac{A_w}{A_{t1}} F_{wt1} = \frac{A_s}{A_{t2}} F_{st2} = F_{t2s} \tag{4.85}$$

$$F_{t2w} = \frac{A_w}{A_{t2}} F_{wt2} = \frac{A_s}{A_{t1}} F_{st1} = F_{t1s} \tag{4.86}$$

Thereby, the system is reduced to one equation with only one unknown.

$$F_{tt} = \frac{1 - F_{t1w} - F_{t1s}}{2} = \frac{1 - F_{t2w} - F_{t2s}}{2} \tag{4.87}$$

Once all the view factors are established, the problem can be focused on the thermal circuit of the Figure 35.

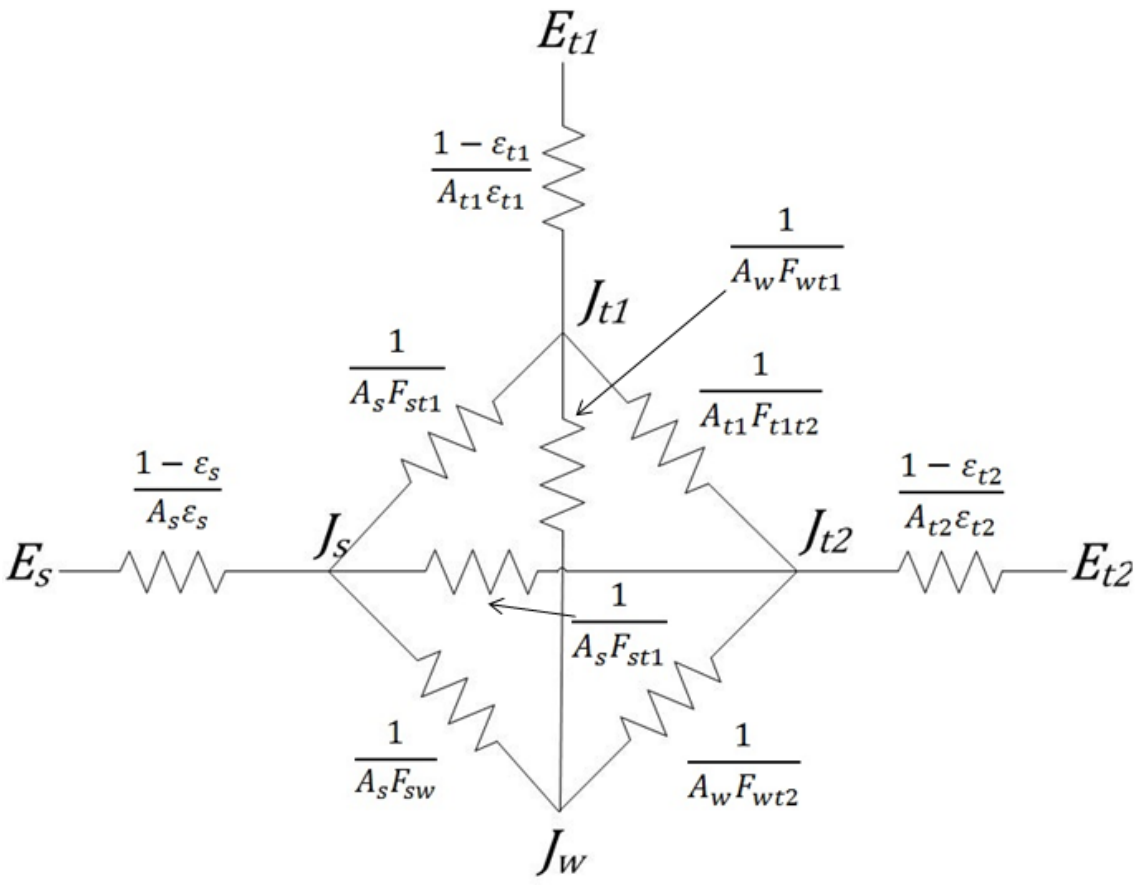

Figure 35: Two-row radiation circuit

The starting energy to be introduced into the problem is the total heat involved in the receiver for each of the rows. This covers the heat needed in the tubes plus the heat lost by convection outside the tubes, which depends on wind velocity.

$$q_{t1} = q_{tube1} + q_{conv1}$$
$$q_{conv1} = q''_{conv1} \cdot \pi \cdot d_{tube,ext} \cdot L_{tube} \quad (4.88)$$

In order to get a plausible system of equations, the heat transfer and external tube temperature of the inner row, q_{t2} and T_{t2}, must behave as unknowns.

The first equations that can be solved are J_{t1} and J_s since T_{t1}, T_s and q_{t1} have already been obtained.

$$q_{t1} = \frac{J_{t1} - E_{t1}}{\frac{1-\varepsilon_{t1}}{A_{t1}\varepsilon_{t1}}} \quad (4.89)$$

$$E_{t1} = \sigma \cdot T_{t1}^4 \quad (4.90)$$

$$E_s = \sigma \cdot T_s^4 \quad (4.91)$$

To sum up, the unknowns will be the radiosities J_s, J_w, the radiation coming from the field of heliostats, G, and q_{t2} and T_{t2}, previously declared. This shows a system of equations with five unknowns and 4 equations. Thereby this problem is solved following a fixed-point iteration. Firstly, the external tube temperature for the inner row is fixed, obtaining a heat transfer in the inner row. This heat transfer gives again an external tube temperature of the inner row, which is compared with the previously fixed temperature until in converges.

$$q_{t2} = \frac{J_{t2} - E_{t2}}{\frac{1-\varepsilon_{t2}}{A_{t2}\varepsilon_{t2}}}$$
$$E_{t2} = \sigma \cdot T_{t2}^4 \quad (4.92)$$

Therefore, this design plays with 4 equations and 4 unknowns. The equations are found following again the nodal method.

$$0 = \alpha F_{sw} A_s G + \frac{J_{t2} - J_w}{\frac{1}{A_{t2}F_{t2w}}} + \frac{J_{t1} - J_w}{\frac{1}{A_{t1}F_{t1w}}} + \frac{J_s - J_w}{\frac{1}{A_s F_{sw}}} \quad (4.93)$$

$$\frac{J_s - \sigma T_s^4}{\frac{1-\varepsilon_s}{A_s \cdot \varepsilon_s}} = \frac{J_{t1} - J_s}{\frac{1}{A_s \cdot F_{st1}}} + \frac{J_{t2} - J_s}{\frac{1}{A_s \cdot F_{st2}}} + \frac{J_w - J_s}{\frac{1}{A_s F_{sw}}} \quad (4.94)$$

$$q_{t1} = \frac{J_{t2} - J_{t1}}{\frac{1}{A_{t1}F_{t1t2}}} + \frac{J_w - J_{t1}}{\frac{1}{A_{t1}F_{t1w}}} + \frac{J_s - J_{t1}}{\frac{1}{A_{t1}F_{t1s}}} + \alpha F_{st1} A_s G \qquad (4.95)$$

$$q_{t2} = \frac{J_{t1} - J_{t2}}{\frac{1}{A_{t2}F_{t2t1}}} + \frac{J_w - J_{t2}}{\frac{1}{A_{t2}F_{t2w}}} + \frac{J_s - J_{t2}}{\frac{1}{A_{t2}F_{t2s}}} + \alpha F_{st2} A_s G \qquad (4.96)$$

Then, once more, the aim is to work with matrix analysis. Thereby, following similar operations as in 4.3.2.1, the matrix system Ax=B is as shown in (4.98), (4.99) and (4.100).

In order to reduce the matrix size, the next constant is declared.

$$a = \frac{1 - \varepsilon_{t2}}{A_{t2}\varepsilon_{t2}} \qquad (4.97)$$

Therefore the system of equations is defined in the following matrices.

$$A = \begin{pmatrix} A_{t1}F_{t1w} + A_{t2}F_{t2w} + A_sF_{sw} & A_sF_{sw} & -\alpha F_{sw}A_s & -A_{t2}F_{t2w}a \\ -A_sF_{sw} & \frac{A_s\varepsilon_s}{1-\varepsilon_s} + A_sF_{sw} + A_sF_{st1} + A_sF_{st2} & 0 & -A_sF_{st2}a \\ A_{t1}F_{t1w} & A_{t1}F_{t1s} & \alpha F_{st1}A_s & A_{t1}F_{t1t2}a \\ -A_{t2}F_{t2w} & -A_{t2}F_{t2s} & -\alpha F_{st2}A_s & a(\frac{1}{a} + A_{t1}F_{t1t2} + A_{t2}F_{t2w} + A_sF_{st2}) \end{pmatrix} \quad (4.98)$$

$$\vec{B} = \begin{pmatrix} A_{t1}F_{t1w}J_{t1} + E_{t2}F_{t2w}A_{t2} \\ A_sF_{st1}J_{t1} + E_{t2}F_{t2s}A_{t2} + E_s\frac{A_s \cdot \varepsilon_s}{1-\varepsilon_s} \\ q_{t1} + J_{t1}(A_{t1}F_{t1t2} + A_{t1}F_{t1w} + A_{t1}F_{t1s}) - E_{t2}A_{t1}F_{t1t2} \\ A_{t1}F_{t1t2}J_{t1} - E_{t2}(A_{t2}F_{t2t1} + A_{t2}F_{t2w} + A_{t2}F_{t2s}) \end{pmatrix} \quad (4.99)$$

$$\vec{x} = \begin{pmatrix} J_w \\ J_s \\ G \\ q_{t2} \end{pmatrix} \quad (4.100)$$

As well as the external tube temperature for the inner row, a properties temperature for the superheated steam passing through these tubes is estimated in order to start the iteration, recalculating it as loops grow. Taking this properties temperature, the heat thermal resistance is calculated as in the design with one row of tubes for the superheated stage, (4.39).

Using the following equations the external temperature of the inner row is obtained. Firstly, the temperature of the vapor at the outlet of the tube, T_{out}, is calculated with (4.101). After this, the external tube temperature for the inner row, T_{t2}, is obtained in order to compare with the previous value given for this variable using equation (4.102).

$$q_{t2} = mC_p(T_{out} - T_{in}) = \frac{\Delta T_{lm}}{R} \tag{4.101}$$

$$\Delta T_{lm} = \frac{(T_{t2} - T_{in}) - (T_{t2} - T_{out})}{\ln \frac{(T_{t2} - T_{in})}{(T_{t2} - T_{out})}} \tag{4.102}$$

Having solved the previous system, the problem is close to its end calculating the final heat loss due to radiation. In this design, the heat loss due to radiation calculated is for a pair of tubes, one of each row.

$$q_{tube.rad} = \frac{J_s - \sigma T_s^4}{\frac{1 - \varepsilon_s}{A_s - \varepsilon_s}} \tag{4.103}$$

$$q_{rad} = q_{tube.rad} \cdot n_{tube} \cdot n_{panel} \tag{4.104}$$

4.4. Load losses

4.4.1. Load losses at the receiver

In order to obtain the pressure losses in the installation, the first step taken in this project is to calculate them at the receiver. These losses are different in each panel due to the different physical states that the HTF goes through. Anyway, the general equation to calculate load losses is Bernoulli equation seen at (4.105).

$$\Delta P_{rec} = \frac{1}{2}\rho \cdot v^2 \left(\lambda \frac{L}{D} + \sum k\right) \tag{4.105}$$

As it can be seen in the previous equation, there are two different reasons that participate in the growth of load losses. The first one is the friction loss which is introduced into the equation with the coefficient λ. This coefficient depends on the inner roughness of the tube and the velocity of the HTF. It is calculated with the help of the Colebrook correlation, equation (4.106), which has to be iterated in order to get the proper value.

$$\frac{1}{\sqrt{\lambda}} = -2\log\left(\frac{\varepsilon/D}{3.7} + \frac{2.51}{Re\sqrt{f}}\right) \tag{4.106}$$

The second ones are the secondary losses which come from different geometries and devices that the HTF may find during its way through the receiver. These secondary losses will be taken according to Figure 24.

4.4.2. Load losses at the tower

In the case of the tower, the load losses come from the same facts as in the receiver plus the height that the water must overcome in order to feed the receiver.

$$\Delta P_{tower} = \frac{1}{2}\rho \cdot v^2 \left(\lambda \frac{L}{D} + \sum k\right) + \rho \cdot g \cdot h \tag{4.107}$$

As it can be observed in equation (4.107), the Bernoulli equality is used again, with the addition of the hydrostatic pressure due to the HTF column above the pump.

4.4.3. Pumping power

Last step is to obtain the pumping power needed in order to overcome the previously explained load losses. This power comes from the multiplication of the load losses plus the pressurization of the HTF due to the cycle and the water flow.

$$\Delta P_{total} = \Delta P_{rec} + \Delta P_{tower} + \Delta P_{cycle} \tag{4.108}$$

$$P_{pump} = \Delta P_{total} \cdot Q \tag{4.109}$$

4.5. Solar radiation

Due to the high dependency of both the performance and the profitability of this kind of power plant on the solar radiation along a whole day, the first step in order to get a proper design is to model how the Sun radiates the Earth. This model depends on the day of the year

and the location of the power plant, so it is key to choose an optimum place and a day which gives equilibrium to the plant performance.

In order to simplify the algorithm, the solar radiation is taken at its maximum value on the day that has been chosen, which happens at local noon.

However, even taken into account the previous statements, the angle that forms the line from the heliostat to the sun, and the line from the heliostat to the receiver, θ, has much to do with the amount of energy that will reach the HTF. In the Figure 36 the angles that needs to be calculated for this purpose are shown.

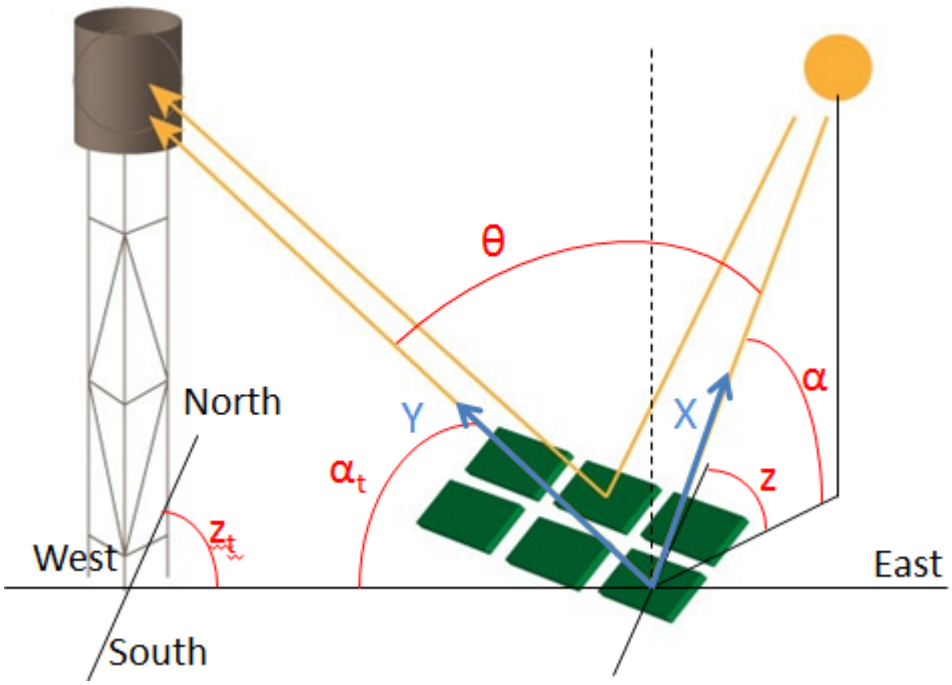

Figure 36: Solar Angle diagram for the field of heliostats

In the image above, the angle that have been described are, for the tower, the azimuth angle and the tower altitude angle, and for the Sun, the azimuth angle and the solar altitude angle. Using these angles, unit vectors **X** and **Y** are defined.

$$\vec{X} = cos\ \alpha \cdot cos\ z\ \vec{\imath} + sin\ \alpha \cdot sin\ z\ \vec{\jmath} + sin\ \alpha\ \vec{k}$$

$$\vec{Y} = cos\ \alpha_t \cdot cos\ z_t\ \vec{\imath} + sin\ \alpha_t \cdot sin\ z_t\ \vec{\jmath} + sin\ \alpha_t\ \vec{k} \qquad (4.110)$$

Furthermore, using the definition of the cross product, the angle θ can be obtained.

$$cos\ \theta = \frac{\vec{X} \cdot \vec{Y}}{|\vec{X}| \cdot |\vec{Y}|} \qquad (4.111)$$

$$\cos\theta = \cos\alpha \cdot \cos z \cdot \cos\alpha_t \cdot \cos z_t + \cos\alpha \cdot \sin z \cdot \cos\alpha_t \cdot \sin z_t + \sin z \cdot \sin z_t$$

Once this angle is obtained, the problem must face the step where the direct solar radiation is received on the surface of the heliostats and is concentrated at the receiver.

4.6. Design of the field of heliostats

Like it was said previously in the report, the field of heliostats is designed based on the radiation needed at the tubes in order to obtain the stated power in the turbine. This radiation has to be fulfilled with the maximum value for the solar radiation in the chosen day for this project. If the radiation per unit area, *G*, is multiplied by the frontal area of the receiver which is constrained by each sector, the total power needed from the field of heliostats for each sector is obtained.

$$q_G = G \cdot \alpha_{sector} \cdot r_{rec} \cdot L_{tube} \qquad (4.112)$$

This, together (4.111), which gives the angle between the sun, the heliostat and the receiver, and the solar radiation at local noon at the chosen location allows to calculated the needed field of heliostats in order to give the HTF the proper energy. The geometry that is going to be used in the design of the field of heliostat is described as follows:

- As seen in 3.1.4, the heliostats are mirrors with rectangular or squared form. Different sizes of heliostats will be taken into account in order to compare the different pros and cons can appear in the use of an optimum size.
- The heliostats will be distributed in concentric rings around the tower. The number of rings will vary according to the sector it concentrates the radiation to. As a reminder, the sectors are defined by the different panels the receiver is made of.
- Special attention must be focused into the distance between heliostats, both between heliostats of the same ring, from now on transversal distance, and between heliostats on the previous and next ring, from now on longitudinal distance. This point comes from the fact that each heliostat projects a shadow that can avoid the optimum performance of the heliostats. Taking Gemasolar power plant as point of reference, the distance between heliostats will be described below:
    - From the first to the fifteenth ring, both transversal and longitudinal distances will remain constant with a value of one heliostat and a half.
    - From the fifteenth on, the transversal distance raises a 10% of the width of the heliostat at each ring, and the longitudinal distance rises at a rate of 0.1 meter per ring.
- The number of heliostats in each is defined with equation (4.113). What it really does is to divide the arc of the ring in equal parts of the same length as the transversal distance that corresponds to the given ring. It is taken the arc, and not the whole circumference since some of the sectors will not need more rings when they can concentrate the needed energy in the receiver.

$$N_{helio} = \frac{arc\ of\ the\ ring}{transversal\ distance} \qquad (4.113)$$

With the design that has been described, the field of heliostats will have a different radius for each sector, which will give a non-uniform field. The algorithm starts from a first ring, placed at a radius of 20 meters from the base of the tower, and starts to install more rings until each sector fulfills the energy condition at the receiver. All this algorithm can be observed in Annex VI -

4.7. Global performance

It is important to obtain the global performance of the power plant. Like in other cases, the performance is a comparison of the input and output of a system.

In this case, the first step is to calculate the performance of the field of heliostats. This performance is a fraction that compares the concentrated radiation at the receiver with the total radiation that reaches the field directly from the Sun, as shown in equation (4.114).

$$\eta_{field} = \frac{Concentrated\ radiaton\ at\ the\ receiver}{Radiation\ on\ the\ field\ directly\ from\ the\ Sun} = \frac{G \cdot A_{rec}}{g_{sun} A_{field}} \qquad (4.114)$$

The second performance is a comparison between the final electrical output and the concentrated radiation at the receiver, equation (4.115). As a reminder, the total electrical output of the power plant takes into account the power that the pump needs to overcome pressure losses.

$$\eta_{rec} = \frac{Electrical\ Power}{Concentrated\ radiaton\ at\ the\ receiver} = \frac{W}{G \cdot A_{rec}} \qquad (4.115)$$

4.8. Natural Gas support

During winter and autumn months, solar radiation is lower than needed. Thereby, the power plant cannot reach the conditions for which it is designed. For these months, the plant needs a back-up, which is performed with a natural gas boiler.

In order to dimension the natural gas installation, the first step taken is the one that allows obtaining the radiation that the power plant is able to absorb during those cold months and the design month. For this purpose a percentage of energy absorption is obtained using equation (4.116). In the given equation, $P_{thermal\ cycle}$ is the power calculated with equation (4.7) and G is the radiation concentrated at the receiver for the design month.

$$\%E_{ab} = \frac{P_{thermal\ cycle}}{G \cdot A_{rec}} \qquad (4.116)$$

Having obtained the previous data, the second step is to calculate the energy absorbed at the receiver. This energy is calculated using equation (4.117) which introduces the time during the plant is able to produce electricity.

$$E_{abs} = \%E_{ab} \cdot G \cdot A_{rec} \cdot t \qquad (4.117)$$

This energy has to be compared with the energy needed in order to make the plant to produce electricity at design conditions. Thereby, this energy is calculated with equation (4.118) where t is the time during the plant is working at the design point every day.

$$E_{need} = P_{thermal\ cycle} \cdot t \qquad (4.118)$$

Once both energies are obtained, the difference of energy between the absorbed and the needed energies, which will be covered by the natural gas boiler, is calculated using equation (4.119).

$$E_{sup} = E_{need} - E_{abs} \qquad (4.119)$$

With these results, it can be obtained the percentage of support given by the natural gas boiler, both along a month and along the whole year.

$$\%support = \frac{E_{sup}}{E_{need}} \qquad (4.120)$$

4.9. Behavior of heliostats during hot months

As well as in the previous section, in this case of hot months it is needed to take some heliostats out of focus. This happens due to the high temperature that could get the tubes of the receiver because of a big amount of solar radiation concentrated on it. Thereby, since the design of the power plant is based on a medium solar radiation month, there are more heliostats than needed for those hot months.

Then, the prime aim is to redesign the power plant for a representative day of each of the hot months in order to compare it with the design month. After that, it will be possible to obtain the number of heliostats that have to be taken out of focus and where these heliostats are inside the field of heliostats.

Chapter 5 Results

During this chapter all the results obtained through the model described in Chapter 4 are presented. It includes comparisons and alternatives to take, in the following chapter, the optimum design of a direct steam solar-thermal power plant.

In order to take the ambient and radiation data it has been used an electronic source of radiation data (Agencia Andaluza de la Energía 2013). It has been decided to place the power plant at Gibraleón, Huelva, province of Andalusia , Spain. The reasons to choose this location are the amount of solar radiation it receives during the whole year, strong Chemical and Mechanical engineering industry and University in the surroundings, and the high unemployment rate of the province, which could be soften with this kind of projects.

As a reminder, shows a brief summary of the particularities of each design, which will be compared now on.

	Design 1	Design 2	Design 3	Design 4
No. of rows at the receiver	1	2	2	2
Reheating process	No	Yes	No	Yes
Opening sector at outer row of the receiver	No	No	Yes	Yes

Table 1: Characteristics of the four studied designs

5.1. Chosen day

As it was said at section 4.4, in order to design the power plant, one day must be chosen as reference. The chosen day is usually taken at a medium value for the solar radiation. This value is given during a day on spring or autumn. For the present project, March 20th has been the chosen day.

The previously cited electronic resource (Agencia Andaluza de la Energía 2013) helps to get the solar radiation values, which for the chosen day gives the distribution of the Figure 37.

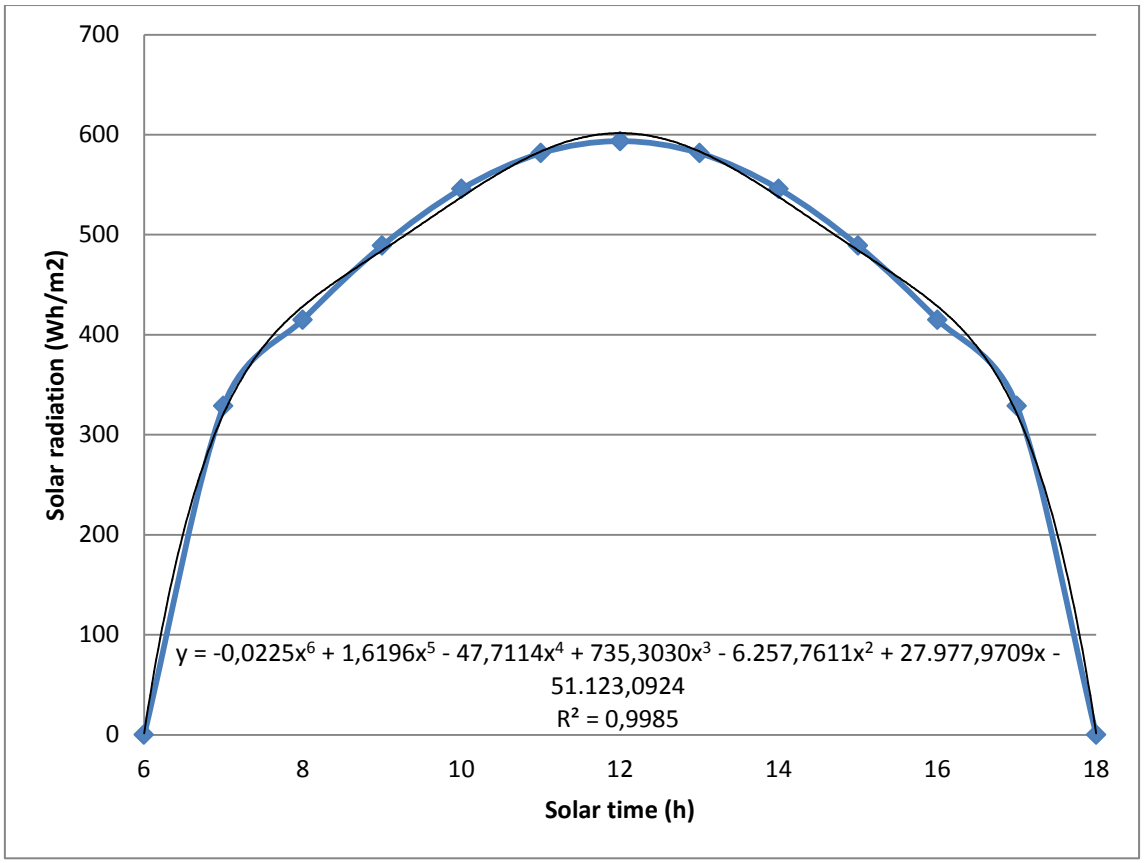

Figure 37: Direct radiation on March 20th. Source: (Agencia Andaluza de la Energía 2013)

Local time	Direct Radiation, Wh/m2
6	0
7	328,8
8	415
9	489
10	545,8
11	581,5
12	593,6
13	581,5
14	545,8
15	489

16	415
17	328,8
18	0
TOTAL	**5313.8**

Table 2: Solar radiation along March 20th. Source: (Agencia Andaluza de la Energía 2013)

Therefore, the treatment of the solar radiation will be as follows. As seen in equation (5.1), the intensity of solar radiation used is the average of the chosen day.

$$I_{ave} = \frac{\int I(t)}{t} \qquad (5.1)$$

$$I(t) = -0.0225 \cdot t^6 + 1.6196 \cdot t^5 - 47.7114 \cdot t^4 + 735.3030 \cdot t^3 - 6{,}257.7611 \cdot t^2 + \\ + 27{,}977.9709 \cdot t - 51{,}123.0924$$

Apart from that value, the cosine of theta described in equation (4.111) is taken at noon time. This is made as simplification based on the fact that this value is close to be the average of the whole day.

5.2. Thermal cycle

5.2.1. First design, regular Rankine cycle

In this section the thermal cycle will take values in order to see what the needs are in order to obtain a nominal power of 50MW. The first steps are to fix the pressure at which both condensation and evaporation will take place. Based on other projects and references, the high pressure value, at which steam is obtained for the turbine, is fixed at 60bar. To fix the condensation pressure, the ambient temperature of the location has to be taken into consideration. For this project, as previously said, the location is Huelva, at which a maximum temperature of 40ºC is reached. Due to this reason, the value taken for the temperature at the condenser is of 320K, 47ºC, at a pressure of 0.1 bars. Finally, the temperature at the outlet of the boiler is fixed at 873.15K, 600ºC. All the water properties given from this point have been obtained using an internet calculator (Glendoher Engineering 2009).

It has to be taken into account that the results of this section are the same for both design 1 and 2, where no reheating process is accomplished.

Taking the values given in the previous paragraph, both points, 1 and 3, which are the inlet of the pump and the inlet of the turbine respectively, can be described in thermal terms with their enthalpy.

$$h_1 = 191.9\ kJ/kg \qquad (5.2)$$

$$h_3 = 3658.75\ kJ/kg \quad (5.3)$$

Later on, the vapor quality will be obtained in order to describe point 4, the outlet of the turbine. For this purpose, as it has been shown in section 4.1.1 the entropy of the inlet of the turbine is also needed.

$$s_3 = 7169.21\ J/kgK \quad (5.4)$$

Taking into account the previous value, quality vapor at the outlet of the turbine for an isentropic expansion can be given using equation (4.2).

$$\chi_{4s} = 0.8692 \quad (5.5)$$

Using equations (4.3) and (4.4) the isentropic and non-isentropic enthalpies of the outlet of the turbine are shown below. As it was pointed at section 4.1.1, the net efficiency of the turbine was taken as 85%.

$$h_{4s} = 2271.8\ kJ/kg \quad (5.6)$$

$$h_4 = 2479.8\ kJ/kg \quad (5.7)$$

Having obtained these values, the problem faces the first limit, that is the vapor quality limit at the outlet of the turbine. This value is given by equation (4.5), and as a reminder, the maximum fraction of water droplets was 10%. As it can be seen below, this condition is completely fulfilled.

$$\chi_4 = 0.9562 \quad (5.8)$$

The last point of the cycle, which has not been described yet, is the outlet of the pump. Using equation **¡Error! No se encuentra el origen de la referencia.** this value is given as follows.

$$h_2 = 199.02\ kJ/kg \quad (5.9)$$

Having already shown all the points of the cycle, next step, and one of the most important for the description of it, is to calculate the total efficiency and the thermal power needed for the cycle. This step is based on equations (4.6), (4.7) and (4.8). It has to be taken into account that mechanical and electrical efficiencies together decreases the efficiency in about 1%.

$$\eta_{total} = 0.3353 \quad (5.10)$$

$$P_{thermal,cycle} = 149.11\ MW \quad (5.11)$$

Finally, the problem faces the need of calculating the mass flow rate needed to accomplish the given power. Using equation (4.9) this objective can be achieved. The obtained value for the mass flow rate of HTF per tube is given in equation (5.12).

$$\dot{m} = 0.175\ kg/s \tag{5.12}$$

5.2.2. Second design, Rankine cycle with reheat

The first thing that has to be taken as a reminder, is to point out that the temperature at point five, the outlet of the reheating stage, is a fixed value. For this design, points 1, 2 and 3 do not change any of their values. However, point 4 does change its enthalpy value. In this design, values for the isentropic and real enthalpy at point 4 are obtained as follows, using equation (4.10).

$$h_{4s} = 2761.49\ kJ/kg \tag{5.13}$$

$$h_4 = 2896.08\ kJ/kg \tag{5.14}$$

After this, the temperature and pressure for point 4 are shown in equations (5.15) and (5.16). This pressure is the pressure at which the reheating process takes place.

$$T_4 = 436K = 163ºC \tag{5.15}$$

$$P_4 = 6.7\ bar \tag{5.16}$$

Following the same process as in section 4.1.2, next step is to get the point 5. Having obtained the pressure at which reheating takes place and the temperature, the enthalpy at this point is shown at equation (5.17). The temperature, as previously explained, is obtained under an iteration process and for this description will be taken as fixed.

$$T_5 = 595K = 322ºC \tag{5.17}$$

$$h_5 = 3690.06\ kJ/kg \tag{5.18}$$

In contrast, for the design 4, the properties of point five are given in equations (5.19) and (5.20). All the previous results until this paragraph are valid for both design 2 and 4.

$$T_5 = 873K = 600ºC \tag{5.19}$$

$$h_5 = 3700.00\ kJ/kg \tag{5.20}$$

Last point to be described is point 6. Again, the problem follows the same process as in the first design for point 4, but using equations (4.11), (4.12), (4.13) and (4.14). In this case, vapor quality and enthalpy at point 6 are shown in equations (5.21) and (5.22).

$$\chi_6 = 1.08 \tag{5.21}$$

$$h_6 = 2765.4\ kJ/kg \tag{5.22}$$

Furthermore, the previous properties in te case of the two-row receiver with an opening sector are as seen in equations (5.23) and (5.24).

$$\chi_6 = 1.07 \quad (5.23)$$

$$h_6 = 2770.3\ kJ/kg \quad (5.24)$$

As it can be seen in equations (5.21) and (5.23), the value of the vapor quality is higher than 90%. This means that there are water droplets at the outlet of the turbine but in an allowed quantity. Thereby, the condition of the maximum fraction of water droplets at the outlet of the turbine is fulfilled.

Next step, as said in the previous section, is the most descriptive variables where the total efficiency of the cycle and the thermal power are obtained. The power cycle calculated again using equation (4.7), while the total efficiency is taken from equation (4.15). These values are given in equations (5.25) and (5.26).

$$\eta_{total} = 0.3957 \quad (5.25)$$

$$P_{thermal,cycle} = 127.63\ MW \quad (5.26)$$

In the case of the fourth design, the same values are given as seen in (5.27) and (5.28).

$$\eta_{total} = 0.3913 \quad (5.27)$$

$$P_{thermal,cycle} = 127.77\ MW \quad (5.28)$$

Finally, as in the previous section, the mass flow rate of HTF at each tube for design 2, using equation (4.15), can be observed in equation (5.29).

$$\dot{m} = 0.135\ kg/s \quad (5.29)$$

Meanwhile, for design 4 the mass flow rate is given in equation (5.30).

$$\dot{m} = 0.116\ kg/s \quad (5.30)$$

5.3. Design of the Receiver Geometry

In section 4.2 it is described the geometry of the receiver. For the present project, the receiver is formed by 12 panels. As in that section and in section 4.3 was explained, the HTF passes through the receiver dividing it into three different stages. Thereby these stages are assigned to the 12 different panels the receiver has. This division was based on the difference of enthalpy in each of the stages. In equations (5.31), (5.32) and (5.33) these enthalpies are given and correspond to the values of Figure 25.

$$h_{eco} = 1014.38\ kJ/kg \quad (5.31)$$

$$h_{boil} = 1570.90\ kJ/kg \quad (5.32)$$

$$h_{sh} = 874.45\ kJ/kg \quad (5.33)$$

According to the previous data, the panels can be divided into the different stages as shown in equations (4.17). This is done in equations (5.34), (5.35) an (5.36). It has to be taken into account that, as explained in section 4.2, the HTF is divided into two at the entrance of the receiver. This makes the problem to follow the calculations for only one side of the receiver since the other will be completely symmetrical.

$$N_{panels,ec} = 1.76 \quad (5.34)$$

$$N_{panels,boil} = 2.72 \quad (5.35)$$

$$N_{panels,sh} = 1.52 \quad (5.36)$$

It is easy to observe that the stage which needs more energy is the boiling stage. Both the enthalpy of that stage and the number of panels it occupies are the highest of the three.

After this, the same thing is done for the tube length each stage occupies. This length is the distance that a water molecule, whatever its physical state is, move along the receiver from the entrance to the exit. This helps to calculate the heat transfer along the tubes during the different stages, as described with equations (4.18) and (4.19). In equations (5.37), (5.38) and (5.39) the tube lengths of each stage are given.

$$L_{ec} = 21.11\ \text{m} \quad (5.37)$$

$$L_{boil} = 32.69 \quad (5.38)$$

$$L_{sh} = 18.20 \quad (5.39)$$

5.4. Heat Transfer at the receiver

This point is the result of the described process in sections 4.2.1, 4.2.2, 4.2.3 and 4.3.1. Altogether, the heat transfer needed to achieve the desired power and the heat losses due to convection, will give the total heat that will be needed to overcome by solar radiation.

5.4.1. First design, one-row receiver

For the first design all the parameters can be obtained without using section 4.3.2, where radiation losses are explained.

In order to obtain the results, there are several intermediate steps to take. These steps are to obtain formulae for the specific heat, density, viscosity, thermal conductivity for the HTF and thermal conductivity for the material which the tubes are made of, depending on the temperature.

The metals for the tubes are obtained from *Simulation of an integrated steam generator for solar tower* (Ben-Zvi, Epstein and Segal 2011). For the tubes whose temperature does not reach 510ºC, 783K, the chosen material is a carbon steel, SA-192, due to temperature is its limit and a yield strength of 180MPa. On the other hand, for the tubes whose temperature is higher than the previous limit, the metal chosen is a stainless steel called SA-213TP304H, which has a yield strength of 206MPa and an upper limit temperature of 760ºC, 1033K. Figure 38 and Figure 39 show the thermal conductivity for these metals.

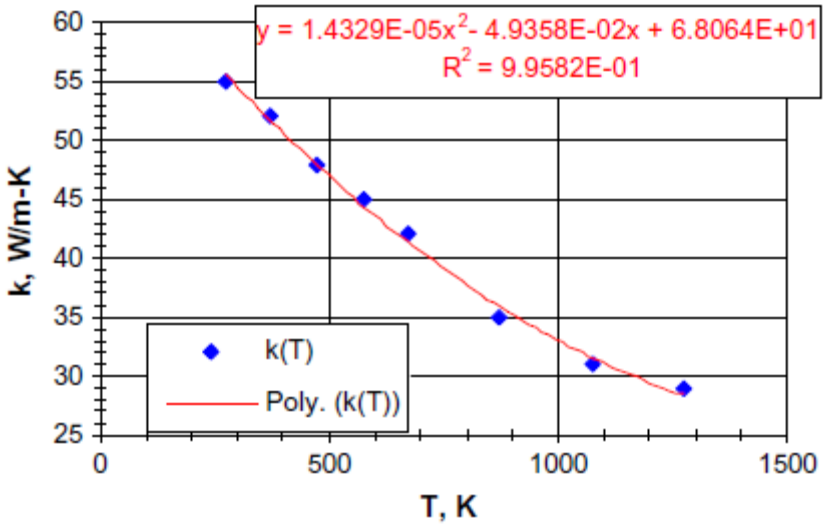

Figure 38: Thermal conductivity vs. temperature for the SA-192. Source: Ben-Zvi, 2012

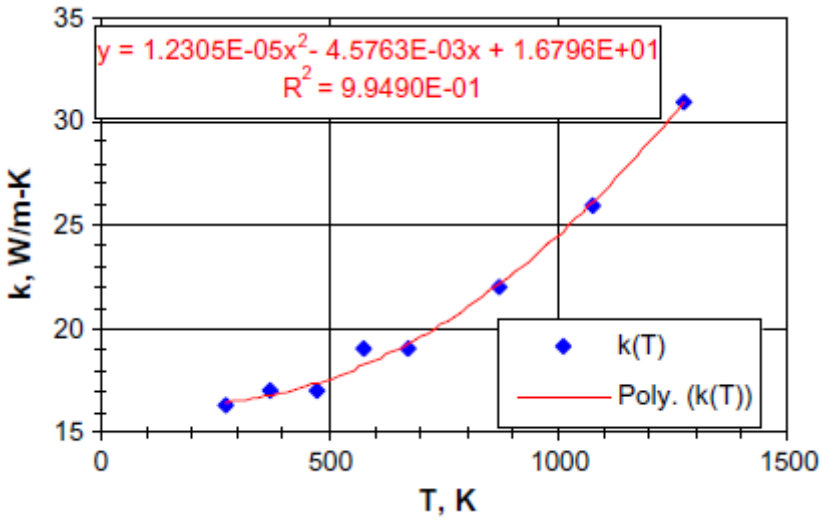

Figure 39: Thermal conductivity vs. temperature for the SA-213TP304H. Source: Ben-Zvi, 2012

Figure 40 and Figure 41 show the relations of the thermal properties previously described for the HTF at the pressure receiver pressure. Only the economizer and superheating stages appear in these images due to thermal properties for the boiling stage are constant since HTF temperature does not change. These relations have been obtained using an website resource for thermodynamic properties of water (Glendoher Engineering 2009).

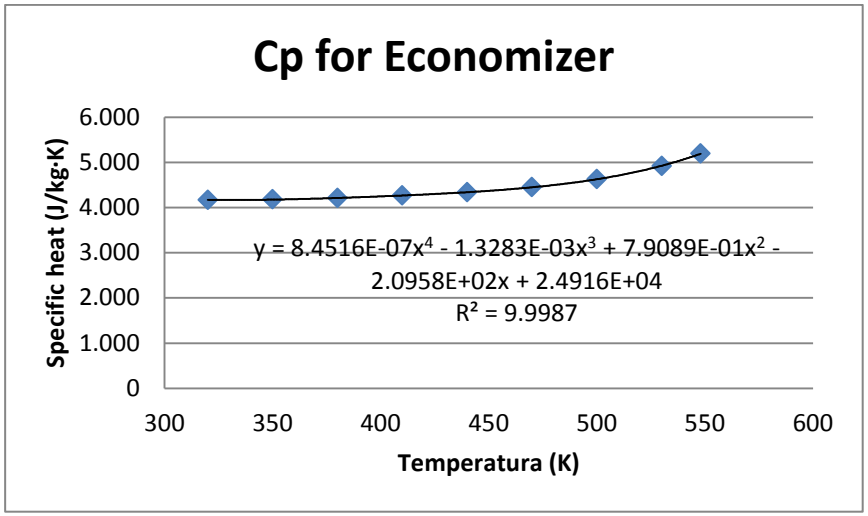

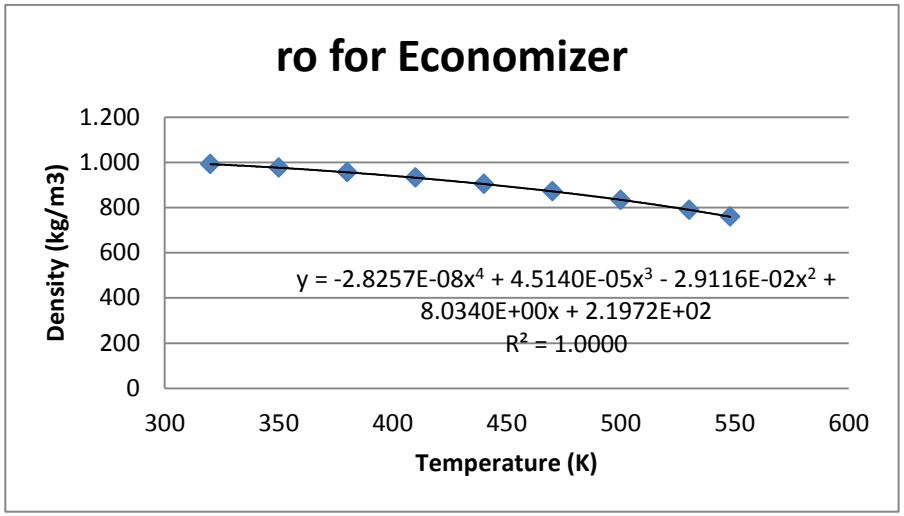

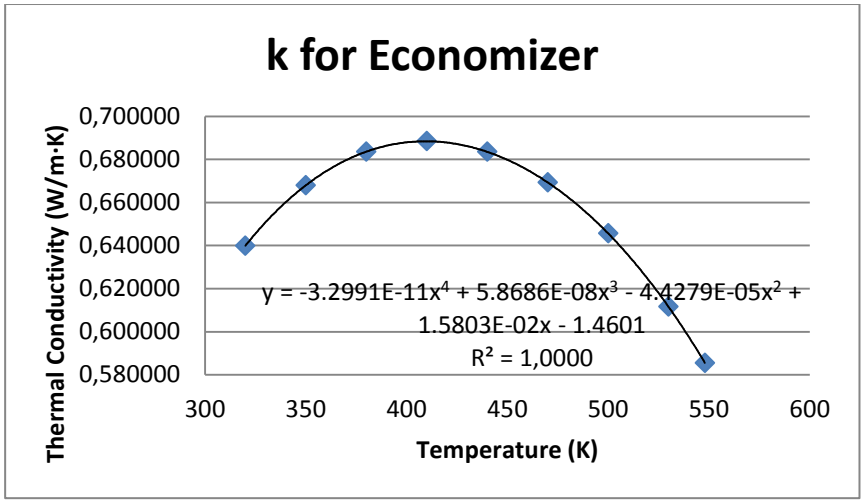

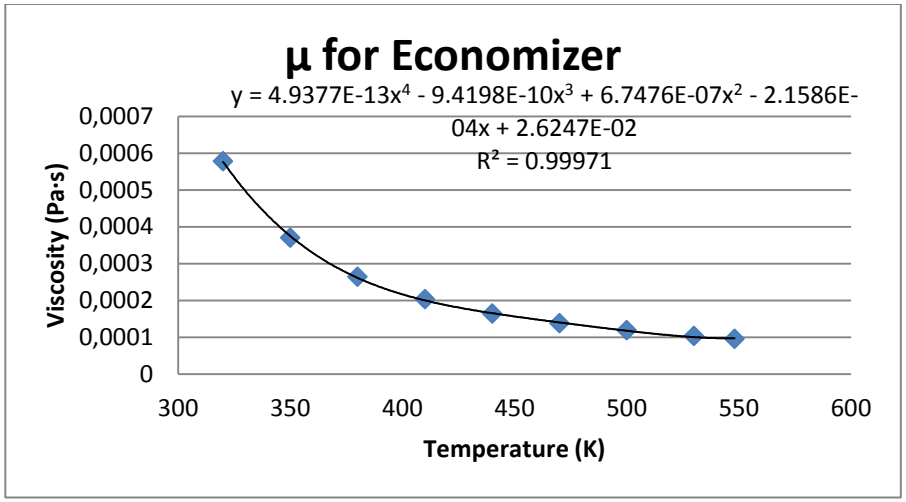

Figure 40: HTF properties for the Economizer stage

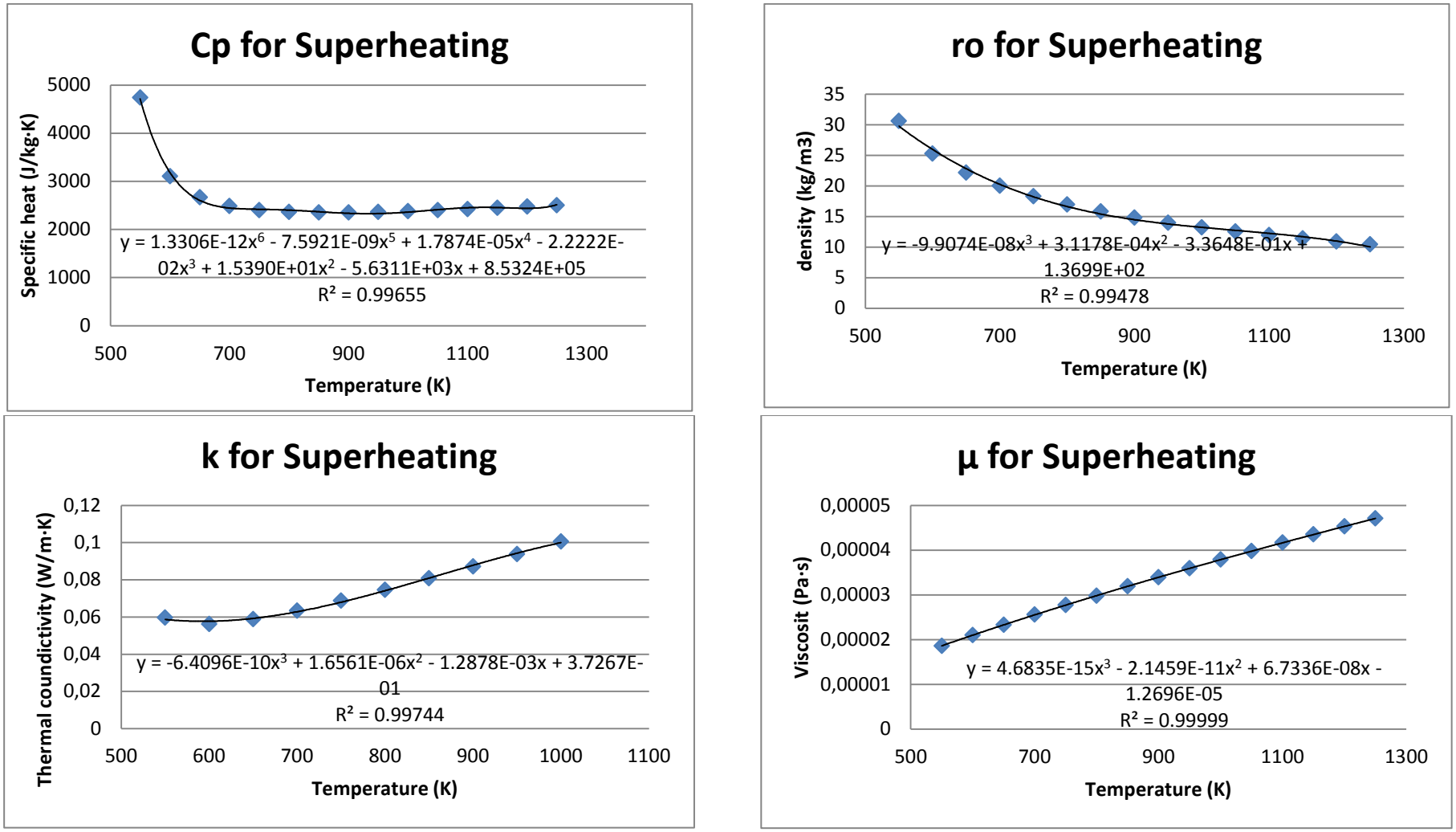

Figure 41: HTF properties for the Superheating stage

In Table 3 the receiver is divided into the stages previously described. The values are given for each tube. The vapor pressure for equation (4.29) is obtained using a tool in the internet (DDBST GmbH 2012) as well as the air properties for convection losses (Wischnewski 2012)

Panel	Stage	q_{conv} (kW)	q (kW)	q_{rad} (kW)	$T_{tube,ext}$ (K)
1	Liq. Water	4.91	100.83	105.74	452.82
2	Liq. Water	6.02	85.86	91.88	553.86
2	Liq. Water+Steam	2.01	45.12	47.13	568.34
3	Liq. Water+Steam	8.36	187.35	195.86	568.34
4	Liq. Water+Steam	8.36	187.35	195.86	568.35
5	Liq. Water+Steam	4.04	90.58	94.62	568.35
5	Steam	6.37	69.97	76.34	701.73
6	Steam	17.72	106.66	124.38	881.72

Table 3: Heat transfer and external tube temperature distribution per stage and panel for design 1

In order to get the total values for the whole receiver each row of Table 3 must be multiplied into the number of tubes per panel and into two, in order to take into account both sides of the receiver. These total values appear in Table 4.

q_{conv} (MW)	q (MW)	q_{rad} (MW)
14.56	220.77	234.81

Table 4: Total Heat transfer at one-row receiver

In the previous tables, q_{rad} is the total heat that has to be overcome by solar radiation in order to meet the plant power, shown in equation (4.62). Another important issue in order to maintain the integrity of the installation, in particular the receiver, is to keep the tube temperature under the limit that was described in previous paragraphs. This limit was established at 1033K, way higher than the maximum tube temperature at the end of superheating stage, Figure 42.

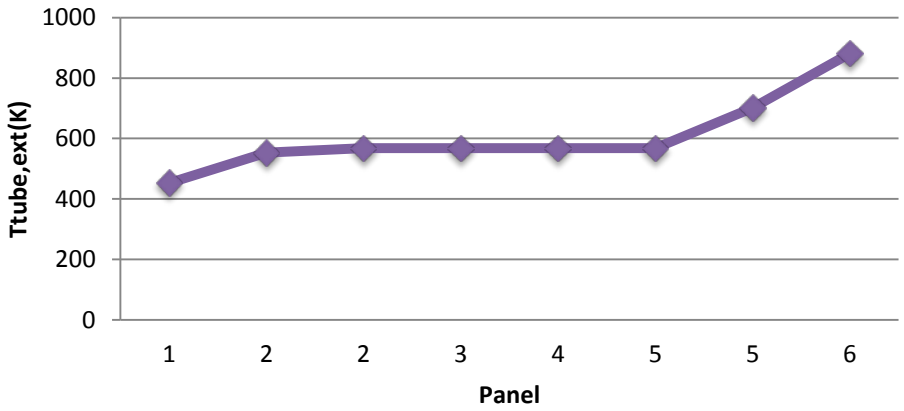

Figure 42: External Tube temperature evolution along the one-row receiver.

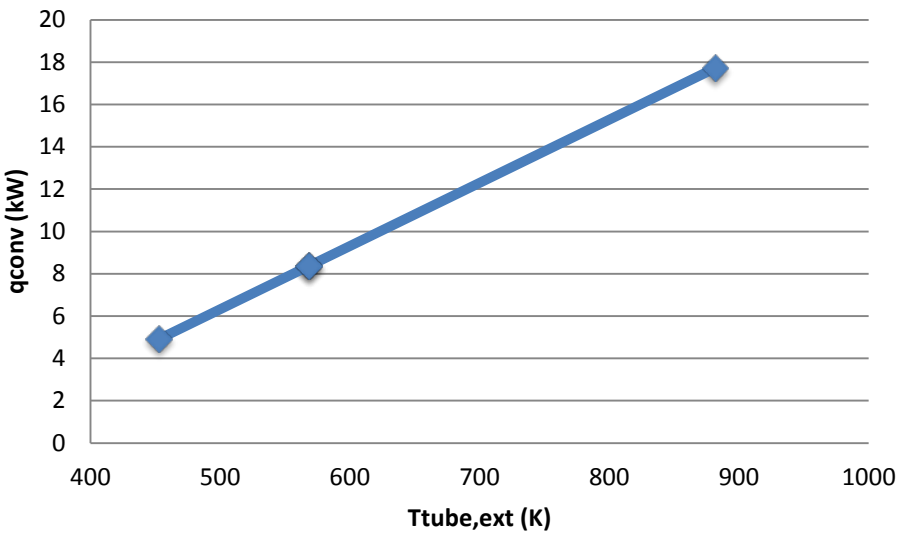

Figure 43: Correlation between external tube temperature and convection losses.

5.4.2. Second design, two-row receiver with reheating

The second design follows a similar model but not equal. The receiver of the second design has a reheating stage which is a reflow of the steam that already left the receiver, when this has been expanded to a certain pressure. So that, this expanded steam passes through a second row of tubes, which can be taken as a second receiver, with the same configuration of tubes and panels. For this design SA-192 steel is considered for the inner row in which reheating process takes place. This gives a cheaper receiver than if this row was made of SA-213TP304H steel.

Apart from that, the mass flow rate is lower than in the first design. This makes the heat needed at each tube of the first row to be lower than in the design of the one-row receiver. However, the relation of the thermal properties of the HTF and its temperature does not vary. Furthermore, it has to be described the behavior of these properties with temperature at reheating pressure using the same resource as in section 5.4.1 (Glendoher Engineering 2009), Figure 44.

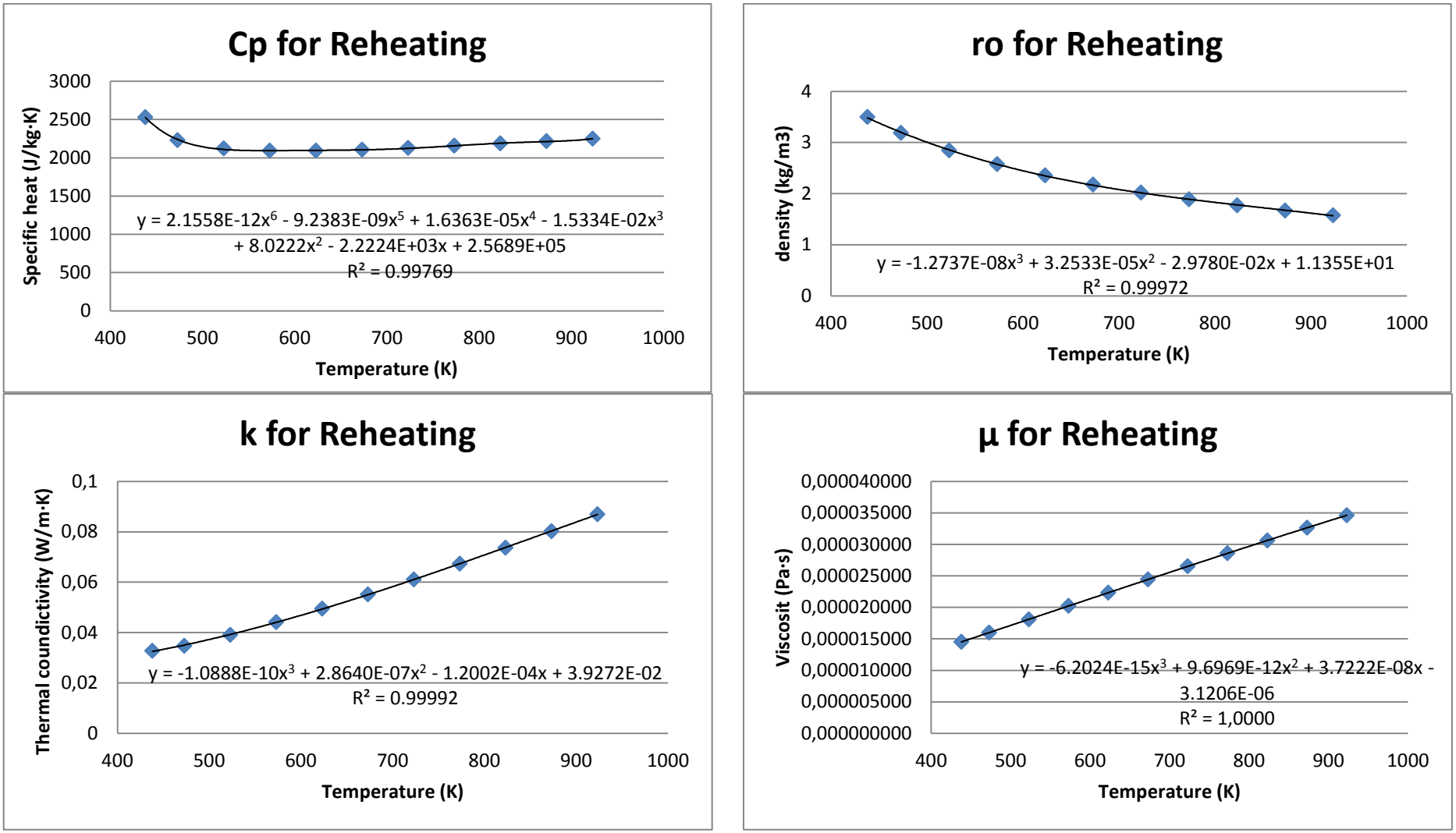

Figure 44: HTF properties for the Reheating stage

In this case, the solar radiation plays an important role to obtain the thermal behavior of the receiver. The heat needed at the first row is easy to get since it follows the model as the first design. But the thermal conditions at the second row depend on the first row. As already explained in section 4.3.2.2, the radiation losses are calculated following iterations. This iteration also gives the temperature of the tubes and heat at those tubes.

	First row (outer)					Second row (inner), Reheating			
Panel	**Stage**	**q_{conv} (kW)**	**q (kW)**	**q_{rad} (kW)**	**$T_{tube,ext}$ (K)**	**q_{conv} (kW)**	**q (kW)**	**q_{rad} (kW)**	**$T_{tube,ext}$ (K)**
1	Liq. Water	5.03	78.85	83.88	456.84	4.38	5.32	9.70	453.12
2	Liq. Water	6.13	67.58	73.71	558.98	3.68	4.63	8.31	468.71
2	Liq. Water+ Steam	2.12	35.30	37.42	583.98	1.29	3.05	4.34	486.29
3	Liq. Water+ Steam	8.82	146.60	155.42	583.98	6.36	11.67	18.03	519.40
4	Liq. Water+ Steam	8.82	146.60	155.42	583.98	7.48	10.55	18.03	557.05
5	Liq. Water+ Steam	4.27	70.87	75.14	583.98	3.91	4.81	8.72	577.22
5	Steam	6.06	55.01	61.07	681.41	4.28	2.40	6.68	583.92
6	Steam	17.70	86.15	103.85	881.07	8.47	2.13	10.60	590.04

Table 5: Heat transfer and External temperature of the tubes distribution per stage and panel for two-row receiver with reheating cycle

As it can be observed in Table 5, the second row, that is the inner one, receives less energy than the outer one. That is the reason why the steam passing through the tubes that form the inner row does not reach the final temperature of the superheating stage of the outer row. Obviously, this all happens because the view factor of the inner row with the surroundings, which is the media that radiates energy, is lower than the view factor of the outer row with that media, giving big convection losses due to the high external temperature of the tubes.

Apart from that, it is easy to see that again the model respects the temperature limit of the temperature that was at 1033K, Figure 45.

First row (outer)			Second row (inner), Reheating			Total		
q_{conv} (MW)	**q (MW)**	**q_{rad} (MW)**	**q_{conv} (MW)**	**q (MW)**	**q_{rad} (MW)**	**q_{conv} (MW)**	**q (MW)**	**q_{rad} (MW)**
14.85	173.11	187.97	10.04	11.23	21.27	24.90	184.34	209.24

Table 6: Total Heat transfer at two-row receiver with reheating cycle

Both in Table 5 and Table 6 q_{rad} is the total energy due to radiation that has to be overcome in order to get the optimum performance of the cycle.

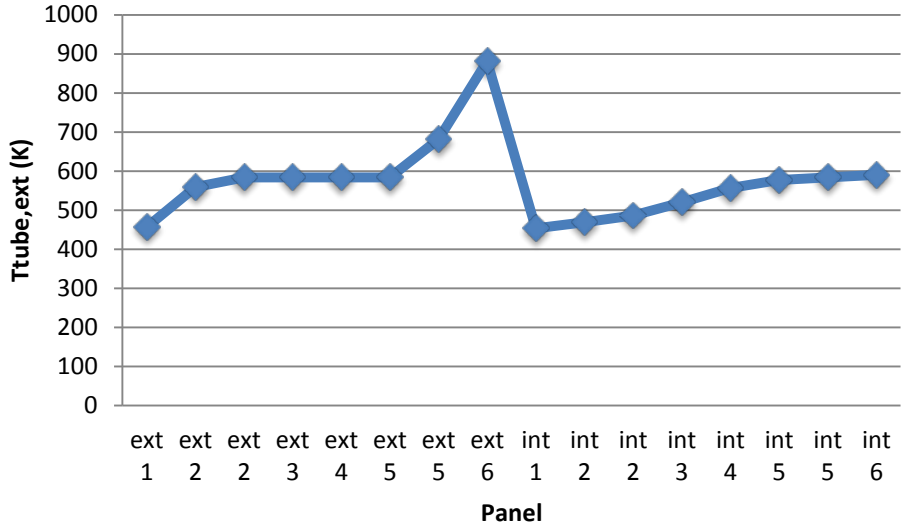

Figure 45: External Tube temperature evolution along the two-row receiver

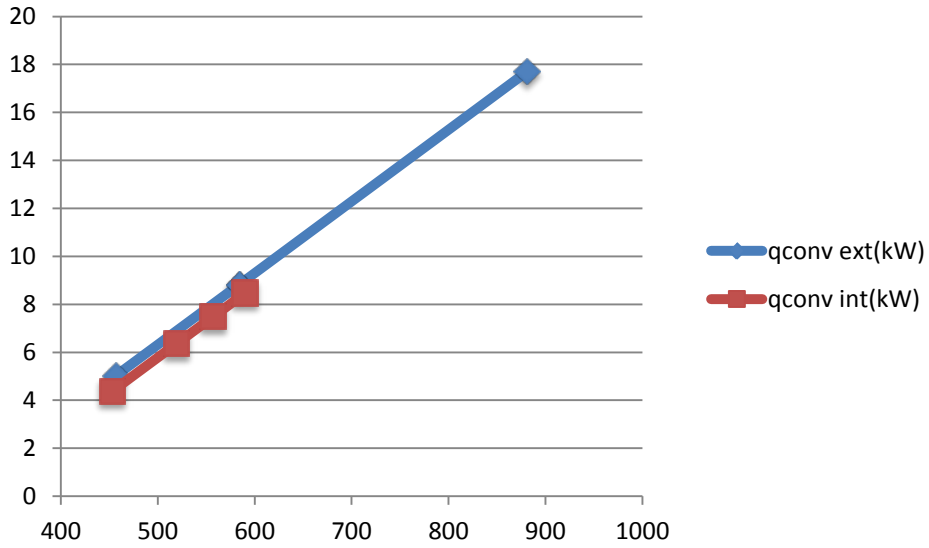

Figure 46: Correlation between external tube temperature and convection losses.

5.4.3. Third design, two-row receiver with opening sector, without reheating

This third case is the one described in section 4.2, which is based on Ben-Zvi's work. It consists of two rows of tubes. The inner one covers all the circumference of the receiver. However, the outer row only covers 5 panels over 6 panels that the receiver has in each of the sides. This design introduces an opening in the north face of the receiver which helps to get the optimum temperature for the cycle. Table 7 shows how the heat transfer behaves in this design.

		First row (outer)				Second row (inner)			
Panel	**Stage**	**q_{conv} (kW)**	**q (kW)**	**q_{rad} (kW)**	**$T_{tube,ext}$ (K)**	**q_{conv} (kW)**	**q (kW)**	**q_{rad} (kW)**	**$T_{tube,ext}$ (K)**
1	Liq.	4.73	90.61	95.34	446.68	7.53	3.62	11.15	558.57

	Water								
2	Liq. Water	7.74	97.45	105.19	557.93	7.60	4.39	11.99	570.98
2	Liq. Water+ Steam	0.34	6.47	6.81	589.78	0.31	0.49	0.80	582.40
3	Liq. Water+ Steam	8.99	169.50	178.49	589.78	8.95	11.90	20.85	606.30
4	Liq. Water+ Steam	8.99	169.50	178.49	589.78	9.86	10.99	20.85	635.23
5	Liq. Water+ Steam	8.99	169.50	178.49	589.98	10.69	10.16	20.85	663.30
6	Steam	-	-	-	-	17.17	104.38	121.55	881.55

Table 7: Heat transfer and External temperature of the tubes distribution per stage and panel for two-row receiver with opening sector without reheating cycle

Meanwhile, in Table 8 the total heat transfer for this receiver is shown.

First row (outer)			Second row (inner)			Total		
q_{conv} (MW)	q (MW)	q_{rad} (MW)	q_{conv} (MW)	q (MW)	q_{rad} (MW)	q_{conv} (MW)	q (MW)	q_{rad} (MW)
10.02	177.16	187.19	15.65	36.77	52.42	25.68	213.94	239.61

Table 8: Total Heat transfer at two-row receiver with opening sector but without reheating cycle

It also can be observed that the tube temperature is under the limit. In this case, Figure 47, there is a little decrease when changing from the outer to the inner row due to the different type of tube material in each row.

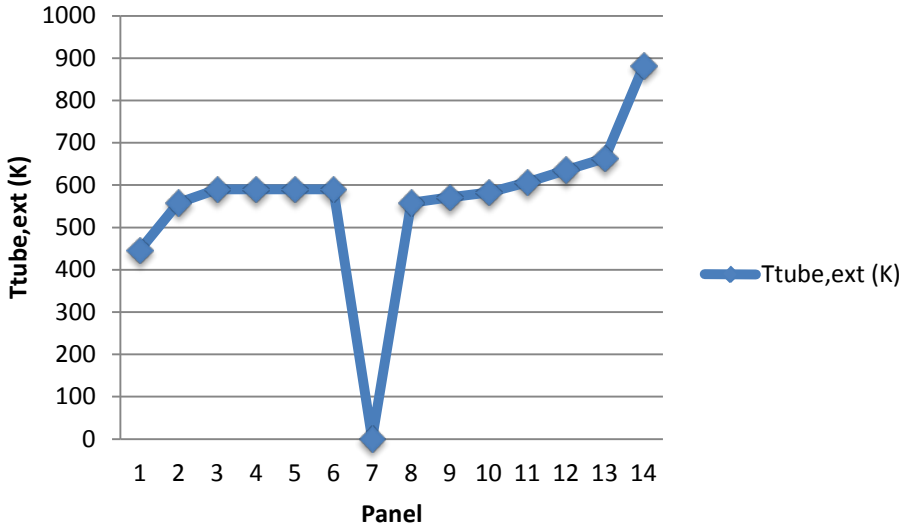

Figure 47: External Tube temperature evolution along the two-row receiver with opening sector

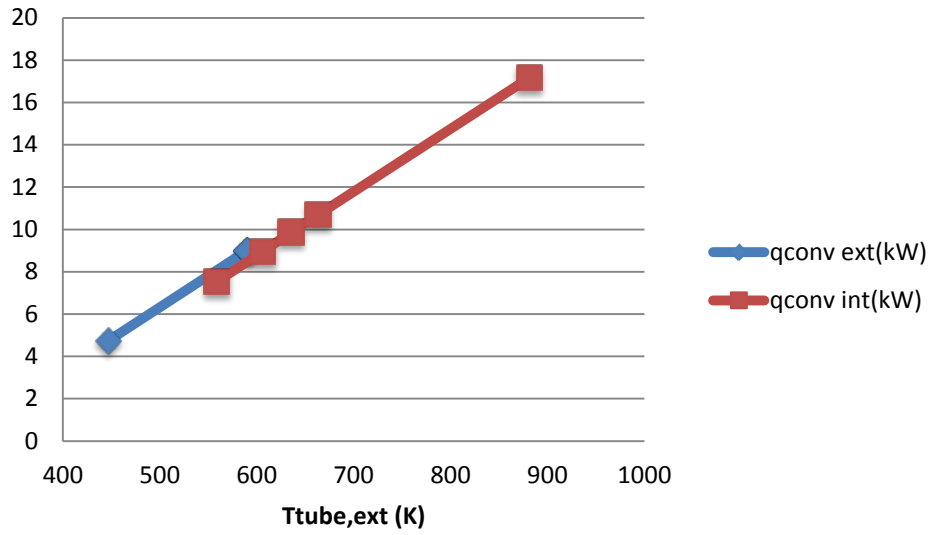

Figure 48: Correlation between external tube temperature and convection losses.

5.4.4. Fourth design, two-row receiver with opening sector and reheating

As a new step, this design is based on Ben-Zvi's. However, it introduces a reheating cycle. In Table 9 the summary of the heat transfer at this receiver is shown in the same format as in the previous designs.

		First row (outer)				Second row (inner), Reheating			
Panel	**Stage**	**q_{conv} (kW)**	**q (kW)**	**q_{rad} (kW)**	**$T_{tube,ext}$ (K)**	**q_{conv} (kW)**	**q (kW)**	**q_{rad} (kW)**	**$T_{tube,ext}$ (K)**
1	Liq. Water	5.77	82.49	88,26	481.68	4.50	5.98	10.48	457.01
2	Liq. Water	8.90	43.93	52.83	568.60	2.29	2.75	5.04	471.09
2	Liq. Water+ Steam	4.73	80.94	85.67	585.23	3.09	6.87	9.96	500.10
3	Liq. Water+ Steam	8.86	151.57	160.43	585.23	7.08	11.57	18.65	543.75
4	Liq. Water+ Steam	6.52	111.59	118.11	585.23	5.95	7.78	13.73	577.31
4	Steam	3.18	29.49	32.67	692.47	2.21	1.81	4.02	587.13
5	Steam	18.81	69.95	88.76	918.35	8.54	2.38	10.92	592.63
6	Steam	-	-	-	-	17.10	104.38	121.48	879.22

Table 9: Heat transfer and External temperature of the tubes distribution per stage and panel for two-row receiver with opening sector with reheating cycle

As well as in the previous designs, Table 10 collects the total heat transfer data for this design.

First row (outer)	Second row (inner),	Total

			Reheating					
q_{conv} (MW)	q (MW)	q_{rad} (MW)	q_{conv} (MW)	q (MW)	q_{rad} (MW)	q_{conv} (MW)	q (MW)	q_{rad} (MW)
14.31	143.63	157.79	12.79	36.17	48.96	27.10	179.80	206.89

Table 10: Total Heat transfer at two-row receiver with opening sector but with reheating cycle

In this design, Figure 49 shows how the external tube temperature of the last panel, 15, rises much comparing to the previous ones due to it is a sector where only one row of tubes is present.

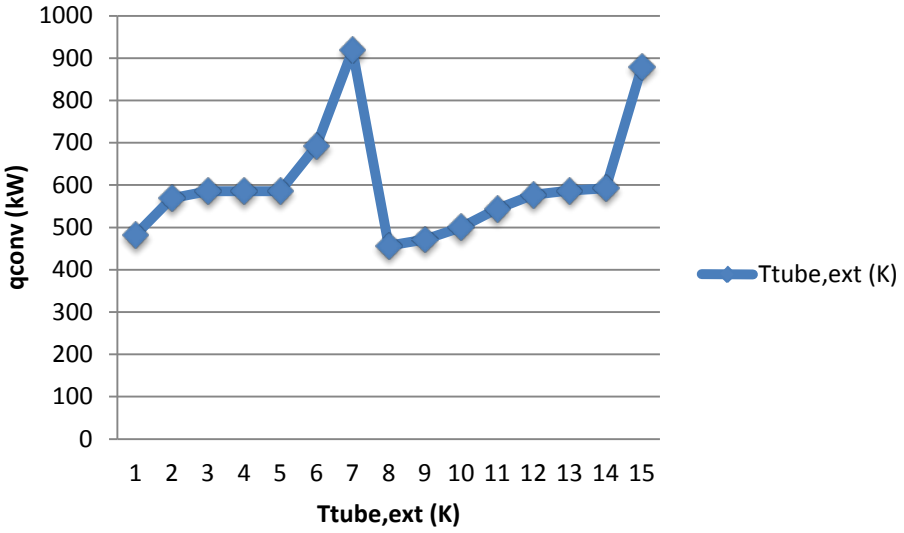

Figure 49: External Tube temperature evolution along the two-row receiver with opening sector

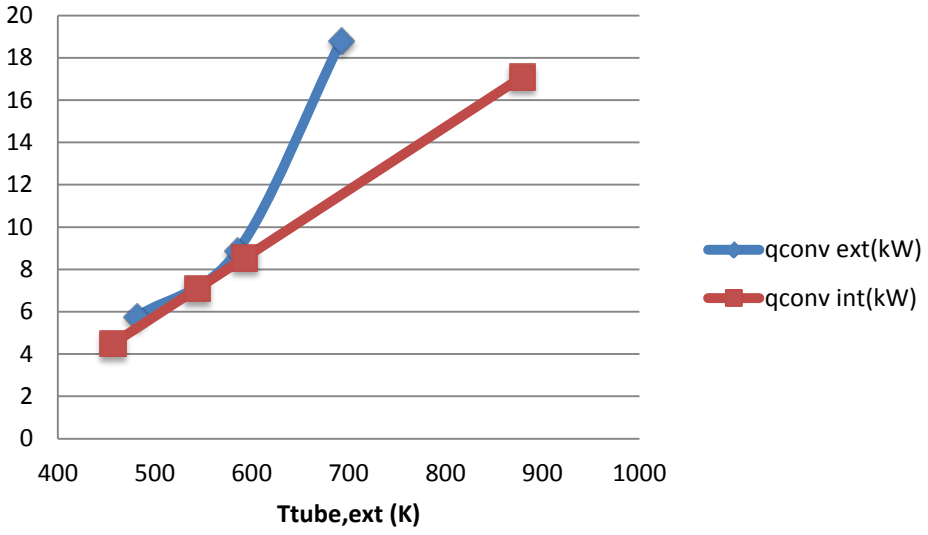

Figure 50: Correlation between external tube temperature and convection losses.

Figure 43, Figure 46, Figure 48 and Figure 50 show the correlation between the external tube temperature and the convection losses. This relation is linear but in the last design in a part where there is a change of tube material.

5.5. Load losses

5.5.1. Load losses at the receiver

This part uses section 4.4.1 in order to obtain the load losses at the receiver. As it was explained in the cited section, the devices installed at the receiver based in Figure 24 are two elbows of 45º and a sudden expansion and a sudden contraction due to the entrance and exit to the HTF collectors between panels. The used elbows are flanged, 90º regular. According to Table 11, the loss coefficient for this kind of elbow is 0.5 if the dimensions of the receiver in section 4.2 are followed.

	Nominal diameter, in								
	Screwed				Flanged				
	½	1	2	4	1	2	4	8	20
Valves (fully open):									
Globe	14	8.2	6.9	5.7	13	8.5	6.0	5.8	5.5
Gate	0.30	0.24	0.16	0.11	0.80	0.35	0.16	0.07	0.03
Swing check	5.1	2.9	2.1	2.0	2.0	2.0	2.0	2.0	2.0
Angle	9.0	4.7	2.0	1.0	4.5	2.4	2.0	2.0	2.0
Elbows:									
45° regular	0.39	0.32	0.30	0.29					
45° long radius					0.21	0.20	0.19	0.16	0.14
90° regular	2.0	1.5	0.95	0.64	0.50	0.39	0.30	0.26	0.21
90° long radius	1.0	0.72	0.41	0.23	0.40	0.30	0.19	0.15	0.10
180° regular	2.0	1.5	0.95	0.64	0.41	0.35	0.30	0.25	0.20
180° long radius					0.40	0.30	0.21	0.15	0.10
Tees:									
Line flow	0.90	0.90	0.90	0.90	0.24	0.19	0.14	0.10	0.07
Branch flow	2.4	1.8	1.4	1.1	1.0	0.80	0.64	0.58	0.41

Table 11: Secondary loss coefficients. Source: (White 2011)

For the sudden expansion equation (5.42) is used and for the sudden contraction equation (5.43). Both expressions have been obtained from *Fluid Mechanics* (White 2011). The diameter of the collector is 38 cm as described in section 4.2.

$$k_{se} = \left(1 - \frac{d^2}{D^2}\right) = 0.99 \qquad (5.40)$$

$$k_{sc} = 0.42\left(1 - \frac{d^2}{D^2}\right) = 0.42 \qquad (5.41)$$

If the Colebrook equation is used, (4.106), and the iteration of Annex V - **,** the value for the friction coefficient is established at around 0.02 for all the tubes. It has to be taken into account that the roughness of a stainless steel is 0.002mm as shown in Table 12.

Material	Condition	ϵ ft	ϵ mm	Uncertainty, %
Steel	Sheet metal, new	0.00016	0.05	± 60
	Stainless, new	0.000007	0.002	± 50
	Commercial, new	0.00015	0.046	± 30
	Riveted	0.01	3.0	± 70
	Rusted	0.007	2.0	± 50
Iron	Cast, new	0.00085	0.26	± 50
	Wrought, new	0.00015	0.046	± 20
	Galvanized, new	0.0005	0.15	± 40
	Asphalted cast	0.0004	0.12	± 50
Brass	Drawn, new	0.000007	0.002	± 50
Plastic	Drawn tubing	0.000005	0.0015	± 60
Glass	—	Smooth	Smooth	
Concrete	Smoothed	0.00013	0.04	± 60
	Rough	0.007	2.0	± 50
Rubber	Smoothed	0.000033	0.01	± 60
Wood	Stave	0.0016	0.5	± 40

Table 12: Roughness for different materials. Source: (White 2011)

Introducing all the previous values into the Bernoulli equation (4.105), the load loss for the receiver is as shown in Table 13.

Panel	HTF state	ΔP_{rec} (kPa)
1	Liq. Water	3.13
2	Liq. Water	2.84
2	Liq. Water+Steam	2.90
3	Liq. Water+Steam	29.02
4	Liq. Water+Steam	62.88
5	Liq. Water+Steam	49.84
5	Steam	69.37
6	Steam	165.27

Table 13: Load losses per panel and stage for the one-row design

For the two-row configuration the model is the same as for the one-row configuration. However, the number of tubes is doubled.

Panel	HTF state outer row	ΔP_{rec} (kPa), outer row	HTF state inner row	ΔP_{rec} (kPa), inner row
1	Liq. Water	1.86	Steam	506.89
2	Liq. Water	1.69	Steam	419.84
2	Liq. Water+Steam	1.72	Steam	196.56
3	Liq. Water+Steam	17.19	Steam	574.65
4	Liq. Water+Steam	37.25	Steam	626.05
5	Liq. Water+Steam	29.52	Steam	375.19
5	Steam	41.10	Steam	403.83
6	Steam	97.92	Steam	690.69

Table 14: Load losses per panel and stage for the two-row design with reheating, second design

In Table 15 the same table is shown for the design where there is no reheating process but the receiver counts with the opening sector in the outer row, design three.

Panel	HTF state outer row	ΔP_{rec} (kPa), outer row	HTF state inner row	ΔP_{rec} (kPa), inner row
1	Liq. Water	3.12	Steam	97.30
2	Liq. Water	3.41	Steam	96.06
2	Liq. Water+Steam	0.86	Steam	19.34
3	Liq. Water+Steam	20.27	Steam	103.82
4	Liq. Water+Steam	50.64	Steam	110.62
5	Liq. Water+Steam	81.00	Steam	117.89
6		-	Steam	160.55

Table 15: Load losses per panel and stage for the two-row design with opening sector but without reheating, third design

After this, Table 16 shows the same data for the two-row receiver with reheating and opening sector, fourth design.

Panel	HTF state outer row	ΔP_{rec} (kPa), outer row	HTF state inner row	ΔP_{rec} (kPa), inner row
1	Liq. Water	1.40	Steam	379.5
2	Liq. Water	0.89	Steam	379.56
2	Liq. Water+Steam	3.97	Steam	217.41
3	Liq. Water+Steam	20.29	Steam	251.20
4	Liq. Water+Steam	27.92	Steam	448.71
4	Steam	18.36	Steam	193.84
5	Steam	70.86	Steam	516.18
6		-	Steam	69.60

Table 16: Load losses per panel and stage for the two-row design with reheating and opening sector, fourth design

To sum up, the total load loss due to secondary losses is shown in Table 17.

ΔP_{rec} first design (MPa)	ΔP_{rec} second design, (MPa)	ΔP_{rec} third design, (MPa)	ΔP_{rec} fourth design, (MPa)
0.38	4.02	0.86	2.60

Table 17: Comparison total load loss at the receiver

5.5.2. Load losses at the tower

In the tower, the device distribution is quite different than at the receiver. There are also two elbows, one at the outlet of the pump and another one at the inlet of the receiver. There is a sudden contraction at the outlet of the tower, and a tee with valve which is used as by-pass for

the receiver. In this case the diameter of the tower is taken as 50 cm, 19.68 inches. Using Table 11, the secondary loss coefficients are shown in Table 18.

Elbow (Flanged, 90º regular)	Tee (Flanged, line flow)	Valve (Flanged, Globe)
0.21	0.07	5.5

Table 18: Secondary loss coefficients for the tower

For the tower, stainless steel is used again. This means that the roughness is 0.002mm. Mixing the previous data with Bernoulli equation, (4.107), where the tower height is taken as 138m, the losses at the tower are as shown in

ΔP_{tow} first design (MPa)	ΔP_{tow} second design (MPa)	ΔP_{tow} third design (MPa)	ΔP_{tow} fourth design (MPa)
95.21	56.40	95.21	42.03

Table 19: Load losses at the tower

The losses at the tower are clearly higher for the one-row design than for the two-row design. This comes, as seen in section 5.2, from the fact that the flow in the two-row configuration is slightly lower than in the one-row design.

5.5.3. Pumping Power

As seen in section 4.4.3, in order to get the pumping power needed, the total load loss must be obtained as well as a definition of the HTF flow. In Table 20 ΔP_{total} includes the needed compression of the HTF in order to pass from the condenser pressure to the boiler pressure.

	ΔP_{total} (MPa)	Q (m^3)	P_{pump} (MW)
Design 1	101.58	0.0445	4.52
Design 2	66.41	0.0343	2.27
Design 3	102.06	0.0445	4.54
Design 4	50.62	0.0296	1.50

Table 20: Total load losses, HTF flow at the pump and Pumping power

As it can be observed in Table 20, the load losses in the two-row receiver are lower as well as the flow. Thereby, the needed pumping power for the two-row model is half the pumping power for the one-row model.

5.6. Field of heliostats

As explained in section 4.6, the field of heliostats is divided in angular sectors according with the panel distribution of the receiver. This model has also been developed in Matlab. The code can be found in Annex VI - . It takes into account both design of the field of heliostats in section 4.6 and solar radiation angles explained in sections 2.4 and 4.4.

The outputs or results of this model are the number of heliostats needed in the field, the number of rings in the field according to the ring distribution explained in section 4.6, the radius of the rings, which will give the final extension of the field, and the average power of solar radiation that gets to the receiver.

As a reminder, 8 different stages have been obtained in the receiver according to the panel and physical state of the HTF. In those 8 stages, there are four, two pairs of stages, what means that those pairs are part of the same panel. If the issue is reduced to a tube, it is easier to see that that pair of stages mean that one stage is at the entrance of the tube, and the other one is at the end of the same tube. However, field is going to be divided in 6 sectors, always having into account that these figures are referred to the half of the receiver and the half of the field of heliostats due to symmetry. In order to get this reduction, (5.42) is used. This equation gives an average of the radiation that the tube must receive.

$$G_{sector} = \frac{G_{stage\ i} L_{tube,stage\ i} + G_{stage\ i+1} L_{tube,stage\ i+1}}{L_{tube}} \quad (5.42)$$

$$L_{tube} = L_{tube,stage\ i} + L_{tube,stag\ i+1} \quad (5.43)$$

In order to get the radiation power of each stage that gets the receiver, G, the systems of equations in sections 4.3.2.1 and 4.3.2.2 are used for one-row and two-row models respectively.

In Table 21 and Table 22 it can be observed the results of the model of the field of heliostats. For this project squared heliostats of 10m width are chosen.

Design 1					
Sector	G (MW)	Rings	Radius (m)	Area (hectare)	Heliostats
1	19.11	47	970.8	24.67	
2	25.30	56	1197.6	37.54	
3	29.50	63	1379.6	49.82	
4	29.26	66	1459.1	55.73	
5	20.56	57	1223.3	39.17	
6	15.73	51	1070.6	30.00	
7	15.49	50	1045.5	28.61	
8	20.53	57	1223.3	39.17	
9	29.34	66	1459.1	55.73	
10	29.27	63	1379.6	49.82	
11	25.01	56	1197.6	37.54	
12	18.86	48	995.6	25.95	
Total	**277.96**	-	-	**473.83**	**8994**

Table 21: Field of heliostats summary for the one-row receiver, first design

Design 2					
Sector	G (MW)	Rings	Radius (m)	Area (hectare)	Heliostats
1	14.21	40	800.0	16.75	
2	20.51	50	1045.5	28.61	
3	24.47	57	1223.3	39.17	
4	23.78	59	1275.0	42.55	
5	16.77	51	1070.6	30.00	

6	13.09	46	946.1	23.43	
7	12.87	45	921.5	22.23	
8	16.82	51	1070.6	30.00	
9	23.81	59	1275.0	42.55	
10	24.29	57	1223.3	39.17	
11	20.95	51	1070.6	30.00	
12	14.65	42	848.3	18.83	
Total	**226.22**	-	-	**363.37**	**7253**

Table 22: Field of Heliostats summary for the two-row design with reheating cycle, second design

Design 3					
Sector	G (MW)	Rings	Radius (m)	Area (hectare)	Heliostats
1	21.43	50	1045.5	28.61	
2	27.87	59	1275.0	42.55	
3	27.74	61	1327.1	46.10	
4	27.59	64	1406.0	51.75	
5	17.39	52	1095.8	31.43	
6	15.18	50	1045.5	28.61	
7	14.96	49	1020.5	27.26	
8	17.41	52	1095.8	31.43	
9	27.67	64	1406.0	51.75	
10	27.65	61	1327.1	46.10	
11	27.59	59	1275.0	42.55	
12	21.15	51	1070.6	30.00	
Total	**273.63**	-	-	**458.22**	**8764**

Table 23: Field of Heliostats summary for the two-row design with opening sector, third design

Design 4					
Sector	G (MW)	Rings	Radius (m)	Area (hectare)	Heliostats
1	16.91	44	897.0	21.06	
2	14.80	42	848.3	18.83	
3	23.75	56	1197.6	37.54	
4	24.59	60	1301.0	44.31	
5	20.50	57	1223.3	39.17	
6	13.59	47	970.8	24.67	
7	13.40	46	946.1	23.43	
8	20.54	57	1223.3	39.17	
9	25.27	61	1327.1	46.10	
10	23.48	56	1197.6	37.54	
11	14.69	42	848.3	18.83	
12	16.69	45	921.5	22.23	
Total	**228,21**	-	-	**372.95**	**7395**

Table 24: Field of Heliostats summary for the two-row design with reheating cycle and opening sector, fourth design

It is clear that the reheating process reduce more the field size than the introduction of a second row of tubes at the receiver. The values are expressed with so many significant figures due to they have been transfer to the report as the where in the programming results.

5.7. Global Performance

In section 4.7 a global performance analysis was carried out. The first analysis was done over the performance of the field of heliostats. Equation (4.114) compared the total radiation that gets to the total area of the field of heliostats with the total radiation that gets to the receiver thanks to the concentration made by the mirrors. In Table 25, a comparison between the four studied models is presented.

η_{field} first design	η_{field} second design	η_{field} third design	η_{field} fourth design
14.36%	15.27%	14.70%	15.04%

Table 25: Field performance comparison

It can be observed that the performance for the two-row design is slightly better. It is due to the fact that the more rings the field have, the more separated the heliostats are both from ring to ring and in the same ring. And this fact was corroborated in section 5.6.

In Table 26 a comparison is done for the receiver performance this time using equation (4.115). As it can be seen, the receiver performance for the two-row design is quite higher than the one-row design. This comes from the fact that the two-row design takes advantage of the second row to absorb more radiation.

η_{rec} first design	η_{rec} second design	η_{rec} third design	η_{rec} fourth design
18.30%	22.44%	18.48%	22.21%

Table 26: Receiver performance comparison

5.8. Natural Gas support

This section gives the results of the explanation seen in section 4.8. The Natural Gas installation supports the power plant during the months in which the solar radiation is not enough in order to make the cycle work at the design day.

In this day, March 20th, the percentage solar radiation absorbed at the receiver is shown in equation (5.44). It has to be highlighted that this day counts with 13 hours of sunlight from sunrise to sunset. Although is a tough approximation, all the hours are taken as valid for the power plant performance, which means that there is no threshold for the valid solar radiation that would make the cycle work.

$$\%E_{ab} = 54\% \qquad (5.44)$$

The cold months cited in section 4.8 are September, October, November, December, January and February. These winter and autumn months are the months in which solar radiation is lower than in the design day and month. Using equation (4.117) the absorbed energy at the receiver for each of the previous months is obtained. Equation (4.118) helps to obtain the needed energy for the design point while (4.119) combines the two previous cited equations giving the energy that the natural gas back-up must provide. Finally, equation (4.120) gives as

result the percentage of energy this back-up provides both at each cold month and during the whole year. Monthly data is given at Table 27.

Month	G (MW)	Time (h)	Eabs (MWh)	Eneed (MWh)	Esup (MWh)	%Esup
September	216.96	13	1525.7		412.8	21%
October	218.17	12	1416.2		522.3	27%
November	102.48	10	554.3		1384.1	71%
December	123.25	10	666.7		1271.7	66%
January	192.14	10	1039.3		899.1	46%
February	253.61	12	1646.2		292.2	15%
March	275.66	13		1938.43		

Table 27: Natural Gas back-up summary

At the end, the total percentage of energy back-up needed for the whole year is given at Table 28. This data takes into account the number of hours that the power plant gives along the different months of the year, which are more during hot months.

%Esup annual
20%

Table 28: Annual natural gas back-up percentage

All this data is the same for all the designs studied in this project. That is why only the first design is shown in this section.

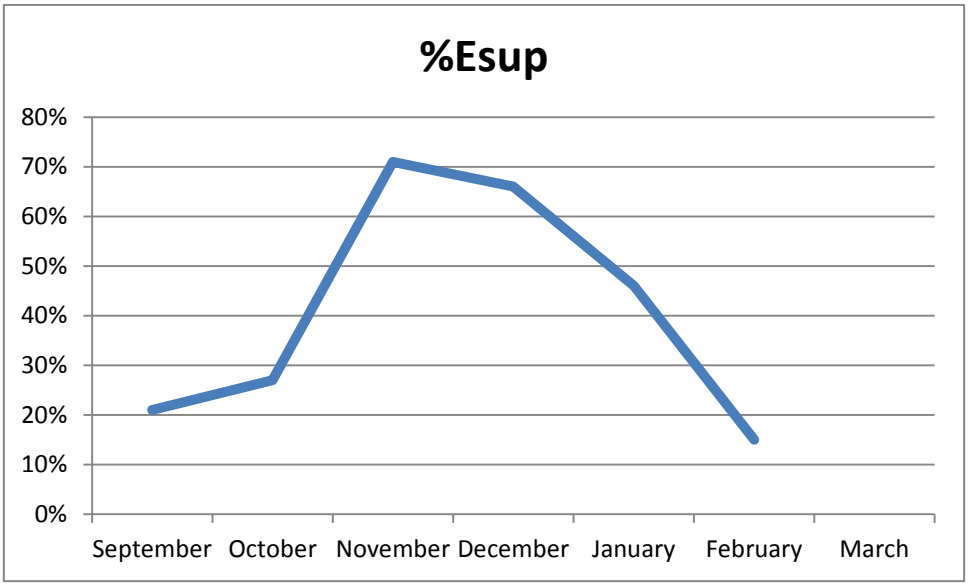

Figure 51: Evolution of the natural gas support along the cold months.

5.9. Behavior of heliostats during hot months

As seen in section 4.9, the objective at this point, in contrast with the previous section, is to figure out how to manage the field of heliostats during hot months, when the solar radiation is higher than in the design month. These hot months are April, May, June, July and August.

In Table 29 there is a scheme of the heliostat needs during this period.

Month	Number of rings by sector, from North, clockwise												Number of heliostats	Percentage of used heliostats
	1	2	3	4	5	6	7	8	9	10	11	12		
March	47	56	63	66	57	51	50	57	66	63	56	48	8994	
April	39	47	59	63	64	58	57	64	64	60	47	41	8664	96%
May	38	45	57	62	64	59	58	63	62	57	45	39	8337	93%
June	34	41	52	57	59	55	54	59	57	52	41	35	7090	79%
July	33	39	50	54	56	52	51	56	54	50	39	34	6448	72%
August	35	41	52	56	56	51	50	56	56	53	42	36	6772	75%

Table 29: Summary of heliostat behavior during summer

As it can be clearly seen in the previous table, there are a huge number of heliostats not needed during summer, not that much during spring months.

As well as in the previous section, these data is equal in all the designs studied during the present project, so that, in this case only the fourth design is shown.

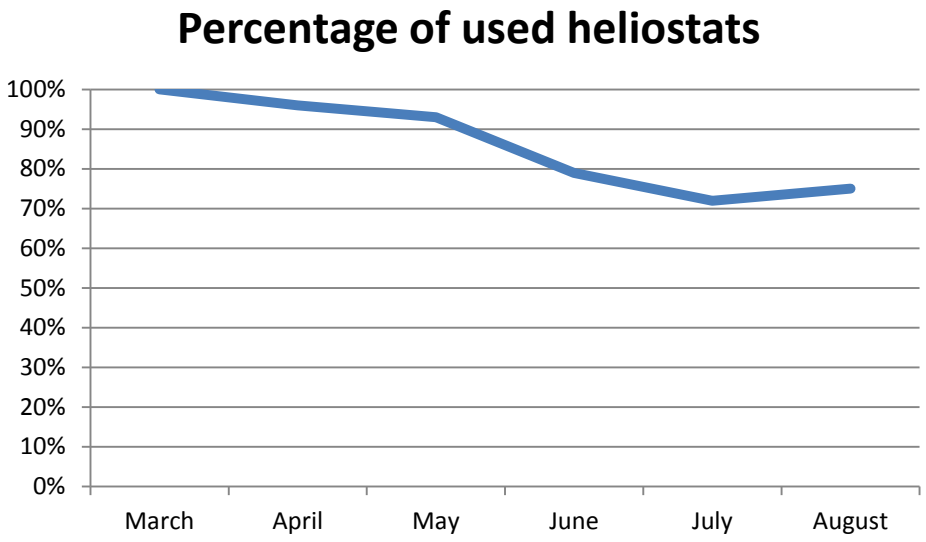

Figure 52: Evolution of the percentage of heliostats used along the year.

Chapter 6 Analysis of the Investment

In this section, an analysis to the total power plant investment is carried out. Firstly the analysis of the investment is given. This first analysis includes the statement of the parameters which influence, a cost assessment, a study of the income this plant is able to produce, lifespan and depreciation period and profitability criteria. After that there is a study of the investment in the plant, giving a summary of the costs of the power plant split into the main parts of it. And finally a financial analysis is given in order to see if the power plant if profitable or not.

6.1. Analysis of the investment

6.1.1. Parameters

When giving an economic analysis there are some important factors which may not be forgot in order to give a good description of the investment, both in short-time and long-time. Table 30 gives a scheme of these parameters.

Time periods	Investment
Lifespan of the power plant	Project Investment
Amortization time	Operation costs
Income	**Others**
Electric bill	Consumer Price Index, (CPI)
kWh Price	Taxes
	Interest rate

Table 30: Parameters influencing in investment analysis

6.1.2. Cost assessment

In the most general way, the costs of the power plant can be divided into two different groups, investment costs and operation costs.

Investment costs are formed, as a rough approximation, by the following concepts:

- Engineering
- Field of heliostats
- Power building
- Electrical system
- Control system
- Building
- Water storage and treatment
- Security systems
- Operation license
- Financial costs

In contrast, operation costs are formed by the other concepts:

- Working cost
- Maintenance
- Spare parts and consumer materials
- Land costs
- Insurance
- Taxes

6.1.3. Income

In order to obtain the total income of the power plant, there is an issue to deal with. This issue is the power plant electric bill. This means that the net power production take into account the own electric consumption due to lighting, electrical and mechanical equipment, temperature and humidity control inside buildings, water treatment, security systems, etc. This consumption can be estimated to be around a 6%.

The product of the power plant is the electricity, which price is regulated by the Spanish government. This price can be obtained from Table 31. It can be seen that for the first 25 years, the price for installations in category b.1.2. is 29.8873c€/kWh and from that time is 23.9097 c€/kWh

3. *Tarifas, primas y límites, para las instalaciones de la categoría b) del artículo 2 del Real Decreto 661/2007, de 25 de mayo*

Grupo	Subgrupo	Potencia	Plazo	Tarifa regulada c€/kWh	Prima de referencia c€/kWh
b.1	b.1.1	P≤100 kW	primeros 30 años	48,8606	0
		100 kW<P≤10 MW	primeros 30 años	46,3218	0
		10<P≤50 MW	primeros 30 años	25,4926	0
	b.1.2		primeros 25 años	29,8873	0
			a partir de entonces	23,9097	0

Table 31: Fares, primes and limits (Orden IET/221/2013, de 14 de febrero, por la que se establecen los peajes de acceso a partir de 1 de enero de 2013 y las tarifas y primas de las instalaciones del régimen especial 2013)

Since temporary variations can happen along the whole lifespan of the power plant, these prices will be increased using the CPI. In Table 31 b.1.1 is the subgroup where photovoltaic installations are covered while b.1.2 is the subgroup where solar thermal power installations are introduced.

6.1.4. Lifespan and depreciation period

Firstly, both lifespan and depreciation period have to be explained.

Lifespan is the estimated time of operation of the power plant, which as in other projects, is taken as 40 years.

Depreciation period is the decrease in value of the assets of the installation due to the operation and use of them in order to obtain the product, which in this case is the electric power. Thereby, this cost is taken as if at the end of this period, all the assets would be replaced. This depreciation is going to be taken as linear along a period of 20 years, half the lifespan.

6.1.5. Profitability criteria

When project profitability is analyzed in order to decide whether this is worth or not there are two main criteria among many others which have to be taken into account. These are the following ones.

6.1.5.1. Net Present Value, NPV

Net present value compares the value of the money today to the value of the money in the future taking into account inflation and returns. This is based on the expression *a dollar today is worth more than a dollar tomorrow*. Its expression is shown at equation (6.1), where R_t is the net cash flow, t is the time of the cash flow in years and I is the discount rate. This discount

rate is the rate of return that can be earned if the same amount of money would be invested in the financial market on another investment with similar risk.

$$NPV(i,N) = \sum_{t=0}^{N} \frac{R_t}{(1+i)^t} \qquad (6.1)$$

In this kind of project is normal to have big down payment and variable cash flows in the successive periods of time.

6.1.5.2. Return on Investment, ROI

This criterion gives a rate of return that makes zero the net present value. In mathematical terms the expression stays as shown in equation

$$0 = R_0 + \sum_{t=0}^{N} \frac{R_t}{(1+ROI)^t} \qquad (6.2)$$

For this interest rate the project does not give any benefit but pays off the total investment.

This interest rate must be higher than the discount rate in order to give net profit. If lower, the project does not cover the total investment, therefore, it would be better to look for another kind of project that could be profitable. Among different projects, the one with the highest TIR must be chosen since this rate expresses the profitability in terms of percentage.

6.2. Power plant investment

During this section the cost of investment of the different parts of the power plant is given. It is going to be split into two main parts, field of heliostats and power building. The field of heliostats is mainly composed of the receiver, the tower and the heliostats. Meanwhile the power building is mainly formed by the turbine. The costs of each of the concepts are based in another bachelor project, *Diseño de una planta termosolar de receptor central con almacenamiento de sales fundidas* (Joga López 2012), scaling them in order to adjust the costs to the characteristics of the present project.

6.2.1. Field of heliostats

As it can be seen in Table 32, the main concepts of the investment in this part are the receiver, the tower and the mirrors with their control system.

Comparing the design with one row of tubes at the receiver and the design with two rows, it is clear that this device has more importance on the second design due to its complexity and size. Nonetheless, due to the smaller amount of mirrors needed in the second design, the investment related to them are significantly lower.

Figure 53, Figure 54, Figure 55 and Figure 56 show the investment distribution for the field of heliostats of each design.

FIELD OF HELIOSTATS				
Concept	Cost (million Euros)			
	First design	Second design	Third design	Fourth design
Receiver	50	75	69	69
Tower	11	14	13	13
Heliostats structure	22	18	22	18
Heliostats supports	4.2	34	4.1	3.5
Foundations	19	15	18	15
Local control	27	21	26	22
Mechanisms	67	54	65	56
Mirrors	82	66	80	68
Land work	24	19	24	20
Assembly in factory	7.1	5,7	6.9	5,9
Assembly and adjustments at the field	15.9	12.8	15.5	13.2
Wiring and instrumentation	35.3	285	34.4	29.4
TOTAL	**365**	**332**	**378**	**333**

Table 32: Investment in the field of heliostats

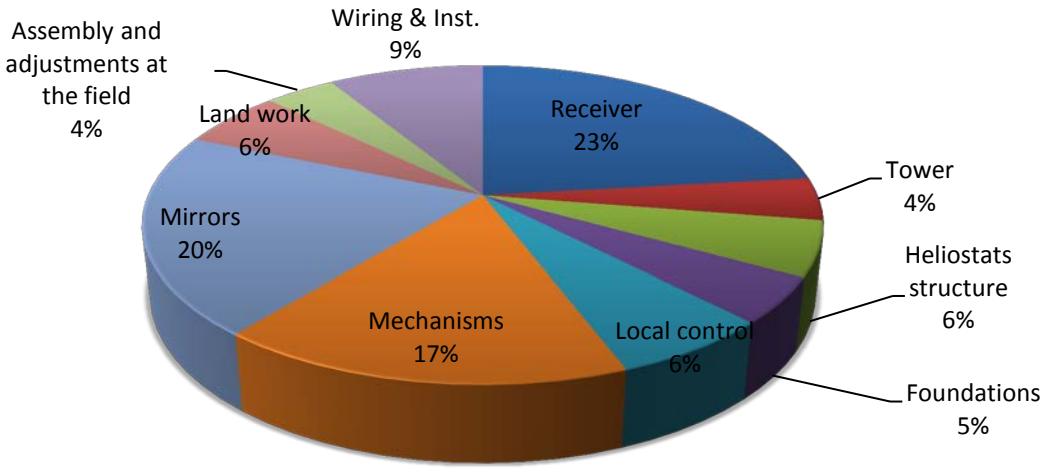

Figure 53: Investment distribution of the field of heliostats for the first design

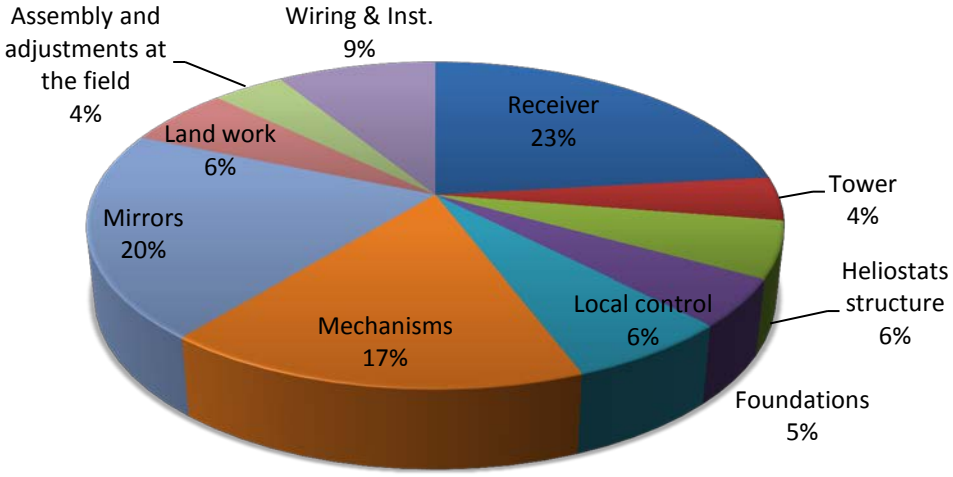

Figure 54: Investment distribution of the field of heliostats for the second design

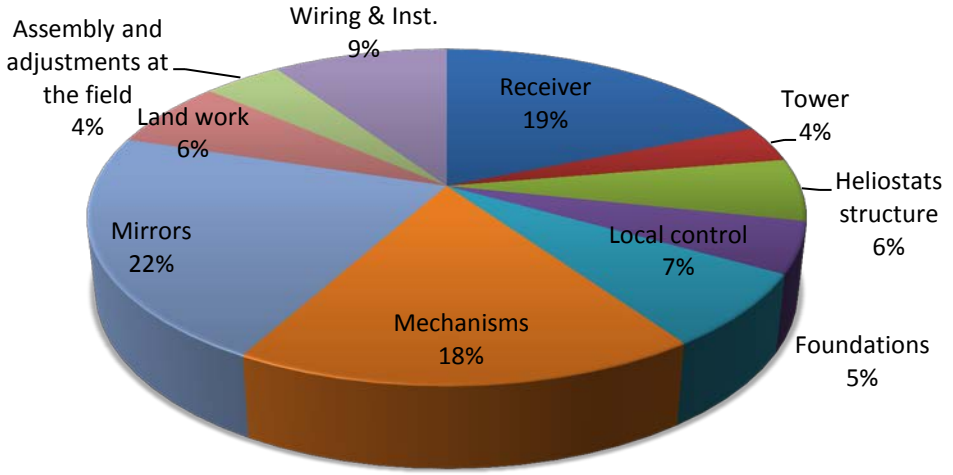

Figure 55: Investment distribution of the field of heliostats for the third design

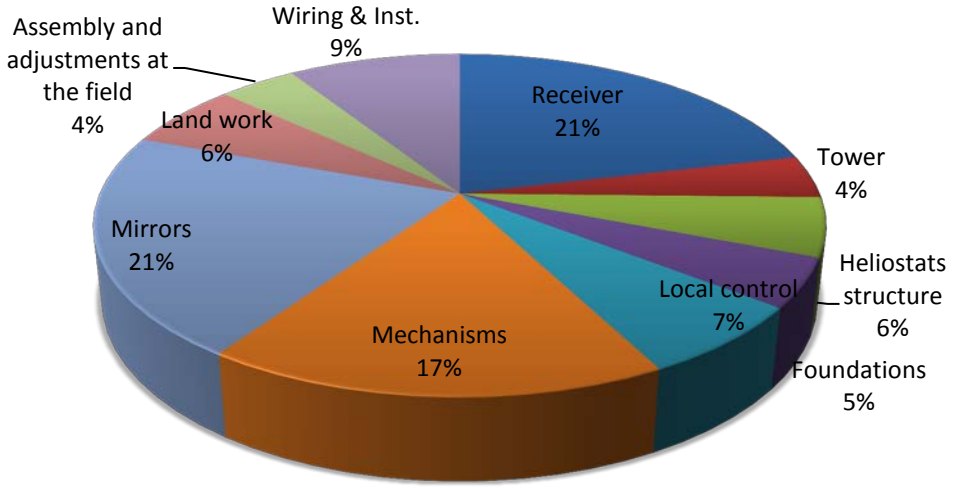

Figure 56: Investment distribution of the field of heliostats for the fourth design

6.2.2. Power building

In the power building the main device is the turbine. In this project the two studied designs present a two principle differences. The first difference is that the first design counts with one turbine while the second design needs two different turbines in order to make possible the reheating cycle.

The second difference is the size of the turbines. In the second design both turbines are smaller either in size, pressure and flow.

Due to the complexity of the reheating process with two different turbines, all the concepts related to the turbines have a higher cost in the second design than in the first design as can be observed in Table 33. Figure 57 and Figure 58 show the investment distribution for the power building of each design.

POWER BUILDING				
Concept	**Cost (million Euros)**			
	First design	**Second design**	**Third design**	**Fourth design**
Building	7	9	7	9
Mechanical equipment	40	56	40	56
Mechanical assembly	4.5	5	4.5	5
Electrical equipment	5	5.5	5	5.5
Electrical assembly	2	2	2	2
Instrumentation and control equipment	1.5	2	1,5	2
Instrumentation and control assembly	0.2	0.5	0.2	0.5
Tubes, valves, isolation and supports	6.5	8	6.5	8
TOTAL	**66.7**	**88**	**66.7**	**88**

Table 33: Investment in the power building

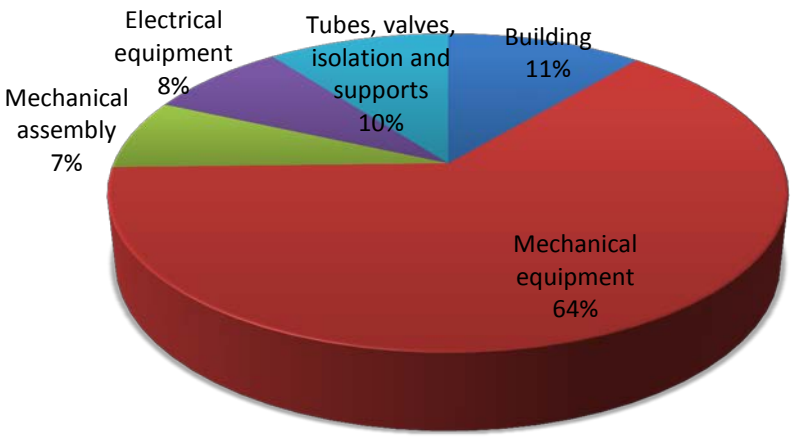

Figure 57: Investment distribution of the power building for the first and third designs

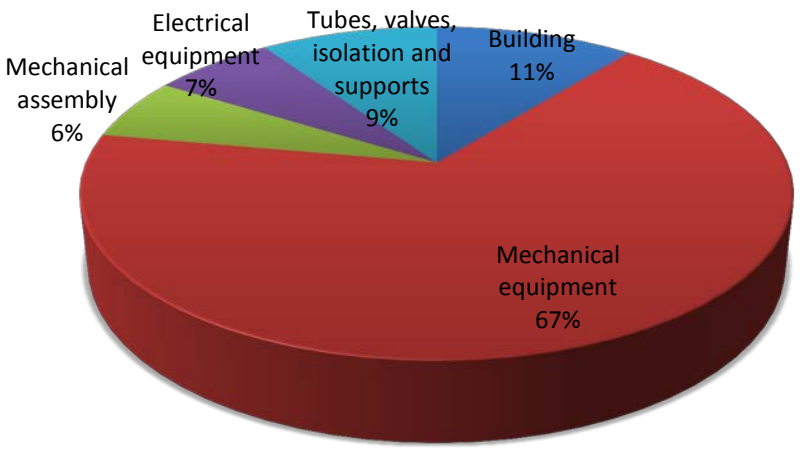

Figure 58: Investment distribution of the power building for the second and fourth designs

6.2.3. Total investment

Finally, as it can be seen in Table 34, the total investment is obtained. For an easier analysis, this final distribution is divided into four main concepts. The field of heliostats covers all the systems that are related to the collectors, both the mirrors themselves and their system. The receiver and the tower come together as one concept because of their role in the system. The power building is the same point as the one developed in section 6.2.2. And finally the Land and other concepts point is related to the cost of buying the land as well as other buildings that has not direct participation on the electricity production.

Comparing Figure 59 and Figure 60, it can be observed that the field of heliostats plays a significant role in both designs, but it is more important in the one-row design. Due to complexity, in the two-row design the weight of the receiver, the tower and the power building grows with respect to the first design. The distribution for the total investment of each design can be observed in Figure 59, Figure 60, Figure 61 and Figure 62.

TOTAL INVESTMENT				
Concept	**Cost (million Euros)**			
	First design	**Second design**	**Third design**	**Fourth design**
Field of heliostats	235.6	190.3	229.2	193.1
Receiver and tower	61.0	89.0	82.0	82.0
Power building	66.7	88.0	66.7	88.0
Lands and others(licenses, personnel)	60.0	40.0	58.0	41.0
TOTAL	**423.3**	**407.3**	**435.9**	**404.1**

Table 34: Total Investment

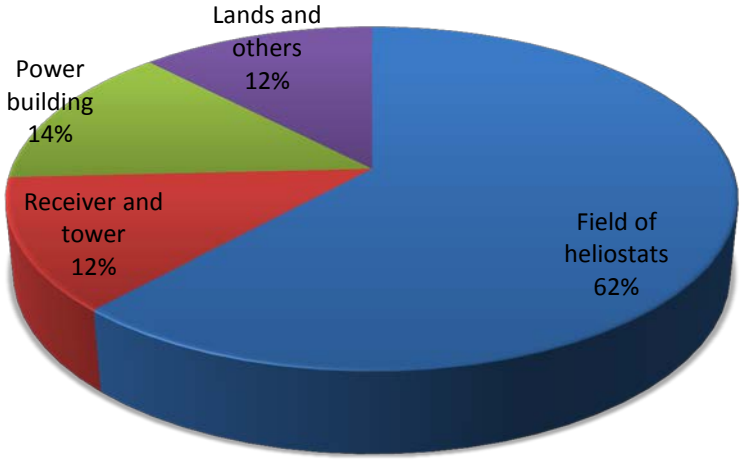

Figure 59: Total investment distribution for the first design

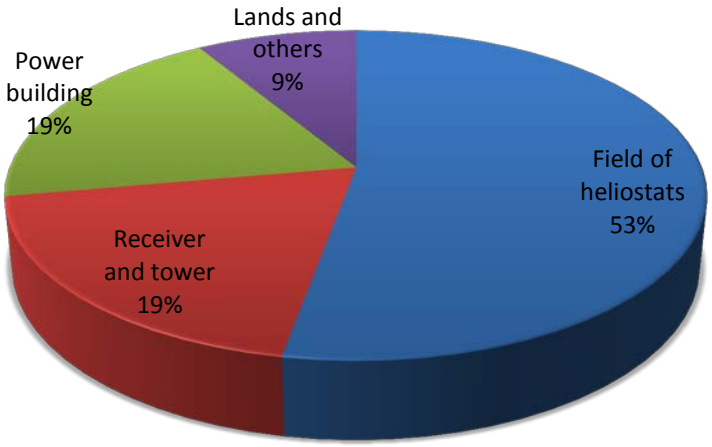

Figure 60: Total investment distribution for the second receiver design

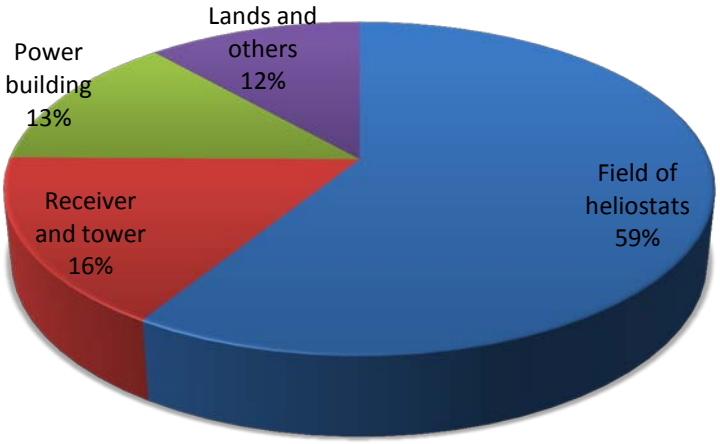

Figure 61: Total investment distribution for the third receiver design

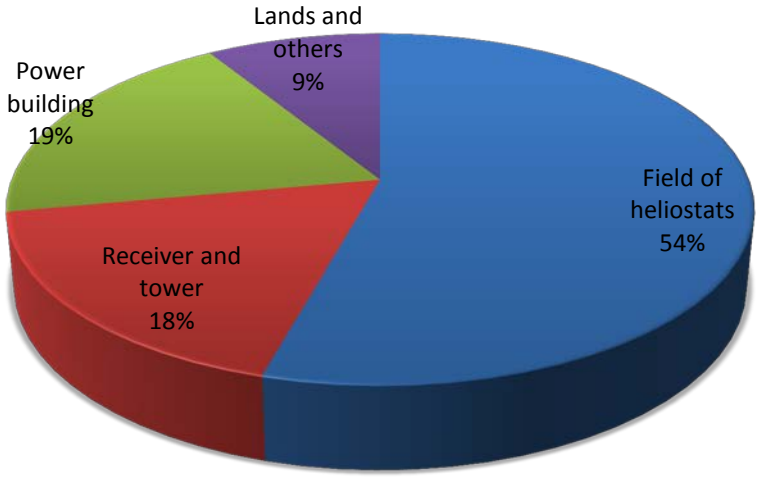

Figure 62: Total investment distribution for second receiver design

6.3. Financial analysis

During this section a detailed financial analysis of the project is presented in order to obtain both profitability indicators seen in section 6.1.5, NPV and ROI. After this, the reader will be in the position to choose whether the present project is worth to invest in or not. It has to be taken into account that, according to the total cost of the project in Table 34, the case studied is for the fourth design, the cheapest one.

As this analysis depends much in a temporary variable, there are some points that must be established before going into the calculation.

Firstly, the investment needed in order to develop the project is of 346.7 million Euros. The investor is able to put 60 million Euros at the very beginning without financial aid. This makes the investor to take 286.7 million Euros on a loan at an interest rate of 8% for 25 years. In this project a grace period of two years, the same period that takes the construction of the power plant, is taken, with no necessity of interest payment before those two years. However, the interests raise the debt from the very beginning.

The CPI will be taken in three different scenarios. As it can be seen in Figure 63, there are two clear extremes in the temporary evolution of the CPI in Spain of the last 10 years. The lower is a -0.2% which will be eliminated as well as the upper limit of 4.1. Thereby, a lower limit of 1.5% and an upper limit of 3.5% are reasonable approximations.

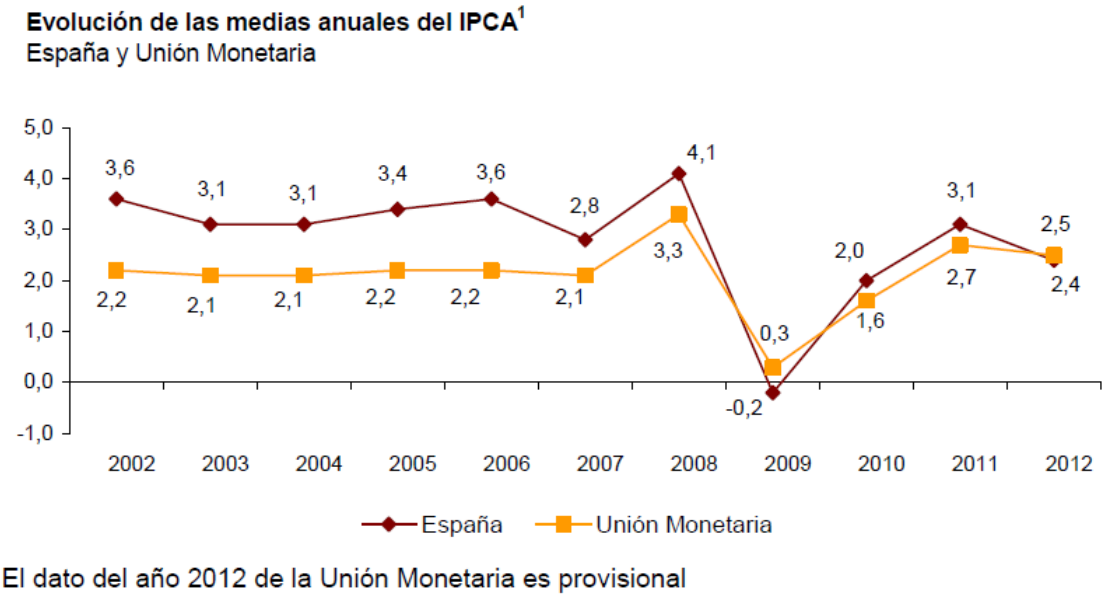

Figure 63: Temporary evolution of the CPI in Spain and European Union. Source: (Instituto Nacional de Estadística de España 2013)

The following data that has to be given is the discount rate to be used in this analysis. The Spanish ten-year bond is around a 4.443% (Agencia EFE 2013) which seems to be a good indicator. This rate is high comparing to stable periods when it has been around 3%.

According to section 6.1.3 the income is of 29.8873c€/kWh which will grow according to the CPI. However, from year 26 the income is reduced. Nowadays this reduction is of around 20%. The annual power production is 216 GWh.

The price of the natural gas is of 26.40 €/MWh which will grow with the CPI. (Comisión Nacional de Energía 2013)

In the case of the needed personnel, 400 workers are needed during the first two years with an average wage of 30,000€ per year. By the time the power plants starts to operate only 50 workers are needed with an average salary of 35,000€. Due to the present economic situation in which Spain is immersed in a growth deceleration, the wages will grow at a 0.5% during the first 10 years and at 2% from that time on.

Maintenance includes the replacement of all the damaged devices, water supply for refrigeration and cleaning of the mirrors, office expenses, travel expenses, etc. These expenses will also grow with the CPI.

For the location of the power plant, as already mentioned in Chapter 5, a land is needed near Gibraleón, a town in the Spanish province of Huelva. In order to purchase the area given in section 4.6, 5 million Euros are needed. This concept is already included in the assessment of section 6.2.3.

As well as because of the sale of the land, the local administration will collect money due to two different fees. The first one is the so called in Spanish *Impuesto de Construcciones, Instalaciones y Obras*. This local fee is of a 2.9% of the material investment without taking into account the personnel expenses (Excmo. Ayuntamiento de Gibraleón 2003). The second local fee is the so called in Spanish "Impuesto sobre Bienes Inmuebles". This local fee is 1.3% for special use, as in this project. The amount is calculated taking as tax base the land price. (Excmo. Ayuntamiento de Gibraleón 2013)

As well as in every type of material, insurance must be purchased. This insurance will take around a 1% of the initial investment which grows with the CPI.

In Table 36, Table 37 and Table 38 the development of the financial view of the project can be observed. The different scenarios can make an investor to trust the project or not. These tables show a construction period of 2 years. This period is shown in the tables as negative years.

In Table 35 there is a comparison of the different profitability indicators, already seen in section 6.1.5, for the three different scenarios described before in this section. It is easy to see that the higher the CPI is, the better the project results, at least economically. This behavior can be explained based on the loan depreciation.

Scenario	NPV	ROI
CPI=1.5%	€ 246.787.371	2.411%
CPI=3.5%	€ 579.294.385	5.246%
CPI=5%	€ 983.551.644	7.203%

Table 35: Profitability comparison for different economic scenarios

The explanation is that the loan payment remains the same whether the CPI is higher or lower. This is because the given interest rate is fixed. This approximation is quite rough but good enough to give this forecast.

Whether this project is worth or not depends on the investor criteria. The indicators show different answers which have to be read by the investor and may help him/her to make a decision.

It is true that compared to the 4.443% ten-year bond discount rate, at a situation where the prices grow at CPI of 1.5%, this investment would not be worth because would not give as much return as the bonds. In the scenario where the CPI is 3.5%, the project begins to be attractive. This situation is not hard to believe, but depends on the world economy. Although the ROI is higher than the discount rate, it has to be taken into account that it is normal that this investment were riskier than the bonds.

Finally, at a CPI of 5%, which would hardly happen, the project would have a rate of return of 7.203% which is quite high and doubles the return that the ten year bond would give.

In Figure 64, Figure 65 and Figure 66 it is observed how the price of the kWh, following always the CPI assumptions made, always cover the cost of the kWh. This happens stronger as the CPI

is higher. The decreases seen in year 26 come from the fact that the loan payment is over by that year, and the Spanish law decreases the price of the kWh in 20% for the 26th year.

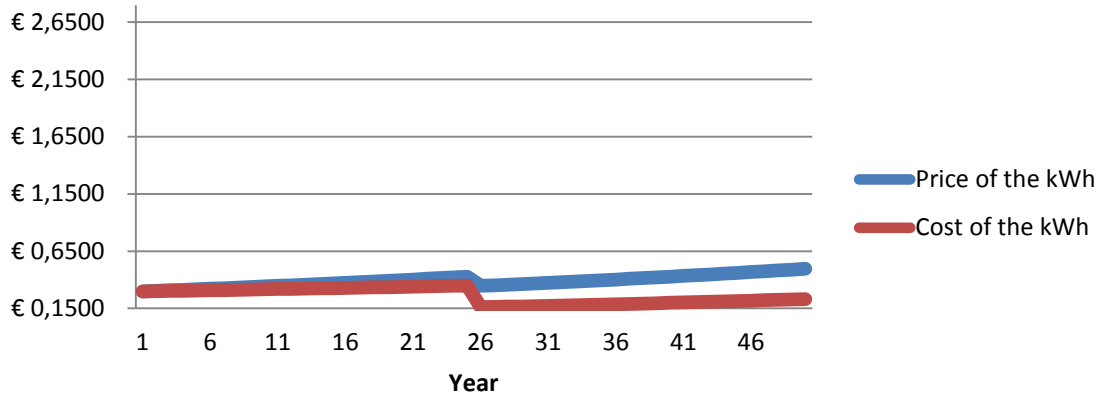

Figure 64: Price vs Cost of the kWh for a CPI=1.5%

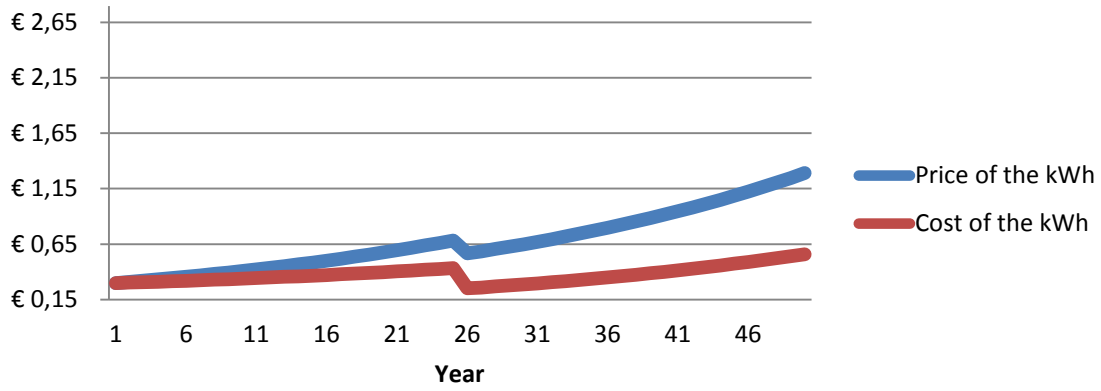

Figure 65: Price vs Cost of the kWh for a CPI=3.5%

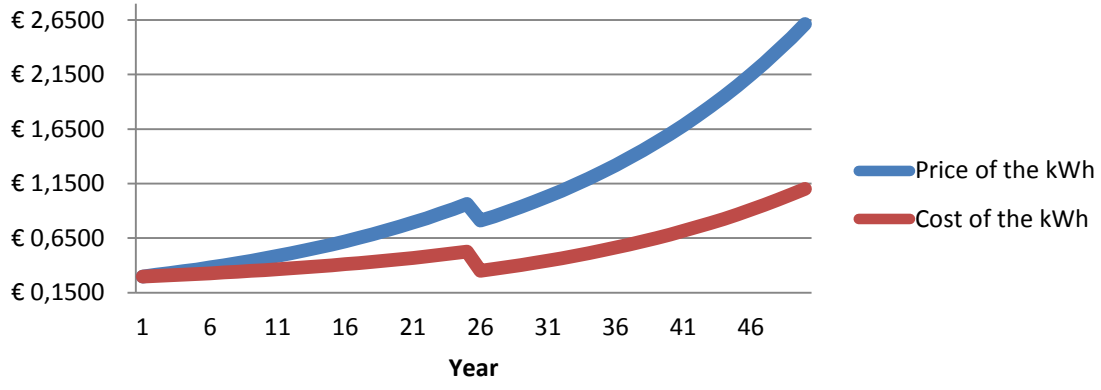

Figure 66: Price vs Cost of the kWh for a CPI=5%

	Year	-2	-1	1	10	25	26	40	50
Loan		€ 369.674.852	€ 406.642.338	€ 447.306.571	€ 373.261.029	€ 39.687.861			
Expenditures	Natural Gas			€ 1.127.887	€ 1.289.615	€ 1.612.318	€ 1.636.503	€ 2.015.772	€ 2.339.385
	Personnel	€ 12.000.000	€ 12.000.000	€ 1.750.000	€ 2.714.824	€ 3.653.796	€ 3.726.872	€ 4.917.529	€ 5.994.440
	Equipment	€ 140.000.000	€ 155.700.000						
	Maintenance			€ 8.000.000	€ 9.147.120	€ 11.436.022	€ 11.607.563	€ 14.297.682	€ 16.593.044
	Land	€ 7.000.000							
	Licenses	€ 20.000.000							
	Local fees			€ 8.666.300	€ 9.908.961	€ 12.388.500	€ 12.574.328	€ 15.488.500	€ 17.975.037
	Insurance			€ 3.467.000	€ 3.964.133	€ 4.956.086	€ 5.030.428	€ 6.196.258	€ 7.191.010
	TOTAL	€ 179.000.000	€ 167.700.000	€ 23.011.187	€ 27.024.653	€ 34.046.723	€ 34.575.693	€ 42.915.740	€ 50.092.916
Income	Energy sale			€ 64.553.131	€ 73.809.403	€ 92.278.882	€ 74.930.452	€ 92.296.014	€ 107.113.292
EBITDA				€ 41.541.944	€ 46.784.750	€ 58.232.159	€ 40.354.759	€ 49.380.274	€ 57.020.376
	Depreciation			€ 5.855.709	€ 12.001.452	€ 39.687.861			
EBIT				€ 35.686.235	€ 34.783.298	€ 18.544.298	€ 40.354.759	€ 49.380.274	€ 57.020.376
	Loan interests	€ 36.967.485	€ 40.664.234	€ 35.572.907	€ 29.427.164	€ 1.740.755	€ -	€ -	
EBT				€ 113.328	€ 5.356.134	€ 16.803.543	€ 40.354.759	€ 49.380.274	€ 57.020.376
	Taxes			€ 28.332	€ 1.339.034	€ 4.200.886	€ 10.088.690	€ 12.345.068	€ 14.255.094
Net Income				€ 84.996	€ 4.017.101	€ 12.602.657	€ 30.266.070	€ 37.035.205	€ 42.765.282

Table 36: Financial analysis for CPI=1,5% scenario

	Year	-2	-1	1	10	25	26	40	50
Loan		€ 369.674.852	€ 406.642.338	€ 447.306.571	€ 373.261.029	€ 39.687.861			
Expenditures	Natural Gas			€ 1.127.887	€ 1.537.194	€ 2.575.337	€ 2.665.474	€ 4.314.588	€ 6.086.152
	Personnel	€ 12.000.000	€ 12.000.000	€ 1.750.000	€ 2.714.824	€ 3.653.796	€ 3.726.872	€ 4.917.529	€ 5.994.440
	Equipment	€ 140.000.000	€ 155.700.000						
	Maintenance			€ 8.000.000	€ 10.903.179	€ 18.266.628	€ 18.905.960	€ 30.602.974	€ 43.168.517
	Land	€ 7.000.000							
	Licenses	€ 20.000.000							
	Local fees			€ 8.666.300	€ 11.811.277	€ 19.788.010	€ 20.480.590	€ 33.151.819	€ 46.763.915
	Insurance			€ 3.467.000	€ 4.725.165	€ 7.916.300	€ 8.193.370	€ 13.262.564	€ 18.708.156
	TOTAL	€ 179.000.000	€ 167.700.000	€ 23.011.187	€ 31.691.640	€ 52.200.071	€ 53.972.266	€ 86.249.473	€ 120.721.179
Income	Energy sale			€ 64.553.131	€ 87.979.291	€ 147.396.003	€ 122.043.890	€ 197.551.777	€ 278.666.292
EBITDA				€ 41.541.944	€ 56.287.651	€ 95.195.932	€ 68.071.624	€ 111.302.304	€ 157.945.112
	Depreciation			€ 5.855.709	€ 12.001.452	€ 39.687.861			
EBIT				€ 35.686.235	€ 44.286.199	€ 55.508.071	€ 68.071.624	€ 111.302.304	€ 157.945.112
	Loan interests	€ 36.967.485	€ 40.664.234	€ 35.572.907	€ 29.427.164	€ 1.740.755	€ -	€ -	
EBT				€ 113.328	€ 14.859.035	€ 53.767.316	€ 68.071.624	€ 111.302.304	€ 157.945.112
	Taxes			€ 28.332	€ 3.714.759	€ 13.441.829	€ 17.017.906	€ 27.825.576	€ 39.486.278
Net Income				€ 84.996	€ 11.144.276	€ 40.325.487	€ 51.053.718	€ 83.476.728	€ 118.458.834

Table 37: Financial analysis for CPI=3.5% scenario

	Year	-2	-1	1	10	25	26	40	50
Loan		€ 369.674.852	€ 406.642.338	€ 447.306.571	€ 373.261.029	€ 39.687.861	-€ 0		
Expenditures	Natural Gas			€ 1.127.887	€ 1.749.723	€ 3.637.549	€ 3.819.426	€ 7.562.203	€ 12.318.032
	Personnel	€ 12.000.000	€ 12.000.000	€ 1.750.000	€ 2.714.824	€ 3.653.796	€ 3.726.872	€ 4.917.529	€ 5.994.440
	Equipment	€ 140.000.000	€ 155.700.000						
	Maintenance			€ 8.000.000	€ 12.410.626	€ 25.800.800	€ 27.090.840	€ 53.638.009	€ 87.370.665
	Land	€ 7.000.000							
	Licenses	€ 20.000.000							
	Local fees			€ 8.666.300	€ 13.444.276	€ 27.949.684	€ 29.347.168	€ 58.105.385	€ 94.647.549
	Insurance			€ 3.467.000	€ 5.378.455	€ 11.181.422	€ 11.740.493	€ 23.245.372	€ 37.864.262
	TOTAL	€ 179.000.000	€ 167.700.000	€ 23.011.187	€ 35.697.904	€ 72.223.250	€ 75.724.798	€ 147.468.498	€ 238.194.948
Income	Energy sale			€ 64.553.131	€ 100.143.093	€ 208.190.299	€ 174.879.851	€ 346.250.143	€ 564.004.998
EBITDA				€ 41.541.944	€ 64.445.190	€ 135.967.049	€ 99.155.053	€ 198.781.645	€ 325.810.050
	Depreciation			€ 5.855.709	€ 12.001.452	€ 39.687.861			
EBIT				€ 35.686.235	€ 52.443.737	€ 96.279.188	€ 99.155.053	€ 198.781.645	€ 325.810.050
	Loan interests	€ 36.967.485	€ 40.664.234	€ 35.572.907	€ 29.427.164	€ 1.740.755	€ -	€ -	
EBT				€ 113.328	€ 23.016.573	€ 94.538.433	€ 99.155.053	€ 198.781.645	€ 325.810.050
	Taxes			€ 28.332	€ 5.754.143	€ 23.634.608	€ 24.788.763	€ 49.695.411	€ 81.452.513
Net Income				€ 84.996	€ 17.262.430	€ 70.903.825	€ 74.366.290	€ 149.086.234	€ 244.357.538

Table 38: Financial analysis for CPI=5% scenario

Chapter 7 Environmental Impact

In this type of power plants, one of the major impacts over the environment is the one made on the landscape. This impact comes from the fact that the installation covers a large area and needs a tower which is high enough to be seen from tens of kilometers of distance to the plant.

As in every single project of this magnitude, the building process affects the flora and fauna of the area. As already mentioned, the power plant needs a huge amount of hectares, which implies the elimination of all the plants and trees that could interfere with the heliostats or in the building process. Apart from that, the noise that the machines emit makes the animals of the surroundings to feel uncomfortable, which would imply that this fauna should go anywhere else losing their natural habitats.

However, since this project is based on renewable energies, a big effect is observed comparing this technology with other non-renewable power plants. The main benefit of the solar plant is the reduction of CO_2 emissions to the air, which helps to not pollute in the air excessively. According to *Observatorio de la Electricidad Agosto 2013* (WWF España 2013), the CO_2 emissions are 240 grams per kW for the national mix. In this project, since a support system based on a natural gas fired-boiler is used, there is an amount of CO_2 emissions that has to be taken into account. The support percentage is a 20% as seen in section 5.8. Considering 212 GWh of annual production, equation gives the amount of CO_2 this power plant does not produce comparing it with other non-renewable power plants.

$$CO_2\ savings = 212\ GWh \cdot (1 - 0.2) \cdot 0.24\ {}^{CO_2 kg}/_{kWh} \qquad (7.1)$$

$$= 40.704\ tons$$

Thereby, in equation (7.1) a total of 40.704 tons of CO_2 per year are saved, which is one of the principles of renewable energies.

Chapter 8 Conclusions

8.1. Summary

Through this project, the author wanted to show the process of the design of a solar thermal central receiver power plant using water, in liquid and steam phases, as heat transfer fluid. For simplicity and cost reduction this was done without the use of any type of storage system but a back-up system which consists of a natural gas-fired boiler. The designed plant is able to give 50MW of electric power during the whole year. For this purpose, it has been chosen a representative day which does not oversize much the installation during periods where solar radiation is high. This representative day is March 21st, a spring day, where medium values for solar radiation are obtained compared to the rest of the year.

The prime aim of this project was to design this kind of power plants using different configurations both for the receiver and for the thermal cycle. This work is based on the paper called *Simulation of an integrated steam generator for solar tower* (Ben-Zvi, Epstein and Segal 2011), where a new receiver is described with two rows of tubes which decreases radiation losses. Apart from that, they add an opening sector that helps to get a higher steam temperature to increase efficiency in the cycle. Taking that paper as starting point, the new receiver gives the opportunity to introduce different configurations in the power cycle in order to improve the thermal behavior of the

power plant. A reheating process is the chosen one during this project in order to improve the efficiency of the power plant, knowing that the cost of the turbines is increased due to the need of two different turbines. However, the reheating system decreases the number of heliostats needed in order to reach the design point.

In the following points a more detailed description is given, comparing the different designs with each other and those designs with real power plants.

8.1.1. Comparison of the different designs of the power plant

One of the major objectives of the present project is to compare how good to design a two-row receiver is compared to the more common one-row receiver.

In Figure 67 it can be easily observed that a two-row receiver as design 3, which has no reheating process, only decreases the number of heliostats in 3% compared to design 1. However, with the two-row receiver, whether it has an opening sector or not, the decrease is up to 20% comparing design 1 and design 2 introducing the reheating process in the second design.

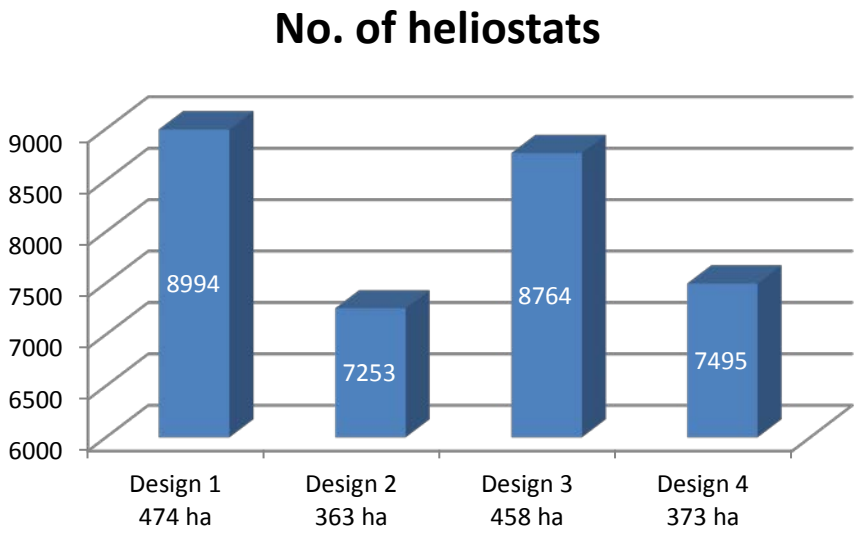

Figure 67: Field of heliostats comparison

What this reheating process implies is the addition of a second turbine, so that, more complexity appears in the design, because this process works both with a high pressure turbine and with a low pressure turbine.

Another important fact that this reheating process gives as a result is that the pumping power also decreases, which means that the net electric power of the plant increases. This can be seen in Figure 68, where the pumping power for the two-row receiver with opening sector and reheating, design 4, is one third of the one-row receiver option, design 1.

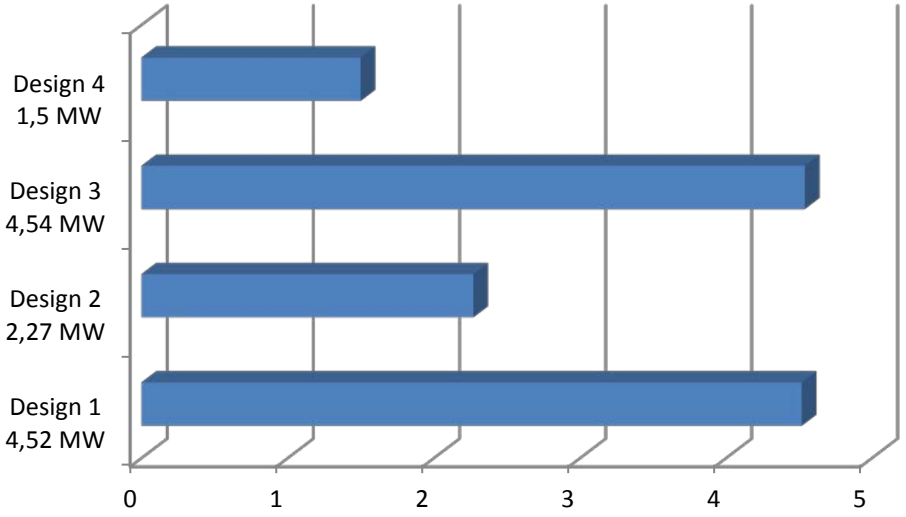

Figure 68: Pumping power comparison

In the pumping power, a variable which has great impact on it is the mass flow rate, which indicates the amount of HTF the power plant needs. Table 39 shows a comparison among the four designs described along this project. It can be observed that when reheating process is included, the mass flow rate decreases up to 33%.

Mass flow rate (kg/s)			
Design 1	**Design 2**	**Design 3**	**Design 4**
0.175	0.135	0.175	0.116

Table 39: Comparison of mass flow rate in each design

What is more, the introduction of the reheating process improves the thermal efficiency of the plat around 6%, as can be seen in Table 40.

Thermal efficiency			
Design 1	**Design 2**	**Design 3**	**Design 4**
33.53%	39.57%	33.53%	39.13%

Table 40: Thermal efficiency comparison

Both Table 39 and Table 40 collect data from section 5.2.

Reheating has an impact on the investment cost of the plant. In Figure 69 it can be observed that the reheating process introduced in designs 2 and 4 are around 40M€ cheaper than the other two options. It is important to remark that the largest amount of money is to purchase and install the field of heliostats with around 60% of the total investment as seen in section 6.2.3. This datum gives a clue of the system of the power plant where more energy has to be put in order to optimize its performance and obtain better results, which would mean a decrease of the cost for future projects.

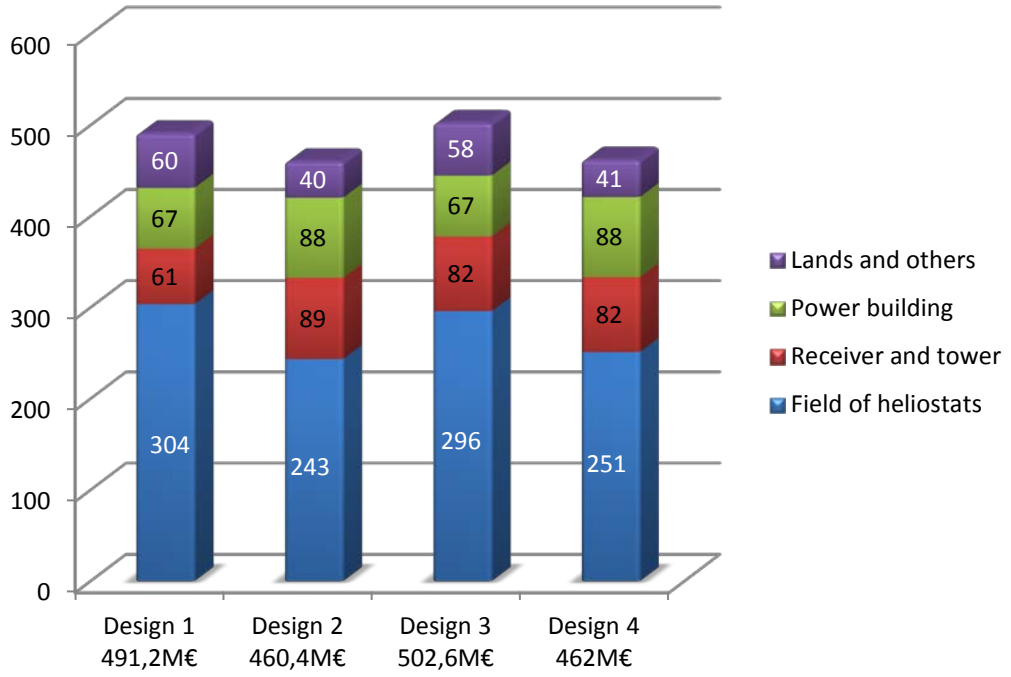

Figure 69: Investment comparison among designs

To conclude, it needs to be underlined the huge improvements that the two-row receiver gives to this kind of technology. In addition, it opens a wide range of opportunities for new solutions in order to develop central-receiver systems. To sum up, the two-row solution makes smaller both the area and the number of heliostats needed in the power plant. It also gives more flexibility to the systems since the two-row receiver behaves like two receivers in one, which can be configured using by-pass valves in order to obtain new results. The two-row configuration does not need a higher tower as in other configurations where two rows are installed but one on top of the other.

8.1.2. Comparison with power plants in operation

Firstly, this section shows a comparison between the four designs of the project and a real central-receiver power plant. This installation is located in Seville and its name is Gemasolar (Torresol Energy 2010). The comparison is done on the basis of the main figures of this kind of power plant in Table 41.

It can be observed that the costs are slightly higher for this project; namely around 130% of the cost of Gemasolar. However, the electric power for Gemasolar is less than half the power of the plant designed here(50MW). Almost the same happens when analyzing the annual production, where the plant of Torresol Energy gives a bit more than a half of the annual production of this project. Consequently, both the field of heliostats area and the number of heliostats are much higher for the present project.

Additionally, there are two key differences between the Gemasolar and the designs developed in this work. One difference is that Gemasolar with molten salt as HTF, while this project uses Water, in liquid and steam phases and the mixture of them. The second difference is that Gemasolar counts with a storage system, which was not selected for this project.

	Gemasolar	Design 1	Design 2	Design 3	Design 4
Total cost of the project (million €)	322.3	491.2	460.4	502.6	462.0
Electric power (MWe)	20	50	50	50	50
Annual energy production (GWh)	110	216	216	216	216
No. of heliostats	2650	8994	7253	8764	7495
Field of heliostats área (ha)	185	474	363	458	373
HTF	Molten Salt	Water/ Steam	Water/ Steam	Water/ Steam	Water/ Steam
Storage	Yes	No	No	No	No

Table 41: Comparison between Gemasolar and this project

A comparison with another real power plant that uses a different concentration system is given. In this case the comparison focuses on the parabolic-trough power plant Andasol, located in Granada and constructed by RREEF, ANTIN and COBRA. (Siemens 2009)

In Table 42, the comparison gives higher costs to the designs of the present project than to the Andasol plant. However, the annual energy production is higher for this project. It may seem confusing since the electric power of all plants is the same and Andasol has a storage system. This is due to approximations taken along the whole project such us no threshold for the minimum solar radiation needed in order to make the power plant work.

In contrast, the area occupied by Andasol is smaller than any of the four designs studied in this project. This issue can play an important role in the decision of which kind of power plant is going to be built when the available area is limited or expensive.

	Andasol	Design 1	Design 2	Design 3	Design 4
Total cost of the project (million €)	260	423,3	407,3	435,9	404,1
Electric power (MWe)	50	50	50	50	50
Annual energy production (Gwh)	157	212	212	212	212
Field of heliostats área (ha)	200	346	266	334	278
HTF	Molten Salt	Water/ Steam	Water/ Steam	Water/ Steam	Water/ Steam
Storage	Yes	No	No	No	No

Table 42: Comparison between Andasol and this project

8.2. Estimation of the cost of the project

Finally, this section shows an estimation of the cost associated to the development and writing of the present project. In order to develop it, it is needed to clarify which are the points that are taken into account.

Firstly, the personnel cost, one of the most important and expensive things. Let the author say that an hour of a junior engineer, the author, costs around 15€ per hour. This project has been done in 750 hours. Apart from this fact, approximately 20 hours of senior engineer, the director, have been needed for the accomplishment of the work. These hours can be estimated to have a price of 30€ per hour.

Secondly, in the case of the equipment, the only device used during the project has been a computer with a cost of 500€ to be paid in 2 years. In this case, 8 months have to be taken into account to obtain what is the depreciation.

According to the software licenses needed for this project, only two of them where required. One of the software is Matlab, with an annual cost of 69€. Moreover, a MS Office package with Excel and Word were needed, with a cost of 119€.

In addition, approximately 50€ can be justified due to the purchase of different products as well as the printing service for needed information.

As the place of residence of the author is far from the University, a monthly pass for public transportation has been purchased with a cost of 63.70€ per month, of which a 20% of the cost can be allotted to the project during 8 months.

Finally, in the item named other expenses it must be introduced the cost of the internet bill, with a 20% allotted to the project, approximately 100€ of electricity and 12 credits of the Bachelor Thesis with a cost of 26.81€ per credit. This credit cost is supposed to cover the access to different databases provided by the University in order to find and download journals, patents and much more information, as well as the renting of the books included in the bibliograph.

To sum up, Table 43, collects all this information to give a more graphic idea of the cost.

	Unit	Quantity	Price (€/Unit)	Cost	Comments
Junior Engineer	h	750	15	€ 11.250,00	
Senior engineer	h	20	30	€ 600,00	
Depreciation of the computer	month	8	20,83	€ 166,67	500€ paid in two years
Software licenses				€ 188,00	Matlab 69€, MS office 119€
Office expenses				€ 50,00	
Travel expenses	-			€ 101,92	monthly pass for public transport
Other expenses	-			€ 501,72	electricity, internet and university fees
TOTAL				**€ 12.858,31**	

Table 43: Project Cost

8.3. Discussion on the assumptions and restrictions

As it was mentioned before, the objective of the project is to introduce new configurations both on the receiver design and the power cycle in this type of installations, central-receiver solar power plant.

Along the development of the project, the author has tried to be the closest as possible to reality taking every single step based on previous works from other researchers. Nevertheless, some simplifications have been made in the calculations in order to not diverge from the scope of this research.

A linear increase of the temperature along the tubes has been considered, making it different for each of the panels. Although it is a good approximation, if that increase had been taken as non-linear, it may have given slightly different results. Furthermore, vapor quality at the boiler is treated in the same manner, taking it as linear for the whole length this stage covers at the receiver. Likewise, different results can be obtained by modifying this approximation.

The convection losses at the receiver for the two-row design are the result of a second approximation: the temperature of the air that surrounds the tubes of the inner row is taken as the ambient temperature. This is not strictly real since the outer row shields in some way the inner row. Thereby, the temperature of the air that surrounds these inner tubes would be higher, which may give a decrease in the convection losses. Hence, being more accurate in such temperature would lead to better results as regard to the convection losses.

Those points do not mean that those approximations lead to a wrong ending, but there could be some deviation in the results.

Another relevant point to take into account is that, according to section 5.8, the support given by the natural gas-fired boiler is too high for this type of power plants, 20%. In order to be considered as special regime and take advantage of their benefits the natural gas support must be no higher than 15% for renewable energies projects. Thereby, in order to meet the requirements, more heliostats would be needed to reduce the dependence on this¡¡e boiler back-up system, which would lead to an increase in the cost of the investment.

Finally, due to political reasons, it is important to bear in mind that these types of power plants are strongly related to government regulations. The analysis of the investment given in Chapter 6 would change much if the price of the energy produced on this power plant was not supported by Spanish government. In that case, the economic feasibility of the project would be seriously damaged until the point of considering other investments as better alternatives.

8.4. Further development and new research opportunities

The present project has proven that the two-row receiver design can be a feasible and improved solution for this type of power plant. It is not difficult to notice that there are some new lines for future research based on the results here obtained.

On the one hand, in order to improve the quality of the calculations, it is recommended to be more accurate in all the approximations and simplifications that have been made in the project.

Regarding the calculations of the increase in temperature and vapor quality along the tubes, one way of getting better results could be to divide each tube in different slices or axial sections. Thereby, although a linear treatment would be taken for each slice, it would be non-linear for the entire tube, which would be closer to reality.

In order to improve the calculations of the convection losses at the inner row of tubes for the two-row receiver design, using a more precise air temperature at the surroundings of those tubes could decrease those losses. Thus, further research for calculating this temperature in a two-row configuration would improve the performance of the power plant. Given that the computing workload of the given method is relatively low, this presents the possibility for further research about the optimization of the power plant.

The dependence on the natural gas-fired boiler is another relevant aspect that must be taken into account. As mentioned in sections 5.8 and 5.9, during cold months the field of heliostats is not big enough to supply the needed energy required to get the optimum performance of the power plant. However, during hot months the field of

heliostats is oversized, having some of the heliostats not working in order to protect the receiver against critical temperatures. New research could focus on improving the performance on winter in order to decrease the use of fossil fuel. Nevertheless, this would bring an even more oversized field of heliostats for summer season. This is a matter of a cost-benefit analysis, which involves introducing more heliostats, assuming the investment cost of the new heliostats would arise saving funds year after year by not consuming natural gas, but at the same time assuming the cost of not employing those heliostats in summer time. New lines of investigation can be focused on finding additional uses for the idle heliostats in that period of the year such as designing a second tower or another receiver which could be used as economizer. One more possible alternative, which is out of the objectives of this project, is the introduction of a storage system. This system would give more time of electricity production per day, reducing the natural gas use considerably. However, this solution would also imply the addition of more heliostats to the field, getting a similar cost-benefit analysis result to the one that has been already mentioned.

Finally, although the results have been verified by using common sense and previous papers results, such as in the work by Ben-Zvi, it would be positive to compare those results with experimental data in order to give a true validation to the model.

Chapter 9 Bibliography

Agencia Andaluza de la Energía. *Radiación Solar en Andalucía.* Agosto 24, 2013.

Agencia EFE. "Expansión." *Expansión.* 08 26, 2013. http://www.expansion.com/agencia/efe/2013/08/26/18678463.html (accessed 08 27, 2013).

Alexopoulos, Spiros, and Bernhard Hoffschmidt. "Solar tower power plant in Germany and future perspectives of the development of the technology in Greece and Cyprus." *Renewable Energy*, 2010: 1352–1356.

Ben-Zvi, R., M. Epstein, and A. Segal. "Simulation of an integrated steam generator for solar tower." *Solar Energy*, 2011: 578-592.

BVA Media Group. *Sun & Wind Energy.* 2012. http://www.sunwindenergy.com/news/new-parabolic-trough-collector-3m-and-gossamer (accessed August 20, 2013).

Comisión Nacional de Energía. "Informe mensual de supervisión del mercado mayorista de gas." 2013.

Darvill, Andy. *Energy sources.* 2012. http://www.darvill.clara.net/altenerg/index.htm (accessed August 20, 2013).

DDBST GmbH. *Saturated Vapor Pressure.* 2012. http://ddbonline.ddbst.de/AntoineCalculation/AntoineCalculationCGI.exe (accessed August 20, 2013).

Denkenberger, D. C., and J. M. Pearce. "Numerical Simulation of the Direct Application of Compound Parabolic Concentrators to a Single Effect Basin Solar Still." *Proceedings of the 2006 International Conference of Solar Cooking and Food Processing.* 2006. 118.

EsAcademic. *Esacademic.* 2013. http://www.esacademic.com/dic.nsf/eswiki/283402 (accessed August 20, 2013).

Excmo. Ayuntamiento de Gibraleón. "Ordenanza Fiscal reguladora del Impuesto sobre Bienes Inmuebles." Gibraleón, Huelva, March 31, 2013.

—. "Ordenanza Fiscal reguladora del Impuesto sobre Construcciones, Instalaciones y Obras." Gibraleón, Huelva, March 31, 2003.

Favrat, D., and G. Augsburger. "Modelling of the receiver transient flux distribution due to cloud passages on a solar tower thermal power plant." *Solar Energy*, 2012: 42-52.

Forster, H. K., and N. Zuber. "Dynamics of vapor bubbles and boiling heattransfer." *AlChe Journal*, 1955: 531-535.

Geothermal Education Office. *Geothermal Education Office.* 2000. http://geothermal.marin.org/geopresentation/sld015.htm (accessed August 20, 2013).

Glendoher Engineering. "Glendoher Engineering." 10 24, 2009. http://eng-calculations.com/ (accessed August 20, 2013).

Greenewables. *DW Greenewables, Green Renewable Products.* 2013. http://dwgreenewables.com/home/ (accessed August 20, 2013).

Guia Sempio. *Guia Sempio.* 2007. http://guiasempio.com.ar/gs-esp/area-ingenieria/obras/0008-presa-hoover/ (accessed August 20, 2013).

Harrison, G.P., and H.W. Whittington. "Vulnerability of Hydropower Projects to Climate Change." Edinburgh, 2001.

Heras Martín, Jorge. *Diseño y análisis de una planta termosolar de torre central con configuraciones de único o doble receptor operando con sales fundidas.* Bachelor Thesis, Leganés: Carlos III University of Madrid, 2012.

Hottel, H. C. "Radiant heat trasnmission between surfaces separated by non-absorbing media." *Transactions of ASME, Journal of Heat Tranfer*, 1931: 265-273.

Incropera, F. P. *Introduction to heat transfer.* John Wiley and Sons, 2006.

Instituto Nacional de Estadística de España. "Índice de Precios de Consumo (IPC). Base 2011." 2013.

International Energy Agency. *World Energy Outloot 2012.* Paris: IEA Publications, 2012.

Joga López, H. *Diseño de una planta termosolar de receptor central con almacenamiento de sales fundidas.* Bachelor Thesis, Leganés: Carlos III University of Madrid, 2012.

Johansson, T. B. *Renewable energy: sources for fuels and electricity.* Island Press, 1993.

Kalogirou, S. *Solar energy engineering: processes and systems.* Elsevier/Academic Press, 2009.

Meyer, N. I. "European schemes for promoting renewables in liberalised markets." *Energy Policy*, 2003: 665-676.

Milankovitch, M. "Canon of Insolation and the Ice-Age Problem." *Special Publications of the Royal Serbian Academy*, 1941: 484.

Ministerio de Industria, Energía y Turismo de España. *La energía en España 2011.* Madrid: Subdirección general de desarrollo normativo, informes y publicaciones, 2012.

Novatec Solar. *Novatec Solar.* 2012. http://www.novatecsolar.com/ (accessed August 20, 2013).

Orden IET/221/2013, de 14 de febrero, por la que se establecen los peajes de acceso a partir de 1 de enero de 2013 y las tarifas y primas de las instalaciones del régimen especial. España: Boletín Oficial del Estado, 2013.

Protermosolar. "Localización de centrales solares termoeléctricas en España." 2013. http://www.protermosolar.com/boletines/23/Mapa.pdf (accessed August 30, 2013).

Schmitz, M., P. Schwarzbözl, R. Buck, and R. Pitz-Paal. "Assessment of the potential improvement due to multiple apertures in central receiver systems with secondary concentrators." *Solar Energy*, 2006: 111-120.

Şen, Z. "Solar energy in progress and future research trends." *Progress in Energy and Combustion Science*, 2004: 367-416.

Siemens. *Proyectos Siemens Energy: Andasol.* 2009. http://www.swe.siemens.com/spain/web/es/energy/com_energy/proyectos/Pages/proyectos_siemens_energy_andasol.aspx (accessed August 30, 2013).

Solar Energy Topics. *Solar Energy Topics.* 2012. http://www.solarenergytopics.com/solar/parabolic-dish.html (accessed August 20, 2013).

Thermal Engineering and Fluid Mechanics Department. "Supplied information." n.d.

Thome, J. R. *Engineering Data Book III.* Lausanne: Wolverine Tube, Inc., 2004.

Torresol Energy. *Torresol Energy.* 2010. http://www.torresolenergy.com/TORRESOL/planta-gemasolar/es (accessed 30 August, 2013).

United Nations Development Programme. *World Energy Assesment 2000.* New York: Bureau of Development Policy, 2000.

Volker Quaschning. *Technology Fundamentals: Solar Energy.* 2003. http://www.volker-quaschning.de/articles/fundamentals2/index.php (accessed August 20, 2013).

White, F. M. *Fluid Mechanics.* McGraw Hill, 2011.

Wischnewski, B. *Peace Software.* 2012. http://www.peacesoftware.de/einigewerte/luft_e.html (accessed August 20, 2013).

Woodbank Communications Ltd. *Electropaedia.* 2005. http://www.mpoweruk.com/solar_power.htm (accessed August 20, 2013).

World Mysteries. *World Mysteries Blog.* 2011. http://blog.world-mysteries.com/science/ancient-timekeepers-part-1-movements-of-the-earth/ (accessed August 20, 2013).

WWF España. "Observatorio de la Electricidad Agosto 2013." 2013.

Xah Lee. *Xah Arts.* 2011. http://xaharts.org/Whirlwheel_dir/reflecting_disks/reflecting_disks.html (accessed August 20, 2013).

Annexes

Annex I - Power cycle programming

```
%CYCLE CALCULATION-------------------------------------------------
-----------
%Defined to pressure, inlet and outlet pressures of the turbine
(bar)
Pboil=6e6;%60 bar, 548K
Pcond=0.01e6;%0.1 bar, 320K
T3=600+273.15;
Tboil=548;%K
Tcond=320;

h1=191.90e3;
v=1.01e-3;
np=0.85;
h2=h1+v*(Pboil-Pcond)/np


s3=7169.21;%J/kg·K
h3=3658.75e3;%J/kg
sl=649.3;
sv=8150.2;

hl=h1;
hv=2584.7e3;
h4s=2761.49e3
nt=0.85;
h4=h3-nt*(h3-h4s)
T4=436;%K With the result of the previous line, h4, the
temperature is obtained.
```

```
h5=3700e3
T5=873;%K With the result of the previous line, h5, the
temperature is obtained.
s5=8217.64
X6s=(s5-sl)/(sv-sl)
h6s=(1-X6s)*hl+X6s*hv
h6=h5-nt*(h5-h6s)
X6=(h6-hl)/(hv-hl)

% Then it is calculated the overall yield of the cycle
n=((h3-h4)+(h5-h6)-(h2-h1))/((h3-h2)+(h5-h4))
%the product of the electric and mechanical yields
nprod=0.99;
ntot=nprod*n
Pplant=50;%MW
Pthermal=Pplant/ntot
Pmaxrec=Pthermal

%Temperature and enthalpy differentials for stage calculation
ATheat=Tboil-Tcond;
Tpropheat=(Tboil+Tcond)/2
ATsuper=T3-Tboil;
Tpropsuper=(T3+Tboil)/2
ATreheat=T5-T4;

Cpheat=4.3426*1000;%J/kg·K
Lvap=1575.6*1000;%J/kg
Cpsuper=2.5*1000;%J/kgK
Cpreheat=2.24*1000;%J/kgK
```

Annex II - Heat Transfer Calculation

```
%HEAT TRANSFER CALCULATION-------------------------------------
-----------
h2=1.9902e+5;%J/kg
hl=1213.4e3;%enthaply of the liquid at the boil temperature
hv=2784.3e3;%enthaply of the vapor at the boil temperature
h3=3658.75e3;

hec=hl-h2;
hboil=hv-hl;
hvap=hboil;
hsh=h3-hv;
ht=hec+hboil+hsh;
Notubes=1260;

Npanel=10;
%Mass flow per tube
m=Pmaxrec*1000000/(ATheat*Cpheat+Lvap+ATsuper*Cpsuper+ATreheat*C
preheat)/(Notubes*2/Npanel)
%m=Pmaxrec*10^6/(Notubes*(hec+hboil+hsh));

%Division of panels in stages.
Npanelec=Npanel*hec/ht;
Npanelboil=Npanel*hboil/ht;
```

```
Npanelsh=Npanel*hsh/ht;


Ltube=12;
dext=1.05*2.54*10^-2;
dint=0.742*2.54*10^-2;
Lt=12*Npanel/2;%6 panels per side of the receiver, taking this
one symetric
Lec=Lt*Npanelec/Npanel
dTec=(Tboil-Tcond)/Lec
Lboil=Lt*Npanelboil/Npanel
dx=1/Lboil;
Lsh=Lt*Npanelsh/Npanel
dTsh=(T3-Tboil)/Lsh;

%Air properties
Tamb=15+273.15;%K
Cpair=1006.6258375;%J/kgK
roair=1.226900075;%Kg/m3
vwind=2;%m/s
viscair=1.798414575e-5;%Pa·s
kair=25.308689e-3;%W/mK
nuair=viscair/roair;
Reair=roair*vwind*dext/viscair;
Prair=Cpair*viscair/kair;
Nufc=0.3+0.62*Reair^0.5*Prair^(1/3)/(1+(0.4/Prair)^(2/3))^0.25*(
1+(Reair/282000)^0.625)^0.8;
hfc=Nufc*kair/dext;

%HT IN ECONOMIZER----------------------------------------------
---------
yin=0;
yout=12;
i=1;
Tin=Tcond;
while yout<Lec
    if yin~=0
        Tin=Tin+dTec*(yout-yin);
    end
    Tout=Tin+dTec*(yout-yin);
    Tprop=(Tin+Tout)/2;
    Ltubeeco(i)=yout-yin;

    %Water properties during the economizer stage
    roeco(i)=-3.87E-06*Tprop^3 + 0.0023792*Tprop^2 -
0.8520517*Tprop + 1148.118;%kg/m3;
    veco(i)=m/(roeco(i)*pi*dint^2/4);%m/s
    Cp1(i)=0.0001374*Tprop^3 - 0.151114*Tprop^2 + 56.19775*Tprop
- 2852.383;%J/kgK;
    visc1=4.94E-13*Tprop^4 - 9.42E-10*Tprop^3 + 6.75E-07*Tprop^2
- 0.0002159*Tprop + 0.0262489;%Pa·s
    k1=1.47E-09*Tprop^3 - 7.51E-06*Tprop^2 + 0.0054286*Tprop -
0.3761762;%W/mK

    Reeco(i)=roeco(i)*veco(i)*dint/visc1;
    Pr1=Cp1(i)*visc1/k1;
    Nu1=0.023*Reeco(i)^0.8*Pr1^0.4;

    heco=Nu1*k1/dint;
```

```
    Tt=500+273.15;%external temperature of the tubes
    Ttubeeco(i)=0;
    while abs(Tt-Ttubeeco(i))>Tt*0.005
        ktube=1.2305e-5*Tt^2-4.5763e-3*Tt+1.6796e1;
        Rec=1/(pi*dint*(yout-
yin)*heco)+log(dext/dint)/(2*pi*(yout-yin)*ktube);
        qeco(i)=m*Cp1(i)*(Tout-Tin);
        aux=exp(-1/(m*Cp1(i)*Rec));
        Ttubeeco(i)=(Tin*aux-Tout)/(aux-1);
        Tt=Tt-1;
    end

    %Convection losses
Tbeta=(Tamb+Ttubeeco(i))/2;
beta=1/Tbeta;
Gr=9.81*beta*(Ttubeeco(i)-Tamb)*(yout-yin)^3/nuair^2;
Ra=Gr*Prair;
Nunc=(0.825+0.387*Ra^(1/6)/(1+(0.492/Prair)^(9/16))^(8/27))^2;
hnc=Nunc*kair/(yout-yin);
hconvloss=(hfc^4+hnc^4)^(1/4);
qconveco(i)=hconvloss*pi*dext*(yout-yin)*(Ttubeeco(i)-Tamb);

%iteration helps
    i=i+1;
    yin=yin+12;
    yout=yin+12;


end

yout=Lec;
yaux=12-(yout-yin);
Tt=400+273.15;
Ttube=0;
Ltubeeco(i)=yout-yin;

Tin=Tout;
Tout=Tin+dTec*(yout-yin);
Tprop=(Tin+Tout)/2;
roeco(i)=-3.87E-06*Tprop^3 + 0.0023792*Tprop^2 - 0.8520517*Tprop
+ 1148.118;%kg/m3
veco(i)=m/(roeco(i)*pi*dint^2/4);%m/s
Cp1(i)=0.0001374*Tprop^3 - 0.151114*Tprop^2 + 56.19775*Tprop -
2852.383;%J/kgK
visc1=4.94E-13*Tprop^4 - 9.42E-10*Tprop^3 + 6.75E-07*Tprop^2 -
0.0002159*Tprop + 0.0262489;%Pa·s
k1=1.47E-09*Tprop^3 - 7.51E-06*Tprop^2 + 0.0054286*Tprop -
0.3761762;%W/mK

Reeco(i)=roeco(i)*veco(i)*dint/visc1;
Pr1=Cp1(i)*visc1/k1;
Nu1=0.023*Reeco(i)^0.8*Pr1^0.4;

heco=Nu1*k1/dint;
Ttubeeco(i)=0;
    while abs(Tt-Ttubeeco(i))>Tt*0.005
        ktube=1.2305e-5*Tt^2-4.5763e-3*Tt+1.6796e1;
        Rec=1/(pi*dint*(yout-
yin)*heco)+log(dext/dint)/(2*pi*(yout-yin)*ktube);
        qeco(i)=m*Cp1(i)*(Tout-Tin);
```

```
        aux=exp(-1/(m*Cp1(i)*Rec));
        Ttubeeco(i)=(Tin*aux-Tout)/(aux-1);
        Tt=Tt-1;
    end

%Convection losses
Tbeta=(Tamb+Ttubeeco(i))/2;
beta=1/Tbeta;
Gr=9.81*beta*(Ttubeeco(i)-Tamb)*(yout-yin)^3/nuair^2;
Ra=Gr*Prair;
Nunc=(0.825+0.387*Ra^(1/6)/(1+(0.492/Prair)^(9/16))^(8/27))^2;
hnc=Nunc*kair/(yout-yin);
hconvloss=(hfc^4+hnc^4)^(1/4);
qconveco(i)=hconvloss*pi*dext*(yout-yin)*(Ttubeeco(i)-Tamb);

%HT IN BOILER-----------------------------------------------------
-----------

Tprop=Tboil;
rol=757.993;
rov=30.8154;
ro2=(rol+rov)/2;
Cpl=5.208;
Cpv=4.8531;
Cp2=(Cpl+Cpv)/2;
viscl=9.52467e-5;
viscv=1.85096e-5;
visc2=(viscl+viscv)/2;
kl=0.584294;
kv=0.0599685;
k2=(kl+kv)/2;
dp=6981.24e3-5998.69e3;%Pa
dT=10;
sigma=5.67e-8;

yin=yout;
yout=yin+yaux;
i=1;
while yout<(Lec+Lboil)
    if i==1
        xin=0;
    end
    Ltubeboil(i)=yout-yin;
    xout=xin+dx*(yout-yin);
    x=(xin+xout)/2;

hfz=(kl^0.79*Cpl^0.45*rol^0.49)/(sigma^0.5*viscl^0.29*hvap*0.24*
rov^0.24)*dT^0.24*dp^0.75;

    Re2=m*(1-x)*dint/viscl;
    roboil(i)=1/(x/rov+(1-x)/rol);
    vboil(i)=m/(roboil(i)*pi*dint^2/4);
    viscboil=1/(x/viscv+(1-x)/viscl);
    Reboil(i)=vboil(i)*dint*roboil(i)/viscboil;
    Pr2=Cpl*viscl/kl;
    hdb=0.023*Re2^0.8*Pr2^0.4*kl/dint;

    Xtt=((1-x)/x)^0.9*(rov/rol)^0.5*(viscl/viscv)^0.1;
    F=(1/Xtt+0.213)^0.736;
    Retp=Re2*F^1.25;
```

```
    S=1/(1+2.53e-6*Retp^1.17);

    hevap=S*hfz+F*hdb;

    Tt=800+273.15;%external temperature of the tubes
    Ttubeboil(i)=0;
    while abs(Tt-Ttubeboil(i))>Tt*0.005
        ktube=1.2305e-5*Tt^2-4.5763e-3*Tt+1.6796e1;
        Rboil=1/(pi*dint*(yout-yin)*hevap);
        Rcond=log(dext/dint)/(2*pi*(yout-yin)*ktube);
        qboil(i)=m*(xout-xin)*hv;
        Thtf=Tprop;
        Ttubeboil(i)=Thtf+(Rcond+Rboil)*qboil(i);
        Tt=Tt-1;
    end

        %Convection losses
Tbeta=(Tamb+Ttubeboil(i))/2;
beta=1/Tbeta;
Gr=9.81*beta*(Ttubeboil(i)-Tamb)*(yout-yin)^3/nuair^2;
Ra=Gr*Prair;
Nunc=(0.825+0.387*Ra^(1/6)/(1+(0.492/Prair)^(9/16))^(8/27))^2;
hnc=Nunc*kair/(yout-yin);
hconvloss=(hfc^4+hnc^4)^(1/4);
qconvboil(i)=hconvloss*pi*dext*(yout-yin)*(Ttubeboil(i)-Tamb);

%iteration help
    yin=yout;
    yout=yin+12;
    xin=xout;
    i=i+1;
end

yout=Lec+Lboil;
yaux=Ltube-(yout-yin);
Ltubeboil(i)=yout-yin;
xout=xin+dx*(yout-yin);
x=(xin+xout)/2;

hfz=(kl^0.79*Cpl^0.45*rol^0.49)/(sigma^0.5*viscl^0.29*hvap*0.24*
rov^0.24)*dT^0.24*dp^0.75;

Re2=m*(1-x)*dint/viscl;
roboil(i)=1/(x/rov+(1-x)/rol);
vboil(i)=m/(roboil(i)*pi*dint^2/4);
viscboil=1/(x/viscv+(1-x)/viscl);
Reboil(i)=vboil(i)*dint*roboil(i)/viscboil;
Pr2=Cpl*viscl/kl;
hdb=0.023*Re2^0.8*Pr2^0.4*kl/dint;

Xtt=((1-x)/x)^0.9*(rov/rol)^0.5*(viscl/viscv)^0.1;
F=(1/Xtt+0.213)^0.736;
Retp=Re2*F^1.25;
S=1/(1+2.53e-6*Retp^1.17);

hevap=S*hfz+F*hdb;


    Tt=800+273.15;%external temperature of the tubes
```

```
    Ttubeboil(i)=0;
    while abs(Tt-Ttubeboil(i))>Tt*0.005
        ktube=1.2305e-5*Tt^2-4.5763e-3*Tt+1.6796e1;
        Rboil=1/(pi*dint*(yout-yin)*hevap);
        Rcond=log(dext/dint)/(2*pi*(yout-yin)*ktube);
        qboil(i)=m*(xout-xin)*hv;
        Thtf=Tprop;
        Ttubeboil(i)=Thtf+(Rcond+Rboil)*qboil(i);
        Tt=Tt-1;
    end

%Convection losses
Tbeta=(Tamb+Ttubeboil(i))/2;
beta=1/Tbeta;
Gr=9.81*beta*(Ttubeboil(i)-Tamb)*(yout-yin)^3/nuair^2;
Ra=Gr*Prair;
Nunc=(0.825+0.387*Ra^(1/6)/(1+(0.492/Prair)^(9/16))^(8/27))^2;
hnc=Nunc*kair/(yout-yin);
hconvloss=(hfc^4+hnc^4)^(1/4);
qconvboil(i)=hconvloss*pi*dext*(yout-yin)*(Ttubeboil(i)-Tamb);

%HT IN SUPERHEATER-----------------------------------------------
-------------
yin=yout;
yout=yin+yaux;
i=1;

while yout<=(Lec+Lboil+Lsh)
    if i==1
        Tin=Tboil;
    else
        Tin=Tout;
    end
    Tout=Tin+dTsh*(yout-yin);
    Tprop3=(Tin+Tout)/2;%K
    Ltubesh(i)=yout-yin;

    rosh(i)=-4.37E-07*Tprop3^3 + 0.0010705*Tprop3^2 -
0.8942193*Tprop3 + 271.1968;%kg/m3
    vsh(i)=m/(rosh(i)*pi*dint^2/4);%m/s
    Cp3=-0.0002138*Tprop3^3 + 0.5021893*Tprop3^2 -
391.1837*Tprop3 + 103446.2;%J/kgK
    visc3=1.62E-14*Tprop3^3 - 4.8E-11*Tprop3^2 + 8.74E-08*Tprop3
- 1.76E-05;%Pa·s
    k3=-1.16E-09*Tprop3^3 + 2.77E-06*Tprop3^2 - 0.0020736*Tprop3
+ 0.5546043;%W/mK

    Resh(i)=rosh(i)*vsh(i)*dint/visc3;
    Pr3=Cp3*visc3/k3;
    Nu3=0.023*Resh(i)^0.8*Pr3^0.4;

    hsuper=Nu3*k3/dint;

        Tt=800+273.15;%external temperature of the tubes
        Ttubesh(i)=0;
        while abs(Tt-Ttubesh(i))>Tt*0.005
            ktube=1.2305e-5*Tt^2-4.5763e-3*Tt+1.6796e1;
            Rsuper=1/(pi*dint*(yout-
yin)*hsuper)+log(dext/dint)/(2*pi*(yout-yin)*ktube);
```

```
            qsh(i)=m*Cp3*(Tout-Tin);
            aux=exp(-1/(m*Cp1(i)*Rsuper));
            Ttubesh(i)=(Tin*aux-Tout)/(aux-1);
            Tt=Tt-1;
        end

            %Convection losses
Tbeta=(Tamb+Ttubesh(i))/2;
beta=1/Tbeta;
Gr=9.81*beta*(Ttubesh(i)-Tamb)*(yout-yin)^3/nuair^2;
Ra=Gr*Prair;
Nunc=(0.825+0.387*Ra^(1/6)/(1+(0.492/Prair)^(9/16))^(8/27))^2;
hnc=Nunc*kair/(yout-yin);
hconvloss=(hfc^4+hnc^4)^(1/4);
qconvsh(i)=hconvloss*pi*dext*(yout-yin)*(Ttubesh(i)-Tamb);
    yin=yout
    yout=yin+11.99999999;
    i=i+1;
end
Qeco=qeco+qconveco
Qboil=qboil+qconvboil
Qsh=qsh+qconvsh

%Division in panels and data by panel and not by stage----------
-----------
Q=[Qeco, Qboil, Qsh]
Tt=[Ttubeeco, Ttubeboil, Ttubesh]
Ltubes=[Ltubeeco, Ltubeboil, Ltubesh]
```

Annex III - Radiation Losses Calculation

```
%RADIATION LOSSES-----------------------------------------------
-----------
%Circumference length and number of tubes according to Ben Zvi
design
Lcirc=10/12*2*pi*8
%distance between pipes centers
s=(Lcirc)/Notubes
%heigh of the equilateral triangle configuration
H=sqrt(3)*s/2;
R=s/dext;
%view factor for reradiant surface to tube
Fwt2=-0.0002*R^6+0.0045*R^5-0.0423*R^4+0.189*R^3-0.3552*R^2-
0.0856*R+1.2913
Fwt1=0.00001*R^6-0.00003*R^5-0.0046*R^4+0.0672*R^3-
0.3861*R^2+0.9725*R-0.6499
Fst2=Fwt1
Fst1=Fwt2
Fws=1-Fwt2-Fwt1
Fsw=Fws
As=s*Ltubes(i);
Aw=As;
At=pi*Ltubes(i)*dext;
Ft2w=Aw/At*Fwt2
Ft1s=Ft2w
Ft2s=As/At*Fst2
```

```
Ft1w=Ft2s
Ftt=(1-Ft2w-Ft2s)/2


%Surroundings temperature
eg=0.76;
esky=1;
Tamb=273.15+33;
Tg=Tamb+10;
Tsky=273.15;
es=(esky+eg)/2;
Fsky=0.5;
Fg=0.5;
Ts=((Fsky*esky*Tsky^4+Fg*eg*Tg^4)/es)^(1/4);

%tube emisivity
et=0.925;

%Surroundings and tube area, and error aiming coefficient of
heliostats
Tin=T4;%K Inlet temperature at the lower pressure turbine
qconvreheat=zeros(1, size(Q,2))
for i=1:size(Q,2)

    Ttube2(i)=0;
    Tt2=200+273.15;
    Tprop=479;

    while abs(Tt2-Ttube2(i))>Tt2*0.005

    As=s*Ltubes(i);
    At=pi*dext*Ltubes(i);
    alpha=0.9;
    %Total heat needed in the tube, tube  and Stefan-Boltzmann
constant
    sigma=5.67e-8;
    Jt1=Q(i)*(1-et)/At*et+sigma*Tt2^4;
    Es=sigma*Ts^4;
    a=(1-et)/At*et;
    Et2=sigma*(Tt2)^4;

    %System of equations
    A(1,1)=At*Ft2w+As*Fsw+At*Ft1w;
    A(1,2)=-As*Fsw;
    A(1,3)=-alpha*Fsw*As;
    A(1,4)=-a*At*Ft2w;
    A(2,1)=-As*Fsw;
    A(2,2)=As*es/(1-es)+As*Fst2+As*Fst1+As*Fsw;
    A(2,3)=0;
    A(2,4)=-a*As*Fst2;
    A(3,1)=At*Ft1w;
    A(3,2)=As*Fst1;
    A(3,3)=alpha*Fst1*As;
    A(3,4)=a*At*Ftt;
    A(4,1)=-At*Ft2w;
    A(4,2)=-At*Ft2s;
    A(4,3)=-alpha*Fst2*As;
    A(4,4)=1+a*At*Ftt+a*At*Ft2w+a*At*Ft2s;
    A;
```

```
    B(1,1)=Jt1*At*Ft1w+Et2*At*Ft2w;
    B(2,1)=Jt1*As*Fst1+Et2*As*Fst2+Es*As*es/(1-es);
    B(3,1)=Q(i)-Et2*At*Ftt+Jt1*(At*Ftt+At*Ft1w+At*Ft1s);
    B(4,1)=Jt1*At*Ftt-Et2*(At*Ftt+At*Ft2w+At*Ft2s);
    B;
    M=A\B;
    Jw(i)=M(1);
    Js(i)=M(2);
    G(i)=M(3);
    Qt2(i)=M(4);

        rorh(i)=-0.0000000127*Tprop^3 + 0.0000325*Tprop^2 -
0.0298*Tprop + 11.4;%kg/m3
        vrh(i)=m/(rorh(i)*pi*dint^2/4);%m/s
        Cp= -0.0000000004515*Tprop^5 + 0.000001632*Tprop^4 -
0.002339*Tprop^3 + 1.662*Tprop^2 - 585.5*Tprop + 83860;%J/kgK
        visc=-0.000000000000006202*Tprop^3 +
0.000000000009697*Tprop^2 + 0.00000003722*Tprop -
0.000003121;%Pa·s
        k= -0.0000000001089*Tprop^3 + 0.0000002864*Tprop^2 -
0.00012*Tprop + 0.03927;%W/mK

        Rerh(i)=rorh(i)*vrh(i)*dint/visc;
        Pr=Cp*visc/k;
        Nu=0.023*Rerh(i)^0.8*Pr^0.4;

        hsuper=Nu*k/dint;
        ktube=1.2305e-5*Tt2^2-4.5763e-3*Tt2+1.6796e1;

Rsuper=1/(pi*dint*Ltubes(i)*hsuper)+log(dext/dint)/(2*pi*Ltubes(
i)*ktube);

        Tout(i)=(Qt2(i)-qconvreheat(i))/(m*Cp)+Tin;
        Ttube2(i)=(Tout(i)-Tin*exp(-1/(m*Cp*Rsuper)))/(1-exp(-
1/(m*Cp*Rsuper)));
        Tprop=(Tout(i)+Tin)/2;

        %Convection losses
            Tbeta=(Tamb+Ttube2(i))/2;
            beta=1/Tbeta;
            Gr=9.81*beta*(Ttube2(i)-Tamb)*Ltubes(i)^3/nuair^2;
            Ra=Gr*Prair;

Nunc=(0.825+0.387*Ra^(1/6)/(1+(0.492/Prair)^(9/16))^(8/27))^2;
            hnc=Nunc*kair/Ltubes(i);
            hconvloss=(hfc^4+hnc^4)^(1/4);

qconvreheat(i)=hconvloss*pi*dext*Ltubes(i)*(Ttube2(i)-Tamb);


        if Tt2>Ttube2(i)
            Tt2=Tt2-0.1;
        else
            Tt2=Tt2+0.1;
        end
    end
    Tin=Tout(i);
end
```

Annex IV - Heat Transfer Calculation Last Panel inner row

```
%LAST SUPERHEATING INNER ROW----------------------------------
----------
i=i+1;
Tin=Tout(end)
    Tout(i)=T5
    Tpropsh=(Tin+Tout(i))/2;%K

    rorh(i)=-4.37E-07*Tpropsh^3 + 0.0010705*Tpropsh^2 -
0.8942193*Tpropsh + 271.1968;%kg/m3
    vrh(i)=m/(rorh(i)*pi*dint^2/4);%m/s
    Cprh=-0.0002138*Tpropsh^3 + 0.5021893*Tpropsh^2 -
391.1837*Tpropsh + 103446.2;%J/kgK
    viscrh=1.62E-14*Tpropsh^3 - 4.8E-11*Tpropsh^2 + 8.74E-
08*Tpropsh - 1.76E-05;%Pa·s
    krh=-1.16E-09*Tpropsh^3 + 2.77E-06*Tpropsh^2 -
0.0020736*Tpropsh + 0.5546043;%W/mK

    Rerh(i)=rorh(i)*vrh(i)*dint/viscrh;
    Prrh=Cprh*viscrh/krh;
    Nurh=0.023*Rerh(i)^0.8*Prrh^0.4;

    hrh=Nurh*krh/dint;

        Tt=800+273.15;%external temperature of the tubes
        Ttube2(i)=0;
        while abs(Tt-Ttube2(i))>Tt*0.005
            ktube=1.2305e-5*Tt^2-4.5763e-3*Tt+1.6796e1;

Rrh=1/(pi*dint*Ltube*hrh)+log(dext/dint)/(2*pi*Ltube*ktube);
            qrh=m*Cprh*(Tout(i)-Tin);
            aux=exp(-1/(m*Cprh*Rrh));
            Ttube2(i)=(Tin*aux-Tout(i))/(aux-1);
            Tt=Tt-1;
        end

            %Convection losses
Tbeta=(Tamb+Ttube2(i))/2;
beta=1/Tbeta;
Gr=9.81*beta*(Ttube2(i)-Tamb)*Ltube^3/nuair^2;
Ra=Gr*Prair;
Nunc=(0.825+0.387*Ra^(1/6)/(1+(0.492/Prair)^(9/16))^(8/27))^2;
hnc=Nunc*kair/(Ltube);
hconvloss=(hfc^4+hnc^4)^(1/4);
qconvreheat(i)=hconvloss*pi*dext*Ltube*(Ttube2(i)-Tamb);
Qt2(i)=qconvreheat(i)+qrh;

%RADIATION LOSSES
%Circumference length and number of tubes according to Ben Zvi
design
Lcirc=10/12*2*pi*8
%distance between pipes centers
s=(Lcirc)/Notubes
%view factor for reradiant surface to tube
Fwt=1-sqrt(1-(dext/s)^2)+(dext/s)*atan(sqrt((s^2-
dext^2)/dext^2))
Fws=1-Fwt
```

```
Fsw=Fws
Ftw=s/(pi*dext)*Fwt
Fts=Ftw
Ftt=1-2*Ftw
Fst=Fwt

%Surroundings temperature
eg=0.76;
esky=1;
Tamb=273.15+33;
Tg=Tamb+10;
Tsky=273.15;
es=(esky+eg)/2;
Fsky=0.5;
Fg=0.5;
Ts=((Fsky*esky*Tsky^4+Fg*eg*Tg^4)/es)^(1/4);

%tube emisivity
et=0.925;

%Surroundings and tube area, and error aiming coefficient of
heliostats
As=s*Ltube;
At=pi*dext*Ltube;
alpha=0.9;
%Total heat needed in the tube, tube  and Stefan-Boltzmann
constant
sigma=5.67e-8;
Jt=Qt2(i)*(1-et)/At*et+sigma*Ttube2(i)^4;

%System of equations
A(1,1)=At*Ftw;
A(1,2)=As*Fst;
A(1,3)=alpha*Fst*As;
A(2,1)=As*Fsw;
A(2,2)=-(As*es/(1-es)+As*Fsw+As*Fst);
A(2,3)=0;
A(3,1)=-(As*Fst+At*Ftw);
A(3,2)=As*Fsw;
A(3,3)=alpha*Fsw*As;
A;
B(1,1)=Qt2(i)+Jt*(At*Ftw+As*Fst);
B(2,1)=-As*es/(1-es)*sigma*Ts^4-As*Fst*Jt;
B(3,1)=-Jt*At*Ftw;
B;
M=A\B;
Jw(i)=M(1);
Js(i)=M(2);
G(i)=M(3);%W/m2

qrad(i)=(Js(i)-sigma*Ts^4)/((1-es)/As*es);
```

Annex V - Load Losses and Pumping Power Calculation

```
%LOAD
%LOSSES-----------------------------------------------------------
-------
ro=[roeco, roboil, rosh, rorh]
v=[veco, vboil, vsh, vrh]
Re=[Reeco, Reboil, Resh, Rerh]
Ltu=[Ltubes, Ltubes, Ltube]
rug=0.002;
Dcol=0.38;
kelbow=0.5*2
kse=(1-dint^2/Dcol^2)^2;
ksc=0.42*(1-dint^2/Dcol^2)^2;
kfluid=kelbow+kse+ksc;
for i=1:size(ro,2)
    f1=2;
    f2=0;
    while abs(f1-f2)>f1*0.05
        f2=1/(-2*log(rug/dint/3.7+2.51/Re(i)/(f1)^(1/2)))^2;
        if f1>f2
            f1=f1-0.001;
        else
            f1=f1+0.001;
        end
    end
    dPrec(i)=1/2*ro(i)*v(i)^2*(f2*Ltu(i)/dint+kfluid);
end
dPrec
sum(dPrec)

mtower=m*(2*Notubes/Npanel);
rotow=991.6;%kg/m3
vtow=mtower/(rotow*pi*dint^2/4);
Dtow=0.50;
visctow=0.00056908;
Retow=vtow*Dtow*rotow/visctow;
ksc=0.42*(1-Dcol^2/Dtow^2)^2;
kelbowtow=0.21;
ktee=0.07;
kvalve=5.5;
ktow=2*kelbowtow+ktee+kvalve+ksc;
htow=138;
    f1=2;
    f2=0;
    while abs(f1-f2)>f1*0.1
        f2=1/(-2*log(rug/Dtow/3.7+2.51/Retow/(f1)^(1/2)))^2;
        if f1>f2
            f1=f1-0.001;
        else
            f1=f1+0.001;
        end
    end
dPtow=1/2*rotow*vtow^2*(f2*htow/Dtow+ktow)
dPtotal=sum(dPrec)+dPtow+(Pboil-Pcond)
Qpump=mtower/rotow
Ppump=Qpump*dPtotal
```

Annex VI - Heliostat Field Sizing

```
%ARRAY OF RADIATION NEEDED-------------------------------------
-----------
j=1;
for i=1:size(G,2)
    if i==size(Qeco,2)
        Gt(j)=(Ltubeeco(end)*G(i)+G(i+1)*Ltubeboil(1))/Ltube;
        j=j+1;
    else
        if i==(size(Qeco,2)+1)
        else
            if i==(size(Qeco,2)+size(Qboil,2))
            Gt(j)=(Ltubeboil(end)*G(i)+G(i+1)*Ltubesh(1))/Ltube;
            j=j+1;
            else
            if i==((size(Qeco,2)+size(Qboil,2))+1)
            else
            Gt(j)=G(i);
            j=j+1;
            end
            end
        end
    end
end
for i=1:size(Gt,2)
    Gaux(i)=Gt(size(Gt,2)-(i-1));
end
apanel=2*pi/(2*size(Gt,2));%angle that covers each panel
Gt=[Gaux , Gt]*apanel*Ltube*8


%HELIOSTAT FIELD SIZING-----------------------------------------
-----------

w=10;%width of the heliostat
Ztow=138+Ltube/2;%138m from the center of the mirror to the
bottom of the tower according to Ben-Zvi
Lat=37.267;%Latitud of the location
Long=-7.017;%Longitude of the location

radt=0;
helio=0;
g=0;
rring=zeros(1,size(Gt,2));
ring=1;
R=0;
Rn=0;
Ra=0;
Rt=0;

r=ones(1,size(Gt,2))*6; %Initial radius of the field of
heliostats
A=[ 0 31 59 90 120 151 181 212 243 273 304 334];
```

```
H=10^3*[85.7 124.2 147 155.4 196.3 263.2 278.3 241.9 172.6 120.9
100.4 63.2];
Day=21;
Month=3;
D=Day+A(Month);

delta=23.45*sin((360*(284+D)/365)*pi/180)*pi/180;%Declination
angle

hss=acos(-atan(Lat)*tan(delta))*24/(2*pi);%Time distance of
sunset and sunrise from noon
tsr=12-hss;
tss=12+hss;

m=floor((tss-tsr)*60);
%Number of iterations according to the number of minutes of
sunlight during
%the chosen day
Qint=0;
for i=1:m
    t=i/60+tsr;
    Qint=Qint-0.0225*t^6+1.6196*t^5-47.7114*t^4+735.3030*t^3-
6257.7611*t^2+27977.9709*t-51123.0924
end
%Radiation data
Qrad= Qint/m%W/m2
Time=12;



    Rt=zeros(1,size(Gt,2));
    g=0;
    cont=0;%counter variable for sector which has already
fulfilled radiation condition
    contin=0;%counter variable to indicate the position of the
first sector which has not fulfilled its radiation condition yet
    r=20;
    secind=zeros(1,size(Gt,2));
    g=zeros(1,size(Gt,2));
    helio=0;
        asector(1)=apanel;
    for l=2:size(Gt,2)
            asector(l)=asector(l-1)+apanel;%vector with final
angle of each sector
    end
    while cont<size(Gt,2)

        if ring<=15
            nh=(2*pi-apanel*cont)*r/(1.5*w);
            nh=floor(nh);
        else
            nh=(2*pi-apanel*cont)*r/(2*w+ring*0.1);
            nh=floor(nh);
        end
        helio=helio+nh;
        ztin=apanel*contin+asin(5/r);
        Lsector=r*apanel;
        Lsec(1)=Lsector;
        for l=2:size(Gt,2)
            Lsec(l)=Lsec(l-1)+Lsector;
        end
```

```
            h=(12-Time)*2*pi/24;%hour angle which is zero at
local noon

alpha=asin(sin(Lat)*sin(delta)+cos(Lat)*cos(delta)*cos(h));%Sola
r height
            z=sin(cos(delta)*sin(h)/cos(alpha)); %Azimut angle
            alphat=atan(Ztow/r); %angle of the line from the
heliostat to the receiver and the horizontal plane
            for k=1:nh %Loop for radiation of each heliostat
                danh=(2*pi-apanel*cont)/nh;%angular distance
between heliostats
                if k==1
                    zt=ztin+(k-1)*danh;
                else
                    zt=zt+danh;
                end
                l=1;
                while zt>asector(l)
                    l=l+1;
                end

                contaux=0;
                if secind(l)~=0%Loop to pass to te following
sector which has not been fulfilled
                    while secind(l)~=0
                        l=l+1;
                        contaux=contaux+1;
                    end
                    zt=zt+apanel*contaux;
                end


theta=acos(cos(alpha)*cos(z)*cos(zt)*cos(alphat)+cos(alpha)*sin(
z)*cos(alphat)*sin(zt)+sin(alpha)*sin(alphat));
                Rn=Qrad*cos(theta/2); %Radiation of the n
heliostat at i minute
                ztpos=zt*r;
                l=1;
                while ztpos>Lsec(l)
                    ztpos;
                    Lsec(l);
                    l=l+1;
                end

               prevsec=0;
               nextsec=0;
               k;
               helarea(l)=w^2;
               if l~=1
                   if (ztpos-w/2)<Lsec(l-1)
                       helarea(l-1)=Ltube*(Lsec(l-1)-(ztpos-
w/2));

                       prevsec=1;
                       helarea(l)=helarea(l)-helarea(l-1);
                   end
               else
                   if (ztpos+w/2)>Lsec(l)
                       helarea(l+1)=Ltube*(ztpos+w/2-Lsec(l));
                       nextsec=1;
                       helarea(l)=helarea(l)-helarea(l+1);
```

```
                end
            end

            Rt(l)=Rt(l)+Rn*helarea(l);
            if prevsec==1
                Rt(l-1)=Rt(l-1)+Rn*helarea(l-1);
            end
            if nextsec==1
                Rt(l+1)=Rt(l+1)+Rn*helarea(l+1);
            end

        end

    cont=0;
        for l=1:size(Gt,2)
                g(l)=max(Rt(l),g(l));
            if g(l)>Gt(l)
                secind(l)=ring;
                cont=cont+1;
            end
        end
        l=1;
        aux=0;
        while aux==0 & l<=12
            if secind(l)==0
                aux=1;
            else
                l=l+1;
            end
        end

        contin=l-1;
        for l=1:size(Gt,2)
            if secind(l)==0
                rring(l)=r;
                ringsec(l)=ring;
            end
        end
        ring=ring+1;
        if ring<=15
            r=r+1.5*w;
        else
            r=r+2*w+0.1*ring;
        end
    end
    Rt
ringsec
rring
helio
area=zeros(1,size(Gt,2))
area1=0;
for i=1:size(Gt,2)
    area(i)=(apanel/2)*rring(i)^2;
    area1=area1+area(i);
end
area
area1
```

Annex VII - Performance Calculation

```
%TOTAL PERFORMANCE OF THE FIELD AND THE PLANT-------------------
-----
nfield=sum(Gt)/(area1*Qrad)
nplant=Pplant*10^6/(sum(Gt))
```